GENETIC SUSCEPTIBILITY TO THE MURINE MODEL OF RETINOPATHY OF PREMATURITY: IDENTIFICATION OF A NOVEL ROLE OF *TYROSINASE* IN RETINAL ANGIOGENIC REGULATION

By

Bliss Elizabeth O'Bryhim

Submitted to the graduate degree program in Molecular and Integrative Physiology and the Graduate Faculty of the University of Kansas in partial fulfillment of the requirements for the degree of Doctor of Philosophy

R.C. Andrew Symons, MB BS, Ph.D.
Co-Chairperson

Peter Smith, Ph.D.
Co-Chairperson

Jeff Radel, Ph.D.

John Wood, Ph.D.

Ting Xie, Ph.D.

Date defended:___5/10/2013_____

The Dissertation Committee for Bliss Elizabeth O'Bryhim certifies
that this is the approved version of the following dissertation:

GENETIC SUSCEPTIBILITY TO THE MURINE MODEL OF RETINOPATHY OF PREMATURITY:

IDENTIFICATION OF A NOVEL ROLE OF *TYROSINASE* IN RETINAL ANGIOGENIC

REGULATION

_____

R.C. Andrew Symons, MB BS, Ph.D.
Co-Chairperson

_____

Peter Smith, Ph.D.
Co-Chairperson

Date approved:__5/10/2013_____

ABSTRACT

Retinopathy of Prematurity (ROP) is a major cause of vision loss in the pediatric population. A growing body of evidence suggests that a heritable component contributes to risk of disease development. Identification of genes that modify disease susceptibility may provide a means to determine which children are at higher risk of developing ROP, as well as identify potential pharmacological targets to prevent progression of disease to vision-threatening stages. Using the murine model of ROP, oxygen-induced retinopathy (OIR), we developed a mapping cross that identified 2 quantitative trait loci associated with resistance to OIR. This work also found an association between albinism and reduced retinal avascular area. As albinism in our study was caused by loss of function of *Tyrosinase* (*Tyr*), we confirmed that function of this gene is associated with increased risk of OIR susceptibility using the *Tyr*-null murine strain. *Tyr* function was also found to inhibit endothelial progenitor cell (EPC) proliferation, mobilization, and recruitment to the retina. Subsequent studies exploring the mechanism of these findings demonstrated that *Tyr* function contributes to peripheral production of dopamine, and that dopamine inhibits retinal revascularization and EPC recruitment to the retina by signaling through the D1-like family of receptors. A time course study examining the number of EPCs in bone marrow, blood, and retina using both *Tyr*-null and wild-type mice identified patterns of proliferation, mobilization, and recruitment associated with more and less successful response to OIR. This study additionally suggested that retinal revascularization and associated EPC response in this model begins prior to the customary time point of P12, which has important implication for future studies seeking to modify EPC contribution to

this disease. A microarray analysis comparing transcriptional regulation between strains of mice known to be susceptible and resistant to OIR identified additional pathways that also contribute to disease susceptibility, and identified several areas of interest for future experiments. Together, these studies describe a novel role of dopaminergic signaling in retinal vascularization and identify potential mechanisms that contribute to susceptibility to ROP.

DEDICATION

This work is dedicated to my late father,
Harold Jeremiah Hartnett, Jr.,

In memory of our science projects - watching vinegar and baking soda react, making small explosives out of my chemistry kit, enduring the smell of petroleum waiting for “oil-eating bugs” to work, counting heartbeats of daphnia reacting to caffeine, building a maze for testing rat memory, and our favorite experiment of all, cooking. Thank you for helping me practice all of my science project talks and always asking me the hardest question at the presentation. I miss you every day.

ACKNOWLEDGEMENTS

This endeavor – both the dissertation project specifically and my education generally – would not have been possible without the support and encouragement of many people. The following are those who have played a particularly important role in my scientific development, for which I owe particular thanks:

To my mentor and friend, Dr. Andrew Symons, who has introduced me to the wonders of the retina. You gave me the freedom to become an independent scientist but were always available – even from half a world way – to answer questions, give pep talks, or discuss experimental details. You are a brilliant physician scientist, in the truest definition of the term, and you have encouraged both my clinical and research career to a degree that I did not think possible. I look forward to continue working with you in the future as I advance in my career, always with your advice in mind: ”get data, become famous.”

To Dr. Jeff Radel, who has been a constant and unfailingly patient. Thank you for all of the times that you put aside your own work to answer questions, give life advice, build oxygen chambers, fix lab equipment, and edit countless emails, abstracts, and manuscripts. More importantly, though, thank you for regularly reminding that science is a lot of fun.

To Dr. Joe Bast, who was instrumental in my decision both to pursue an MD/PhD program and to attend KUMC. You took time to meet with me when I was a pre-med

student just starting to explore a newfound interest in research, and you gave me the confidence to apply. Thank you also for your help in selecting a research mentor; more specifically, thank you for your encouragement to take a chance in selecting a brand new faculty member.

To Dr. John Sutphin, thank you for your steadfast support. From my first few months as a student at KUMC, you have encouraged my growing interest in ophthalmology and you have made it possible for me to complete my thesis work in this field. Thank you also for making me feel welcome in your department and in the specialty.

To my comprehensive exam and dissertation committee members: Dr. Ting Xie, Dr. Peter Smith, and Dr. John Wood. Thank you for your constructive criticism, suggestions, and support. I appreciate the different perspectives you each brought to my project.

To the current administration of the MD/PhD Program, Dr. Tim Fields, Dr. Brenda Rongish, and Mrs. Janice Fletcher. Tim, thank you for always having an open door and open ear when I had concerns or needed advice. Dr. Rongish, thank you for helping to ensure that everything was in place to facilitate my dissertation submission, defense, and return to clinics. Janice, thank you for taking care of all of us at every step and turn in our journey to graduation.

To Ms. Deborah Kephardt, the Executive Assistant to the Chair, thank you for all of your help. You always make me feel welcome and at ease at Ophthalmology events, and I appreciate always being able to turn to you with questions.

To my friends in the MD/PhD program, it has been a joy to work with you and to share these unique experiences and challenges. I chose to attend KUMC in part because of the camaraderie I sensed between its students, and I have been blessed to be a part of such a supportive program. I would especially like to thank Dr. Shane Stecklein and Mr. Anand Venugopal. You are both incredible scientists, and I appreciate all of the time you both took to help me with my first dabble in cell culture experiments. Thank you also to Dr.s Elizabeth Taglauer, Hope Karnes, and Megan Jack who regularly offered me encouragement and advice when I needed it most.

To those who have helped with the research described in this dissertation:

To Dr. Beth Levant and Dr. Michelle Healy-Stoffel, I owe sincerest thanks for help with the HPLC study, which was a key component of this project. Thank you, Dr. Levant, for generously sharing your resources and time. Michelle, I can't thank you enough for all of the hours you patiently helped me set up, run, and analyze the experiments, and especially for the late nights you came in to troubleshoot.

To Mrs. Janelle Ryals, who provided assistance, materials, and encouragement when I hit my first roadblock in research.

To Miss Emily Crowley, our student “volunteer”, thank you for photographing and measuring retinas in the time study. It was a joy to work with you, and I am confident that you soon be a fantastic physician.

To Mr. R. Sid White, our laboratory technician, thank you for your help with these projects, purchasing, laboratory organization, and daily animal care.

To Mr. Richard Hastings and Mrs. Alicia Zeiger, thank you both for your technical assistance with and suggestions for flow cytometry, which has been a major tool in my projects. Thank you also for your conversation, which helped to pass the time while hunting for my rare cells.

To those who inspired me to pursue research:

To Dr. Darcy Russell, my beloved undergraduate teacher. You encouraged my love for science as a pre-medical student, and showed me a passion for research. It was in your laboratory courses that I really began to appreciate the dynamic and exciting nature of science, which prompted me to explore it further and set me on the road to pursuing this research.

To Dr.s Sara Antonia Li and Jonathan Li, who took a big chance on a very inexperienced undergraduate student who just wanted to see what research was all about.

You were both incredibly kind and patient as I learned how to do my first "real" experiments, and you gently guided me through the process of creating research questions, designing and executing an experiment, and presenting the data. Your laboratory was a fantastic place to become first exposed to research.

To Dr. John Weroha, who also played a large role in my decision to pursue an MD/PhD program. Even though his time in the Li laboratory overlapped my summer research by only two weeks, I was amazed by your patience and kindness, and I was inspired by your passion for your career as a physician-scientist.

To my major sources of funding that have sponsored my research:

Biomedical Research Training Program: I thank the University of Kansas Medical Center Biomedical Research Training Program fellowship, under the directorship of Dr. Dianne Durham and Dr. Benyi Li, for supporting my research efforts.

Kansas Lions Sight Foundation: I thank the Kansas Lions Sight Foundation, under the directorship of Dr. John Sutphin, for their continued support of my work, and for allowing me to present my work at several conferences.

And, lastly, I would like to thank the people in my life who give meaning to my successes:

To my best friend husband, your unwavering encouragement and support – from birthdays delayed by grant deadlines to re-routed vacations, with an extra year thrown in

for fun – has been a guiding force in my life. I am a better, wiser, and more well-rounded person for knowing you, and I am grateful every day to be your wife.

To my sister, Jennifer, thank you for your patience with me over the years! You were my very first student, and I learned to love teaching from those fledgling experiences of playing school with you.

To my mother, who always has been and always will be my biggest cheerleader. Thank you for understanding when my calls became infrequent, and listening about my laboratory work even if it didn't all make sense. Thank you for teaching me to believe in myself and to never let others tell me I can't do something.

To my father, who was my very first and best science teacher. Thank you for helping me practice all of my science project talks and always asking me the hardest question at the presentation. I miss you every day.

TABLE OF CONTENTS

LIST OF FIGURES

Chapter 1

Chapter 2

Chapter 3

LIST OF TABLES

Chapter 3

Chapter 5

CHAPTER I

INTRODUCTION

LIST OF ABBREVIATIONS

BEAT-ROP – Bevacizumab Eliminates the Angiogenic Threat of ROP
BM – bone marrow
c-2J – B6(Cg)-*Tyr*$^{c-2J}$/J
CRYO-ROP – Cryotherapy for ROP
CXCL12 – chemokine (C-X-C motif) ligand 12, or SDF-1
CXCR4 – chemokine (C-X-C motif) receptor 4
DA - dopamine
Dll4 – Delta-like ligand 4
EC – endothelial cell
EPC – endothelial progenitor cell
EPO - erythropoietin
ETROP – Early Treatment for ROP
FEVR – familial exudative vitreoretinopathy
FZD4 – Frizzled 4 receptor
HIF-1 – hypoxia-inducible factor 1
ICAM-1 –intracellular adhesion molecule 1
ICROP – International Classification of Retinopathy of Prematurity
IGF-1 – insulin-like growth factor 1
IGFBP3 - insulin-like growth factor binding protein 3
LRP5 – low-density lipoprotein receptor-related protein 5
NDP – Norrie disease protein
NV - neovascularization
OIR – oxygen-induced retinopathy
P – post-natal day
PMA – post-menstrual age
QTL – quantitative trait loci
RLF – retrolental fibroplasia
ROP – Retinopathy of Prematurity
RPE – retinal pigment epithelium
SDF-1 – stromal cell-derived factor-1, or CXCL12
SNP – single nucleotide polymorphism
STOP-ROP – Supplemental Therapeutic Oxygen for Pre-threshold ROP
SUPPORT – Surfactant, Positive Pressure, and Pulse Oximetry Randomized Trial
TSPAN12 – tetraspanin-12
Tyr – Tyrosinase
WHO – World Health Organization
VEGF – vascular endothelial growth factor
VEGFR2 – vascular endothelial growth factor receptor 3
VPC – vascular precursor cell

RETINA

The human retina, although less than 10 cm^2 in area (Kolb, 2005), is an exceedingly complex and active tissue. Located along the posterior of the eye, the retina is comprised of 55 distinct types of cells, including 5 types of neurons and 2 types of glia (Ye, Wang et al., 2009), organized into 10 distinct layers (Figure 1.1). Within these layers lie parallel microcircuits made of millions of neurons that work together to receive visual input as light energy and convert it into an electrical signal. This signal is subsequently transmitted via the optic nerve to the visual cortex in the occipital lobe of the brain for processing and perception (Dorrell, Friedlander et al., 2007).

Light transduction is a metabolically demanding process, and the adult retina consumes more oxygen per unit weight of any other tissue in the human body. A sufficient blood supply is therefore critical to its function (Chan-Ling and Stone, 1993; Saint-Geniez and D'Amore, 2004; Sapieha, 2012). To meet the demands of this high level of metabolic activity, two distinct vascular beds serve the retina: the choriocapillaris and the retinal vasculature. The choroidal vasculature is derived from the ophthalmic artery. Located posterior to the retinal pigment epithelium (RPE), it supplies the outer retinal layers, including the outer plexiform and nuclear layers, the photoreceptors, and the RPE. The choriocapillaris additionally supplies the macula, the area of the retina that provides fine visual discrimination (Dorrell, Friedlander et al., 2007; Anand-Apte and Hollyfield, 2010).

The retinal vasculature originates from the central retinal artery. Upon entering the eye, it branches into 4 intraretinal arteries. In higher order mammals, these intraretinal arteries form 3 layers of vessels – the superficial, intermediate, and deep plexuses – which

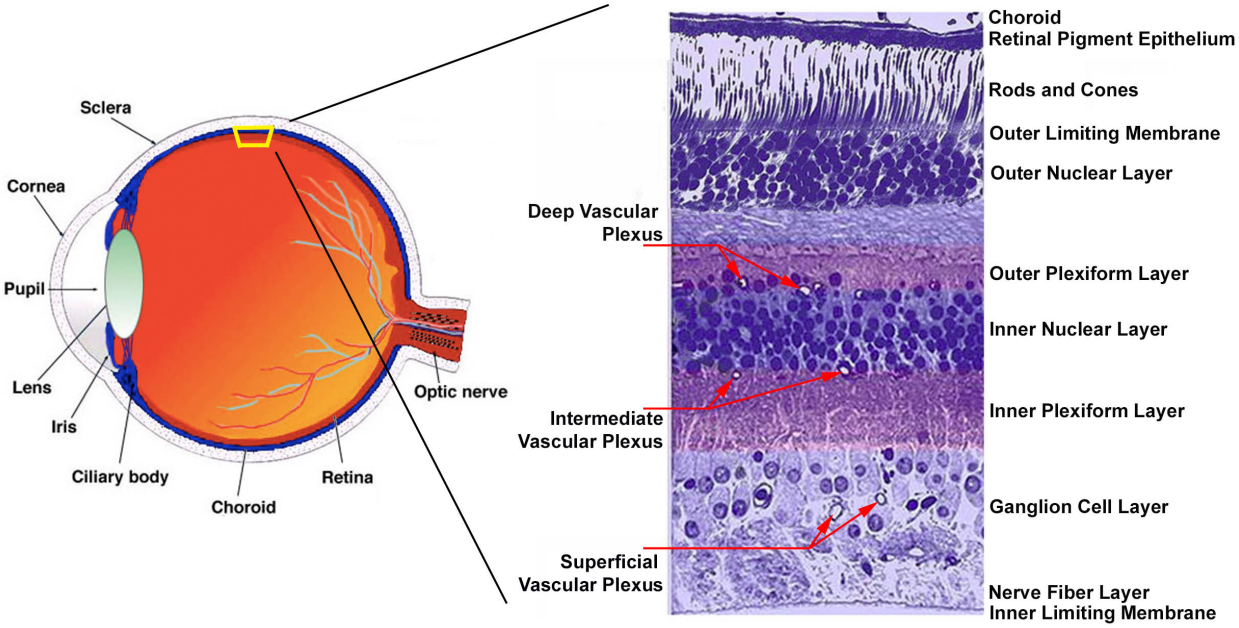
Sclera
Cornea
Pupil
Lens
Iris
Ciliary body
Choroid
Retina
Optic nerve
Choroid
Retinal Pigment Epithelium
Rods and Cones
Outer Limiting Membrane
Outer Nuclear Layer
Deep Vascular Plexus
Outer Plexiform Layer
Inner Nuclear Layer
Intermediate Vascular Plexus
Inner Plexiform Layer
Ganglion Cell Layer
Superficial Vascular Plexus
Nerve Fiber Layer
Inner Limiting Membrane

Figure 1.1. Anatomy and organization of the human retina.
The human retina is located along the posterior wall of the eye. It consists of 10 distinct layers of cells, with 3 vascular plexi. Images adapted from Webvision: The Organization of the Retina and Visual System, Webvision, http://webvision.med.utah.edu, Creative Commons Attribution-Noncommercial license.

are interconnected by capillaries (Gariano and Gardner, 2005). Blood returns via a corresponding venous system that exits the eye as the central retinal vein. The retinal vasculature is responsible for supplying the innermost layers of the retina, including the ganglion cell layer, inner and the nuclear and plexiform layers (Dorrell and Friedlander, 2006).

Appropriate organization of the retinal vasculature is also critical for retinal function. Each vascular plexus has specific and conserved locations within the structure of the retina. The superficial plexus forms within the ganglion cell layer, and the deep and intermediate plexuses form at the outer and inner edges of the inner nuclear layers, respectively (Figure 1.1). If the vasculature does not form, the retina may degenerate due to hypoxic stress. If it forms but is improperly organized, or if vessels are located within regions of the retina that normally remain avascular, such as the photoreceptor layer or the macula, then visual function may be disrupted (Dorrell, Friedlander et al., 2007). Examples of these diseases include neovascular ('wet") age-related macular degeneration and proliferative diabetic retinopathy (Gariano and Gardner, 2005).

RETINAL VASCULAR DEVELOPMENT

Unlike other species, human retinal vascular development occurs almost completely *in utero,* an environment that has relatively low oxygen tension (PaO_2 = 30 mm Hg) (Polverini, Cotran et al., 1977; Fleck and McIntosh, 2008) compared to the extrauterine environment (PaO_2 = 60-100 mm Hg) (Chen and Smith, 2007). This process begins during the second trimester and continues until almost full gestational term, approximately 36 – 40 weeks postmenstrual age (PMA) (Chan-Ling and Stone, 1993).

FETAL BLOOD SUPPLY

The developing eye is supplied by the hyaloid and choroidal vasculature systems. These structures begin to form approximately 5 weeks after conception. The choroidal vasculature arises from the neural tube vasculature and initially forms a large plexus of primitive vessels that extend around the developing optic cup. Over time, this plexus increases in density and size. The growth of the choroidal vasculature is largely dependent on growth factors produced by the RPE (Saint-Geniez and D'Amore, 2004). The choroid begins branching during the eleventh week post-conception and matures during the third and fourth months of gestation (Anand-Apte and Hollyfield, 2010).

The hyaloid artery originates from the primitive dorsal ophthalmic artery and passes through the embryonic fissure into the optic cup. It next extends through the primitive vitreous and reaches the developing lens where it branches to form a dense capillary network around the lens surface. This network anastomoses with the annular vessel at the anterior of the optic cup to connect with the choroidal vasculature, which also serves as a venous drain for the hyaloid artery. The hyaloid system is complete by approximately 11 weeks after conception, and supplies the anterior and intraoptic structures of the developing eye (Saint-Geniez and D'Amore, 2004). The hyaloid vasculature begins to undergo macrophage-mediated apoptosis as the retinal vasculature develops in the later half of gestation and completely regresses by birth (Fruttiger, 2007).

VASCULOGENESIS

Vasculogenesis, or the formation of blood vessels *de novo*, is thought to initiate the development of the retinal vasculature in humans and other primates (Dorrell, Friedlander

et al., 2007). At approximately 14 to 15 weeks PMA (Chan-Ling and Stone, 1993; Hughes, Yang et al., 2000; Fleck and McIntosh, 2008), vascular precursor cells (VPCs) appear at the optic nerve head (Chan-Ling). These progenitor cells are concentrated in 4 lobes that correspond to future artery-vein pairs. VPCs then migrate anteriorly along the retina tissue; cells remaining behind unite to form cords, which become patent, primitive vascular tubes by approximately 15 weeks PMA (Chan-Ling; Hughes, Yang et al., 2000; Fleck and McIntosh, 2008). Vasculogenesis forms the primitive vasculature of a portion of the superficial retinal plexus, the first layer of the retinal vasculature to form (Chan-Ling and Stone, 1993; Dorrell, Friedlander et al., 2007). This process is independent of oxygen-regulated factors and is generally complete by 21 weeks PMA (Chan-Ling; Hughes, Yang et al., 2000; Fleck and McIntosh, 2008).

ANGIOGENESIS

Angiogenesis describes the formation of new blood vessels from existing vasculature. This process is driven by perceived, or "physiologic", tissue hypoxia (Saint-Geniez and D'Amore, 2004). In oxygen-sufficient conditions, prolyl hydroxylase domain proteins hydroxylate specific proline residues in hypoxia-inducible factor-1α (HIF-1α) target proteins. Hydroxylated HIF-1α proteins are recognized by von Hippel-Lindau E3 ubiquitin ligase complex and subsequently degraded. In hypoxic conditions, however, insufficient supply of oxygen prevents hydroxylation of HIF-1α. The more stable, unhydroxylated HIF-1α binds to the HIF-1β subunit. The resulting heterodimer forms an active transcriptional complex that initiates expression of hundreds of genes that promote angiogenesis. Most

important among these HIF-1 target genes is vascular endothelial growth factor (VEGF) (Fraisl, Mazzone et al., 2009).

Retinal vasculature develops in close association with supporting astrocytes (Fleck and McIntosh, 2008). Prior to initiation of vessel growth, astrocytes migrate into the retina and grow peripherally to create a mesh-like template. In response to perceived hypoxia, these cells produce VEGF and other pro-angiogenic HIF-1 gene targets, as described (Chan-Ling; Gariano and Gardner, 2005). Stimulated by these factors, nascent vessels sprout from existing structures formed by vasculogenesis. Each vascular sprout is led by a specialized "tip cell", a type of endothelial cell (EC) that forms filopodia at the leading edge of the developing vascular front, which responds to the gradient of VEGF to guide the developing vessel. To ensure that only one EC becomes a tip cell in each sprout, Notch signaling tightly regulates this response by lateral inhibition. Tip cells express higher levels of Delta-like ligand 4 (Dll4), which acts on neighboring stalk cells' Notch receptors. Upon binding Dll4, Notch is cleaved to release the notch intracellular domain, which is transported to the nucleus to decrease expression of VEGF receptor 2 (VEGFR2). Reduced VEGF signaling in stalk cells results in their proliferation rather than migration, so that they form the length of the nascent vessel. This signaling pathway effectively represses the formation of multiple tip cells (Hellstrom, Phng et al., 2007; Jakobsson, Franco et al., 2010).

In addition to proliferation of existing ECs, bone marrow (BM)-derived endothelial progenitor cells (EPCs) are also incorporated into developing vessels. Mobilization of this cell population from the BM is stimulated by systemic expression of colony stimulating factors, VEGF, and erythropoietin (EPO). Cells subsequently migrate to the site of angiogenesis by unclear mechanisms. It is believed that this critical step relies on cell-cell

interactions between EPCs and existing ECs via integrin expression (Urbich and Dimmeler, 2004). HIF-1α activity stimulates increased production of stromal cell-derived factor-1 (SDF-1), or chemokine (C-X-C) motif ligand 12 (CXCL12), which been shown to be chemotactic for EPCs via interactions with their chemokine (C-X-C) motif receptor 4 (CXCR4) receptor (Semenza, 2009). Once EPCs arrive to the site of angiogenesis, they incorporate into developing vessel walls and differentiate into mature ECs (Urbich and Dimmeler, 2004).

Wnt signaling plays a crucial role in retinal angiogenesis, the importance of which is highlighted in cases of pathology. Wnt molecules are secreted glycoproteins that act on specific families of cell surface receptors and their co-receptors, ultimately producing an intracellular signal to inhibit the degradation of cytosolic β-catenin. β-catenin subsequently translocates to the nucleus where it forms a complex with transcription factors and activates transcription of target genes. In the retina specifically, Muller glial cells produce a non-canonical Wnt ligand, Norrin. Norrin binds with the frizzled 4 receptor (FZD4) and low-density lipoprotein receptor-related protein 5 (LRP5) or 6 co-receptor on both neuronal and vascular cells. Tetraspanin-12 (TSPAN12) is expressed only on ECs, where it binds to FZD4 to enhance signaling, possibly by inducing receptor clustering at the cell surface. Loss of this signaling pathway through mutations in any of the described genes results in delayed and disorganized vascular growth with characteristic retinal defects: loss of the intermediate and deep plexuses, tortuous and dilated primary arteries and veins, delayed regression of the hyaloid vasculature, and frequently intraocular hemorrhage (Ye, Wang et al., 2009).

Angiogenesis begins between 17 and 18 weeks PMA in the human retina (Hughes, Yang et al., 2000; Fleck and McIntosh, 2008) and completes the formation of the nascent retinal vascular system (Fleck and McIntosh, 2008). Sprouting occurs first in avascular spaces between the radial vessels nearest the optic nerve. Over time, vessels form centrally to peripherally, following the centrifugal gradient of VEGF produced by astrocytes. (Gariano and Gardner, 2005). By approximately 25 weeks PMS, branches from the still-developing superficial plexus dive posteriorly to begin the forming the deep plexus (Chan-Ling). The intermediate plexus forms last, and is formed by sprouting from both the superficial and the deep plexuses (Dorrell, Friedlander et al., 2007). Angiogenesis is additionally responsible for the formation of the dense peripheral capillary systems, and numerous arterial-venous arcades (Hughes, Yang et al., 2000; Fleck and McIntosh, 2008). The most peripheral retina is vascularized by approximately 36 to 40 weeks PMA (Polverini, Cotran et al., 1977).

As the vascular front moves peripherally, more central vessels begin to recruit pericytes to initiate vessel maturation and stabilization (Dorrell and Friedlander, 2006). ECs lining nascent vessels secrete platelet-derived growth factor, which acts as a potent mitogen for mural cells (Dorrell, Friedlander et al., 2007). Wnt signaling has also been proven to contribute to vascular stabilization by enhancing EC interactions with pericytes and promoting pericyte proliferation (Ye, Wang et al., 2009). Pericytes then wrap around the ECs and function to create a blood-retinal barrier. During the final stages of vascular development, pericytes stabilize the nascent vessels even as VEGF levels decline, as well as to prevent vessel leakage (Dorrell, Friedlander et al., 2007).

The final steps of retinal vascular development involve pruning of superfluous vessels formed during the process of angiogenesis. The nascent vessels are remodeled in

response to relative tissue hyperoxia (Dorrell and Friedlander, 2006), which leads to up-regulation of intercellular cell adhesion molecule 1 (ICAM-1) on the luminal surface of ECs. Circulating leukocytes bind ICAM-1 via interactions with their surface expression of the CD18 molecule, leading to extravasation and activation of these cells. Activated leukocytes then initiate Fas-ligand-mediated apoptosis of unnecessary vessels. Unstable, mural cell-deficient vessels are leakier, thus favoring increased leukocyte recruitment and apoptosis (Dorrell, Friedlander et al., 2007). This final step in retinal vascularization generates the mature vasculature (Chan-Ling and Stone, 1993).

RETINOPATHY OF PREMATURITY

SIGNIFICANCE

Retinopathy of Prematurity (ROP) is a leading cause of blindness in the pediatric population (Hughes, Yang et al., 2000). A type of retinal vascular disease, ROP affects approximately 16,000 (Hartnett, 2010), or 7.4% of (Lad, Nguyen et al., 2008), premature infants in the US. Among other causes of childhood blindness, ROP is estimated to account for 6-18% of cases in industrialized countries (Coats, 2005). ROP is more prevalent in countries with low infant mortality rates, in large part because those with high mortality rates often lack sufficient resources to care for premature infants. In countries with moderate and low infant mortality rates, ROP is a significant and increasing cause of childhood blindness (Gilbert and Foster, 2001; Wheatley, Dickinson et al., 2002; Coats, 2005). Some studies suggest that the increase in cases from middle income countries in Latin America and Eastern Europe may lead to an epidemic of ROP (Gilbert, 2008).

Although ROP affects a relatively small number of people, it causes disproportionately large burden of disease due to the extremely early onset of visual impairment. Blind children have more frequent and lengthier hospital stays compared to sighted children, and are significantly more likely to have comorbid diseases. Additionally, blindness impacts normal motor, language, and social development (Crewe, Lam et al., 2013). This often necessitates special education and training, despite which blind children have reduced productivity potential. In the US, the federal and state government assumes much of the economic burden, often in the form of disability pay and medical care (Coats, 2005). In developing countries, the costs incurred both from care of a premature infant and the subsequent needs of a blind child may be catastrophic for the family (Gilbert and Muhit, 2012).

In addition to impact overall health and economic expenses, blindness has a staggering emotional cost for both the child and the child's family. ROP often becomes severe enough to threaten vision at approximately the same time as infants become medically stable, exacerbating the emotional impact on parents who have already suffered much anxiety over the health of their premature infant (Ryan, 2001). Furthermore, because ROP is a preventable disease, its associated costs – financial, emotional, and social – are incurred unnecessarily (Coats, 2005). For these reasons, it was identified by the World Health Organization (WHO) as a target cause of preventable blindness in their Vision2020: The Right to Sight global initiative to eliminate avoidable causes of blindness (www.vision2020.org).

HISTORICAL PERSPECTIVES

Originally termed “retrolental fibroplasia” (RLF), ROP was first described in a case study report in 1942. Terry observed the development of bilateral lesions in 7 premature infants, all of which followed 3 characteristics: partial or complete persistence of the hyaloid vasculature, the presence of embryonic connective tissue posterior to the lens, and maintained fibrillar structure of the vitreous (Terry, 1942). Several other cases were subsequently reported that same year, and an epidemic number of cases soon developed both in the US and world-wide (Coats, 2005).

Owens and Owens proved in 1950 that infants were born with a normal hyaloid system and developed RLF post-natally (Owens and Owens, 1950). At that time there was no indication as to the cause of this disease, and initial hypotheses included deficient development of aqueous humor and improper development of the ciliary body (Terry, 1944). X-ray treatment was the first therapeutic attempt to improve the vision of infants with RLF, with very disappointing results (Terry, 1944).

The role of oxygen therapy in the development of ROP was not identified until almost a decade after Terry’s initial observations. In 1951, Campbell reported an increased rate of ROP in infants with higher levels of administered oxygen (Campbell, 1951; Coats, 2005). Shortly after her published results, Patz conducted a randomized, prospective trial of oxygen therapy confirming Campbell’s findings (Patz, Hoeck et al., 1952; Coats, 2005). Oxygen administration had become commonplace in neonatal care in the 1930s and 1940s, with unchecked use (Coats, 2005). After identifying oxygen as a major risk factor in the development of ROP, its use was dramatically curtailed. While rates of blindness dropped from 7.9 cases to 1.2 per 100,000 from 1950 to 1965, it unfortunately also lead to an increase in neonatal morbidity and mortality (Coats, 2005).

The field of neonatal care improved over the following decades such that very low birth weight premature infants, those weighing less than 1,000 g, were surviving in record numbers by the 1970s and 1980s. This lead to a concurrent resurgence of ROP and an interest in better understanding the disease (Coats, 2005). Thus, the International Classification of Retinopathy of Prematurity (ICROP) developed a staging system to more objectively describe disease development and compare outcomes (Lang and Bishop, 1993; Lutty, Chan-Ling et al., 2006), and the first major clinical trial was begun in the mid 1980s (Hartnett and Penn, 2012).

Recently, ROP has become a more prevalent cause of childhood blindness in middle-income countries. Nations such as Sri Lanka, Lithuania, Thailand, and the Philippines have reported their first documented cases of ROP within the last decade. As their neonatal intensive care improves, allowing the survival of increasingly premature infants, ROP is expected to become a more common cause of childhood blindness (Broderick, Hoek et al., 2002; Davies, Eubanks et al., 2003). Accordingly, several international organizations have dedicated resources to ROP prevention and treatment, including the WHO and the Global Initiative for the Elimination of Avoidable Blindness (Broderick, Hoek et al., 2002).

PATHOGENESIS

As vascular development in the human retina is not complete until almost full gestational term (Figure 1.2A), premature children are likely to be born with incompletely vascularized peripheral tissue (Figure 1.2B). The relative hyperoxia of room air (PaO_2 = 60-

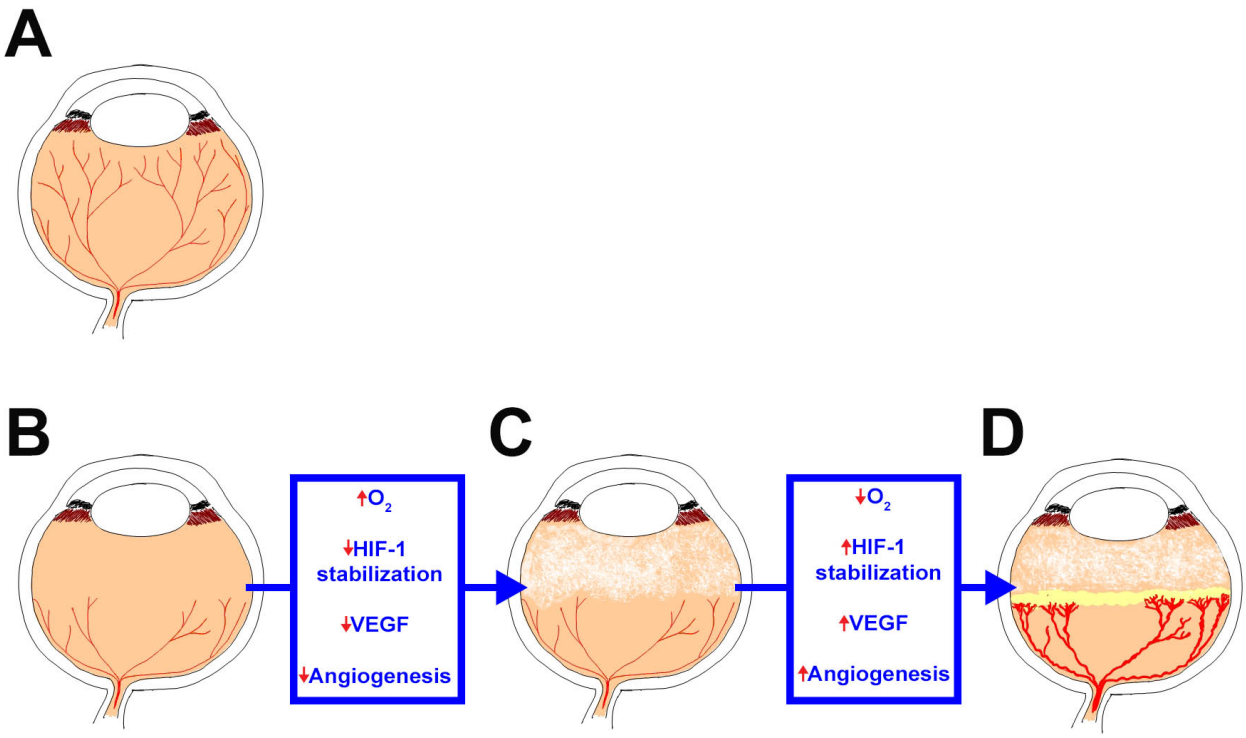
A
B
C
D
↑O2
↓HIF-1 stabilization
↓VEGF
↓Angiogenesis
↓O2
↑HIF-1 stabilization
↑VEGF
↑Angiogenesis

Figure 1.2 Pathogenesis of ROP.
(**A**) An illustration of the retinal vasculature of a full-term child at birth. Blood vessel have grown to supply the peripheral tissue. (**B**) Illustration of the vasculature of a pre-term child at birth. The blood vessels have not yet reached the peripheral retina, and the relative hyperoxia of the extrauterine environment inhibits further vascularization, the first phase of ROP. (**C**) As the retina becomes more metabolically active, the avascular tissue becomes increasingly hypoxic. Astrocytes in these areas express VEGF and other angiogenic factors as a result of increased HIF-1 signaling. This leads to neovascularization at the juncture between vascular and avascular retina (**D**).

100 mm Hg, assuming intact lung function) relative to uterine conditions (PaO_2 = 30 mm Hg) (Chen and Smith, 2007) leads to vasoattenuation and regression of existing vessels (Polverini, Cotran et al., 1977; Chen and Smith, 2007). This creates the first phase of ROP (Figure 1.2C). This stage generally occurs from birth to 30-32 weeks PMA (Chen and Smith, 2007).

The second, or proliferative, stage of ROP begins around 32-34 weeks PMA. As the infant matures, the retinal tissue becomes more metabolically active. Increased demands for oxygen combined with prior attenuation of blood vessels results in hypoxia of the avascular periphery. The ischemic tissue responds by expressing HIF-1 target genes such as VEGF, which can result in neovascularization (NV) at the junction between the vascular and avascular retina (Figure 1.2D). Over time, neovessels can leak or produce a fibrous scar that can retract and cause retinal detachment, the most dangerous complication of ROP (Penn, Tolman et al., 1993; Chen and Smith, 2007).

The development of ROP is divided into 5 clinical stages based on severity of retinal findings during dilated indirect ophthalmic exam, as defined by ICROP (Ryan, 2001; Lutty, Chan-Ling et al., 2006; Hartnett and Penn, 2012). Retinae in the first stage of ROP have a line demarcating vascular and avascular peripheral zones; this is the first clinical sign of ROP development and is pathognomonic for the disease. In Stage 2, this line has grown in both height and width to form an appreciable ridge. Neovascularization of the ridge characterizes Stage 3 ROP, which may be continuous with the ridge or grow perpendicularly to enter the intravitreal space. If the disease progresses to partial retinal detachment, it is classified as Stage 4; the fifth and most severe stage is defined by total retinal detachment. The term "Plus Disease" is often used in conjunction with the staging system to denote that retinal

vessels appear dilated and tortuous, an indication of vascular incompetence and a worsened prognosis (Ryan, 2001; Hartnett and Penn, 2012). Additionally, a diagnosis of "threshold" ROP indicates a 50% likelihood of developing a retinal detachment (Coats, 2005)

Clinically, ROP is also described in terms of the area of retina containing neovascularization. To standardize this, the retina is divided into zones. Zone I includes an area with a radius extending from the optic disk that is twice the distance between the center of the disk and the center of the macula. Disease in this zone is the most difficult to treat, and has the highest risk of recurrence. Zone II encircles Zone I, and extends to the nasal extent of the retina. The radius of Zone II is three times the distance between the center of the disk and the center of the macula. The third and final zone includes the remainder of the retina, and is largely made of peripheral tissue (Ryan, 2001).

ROP is a self-limiting disease, which eventually becomes inactive and can even spontaneously regress. Even in cases of spontaneous regression, however, children with ROP do not return to normal ophthalmological status. Long-term complications include reduced visual acuity, decreased contrast sensitivity, refractive errors, and strabismus. Some premature infants additionally suffer from improperly differentiated macula (Hellstrom, Ley et al., 2010). Over time, the retina may also undergo pigmentary changes, thin, or degenerate (Ryan, 2001). These children also carry a life-long increased risk of glaucoma, cataract formation, retinal breaks, and retinal detachment, all of which threaten vision (Ryan, 2001; Lutty, Chan-Ling et al., 2006; Hellstrom, Ley et al., 2010). Permanent and vision-impairing sequelae are determined by the maximum severity of disease. Approximately half of infants with diagnosed ROP will regresses in early stages, and thus have fewer long-term complications, while the remaining half will progress to severe stages

(Coats, 2005). It is currently unclear why ROP progresses to a severe stage in these children despite timely intervention (Shastry, 2010).

CLINICAL MANAGEMENT

In the US, it is recommended that infants born at less than 30 weeks PMA or weigh less than 1500 g at birth receive a dilated, indirect ophthalmic exam at a chronological age of 4-6 weeks or at post-gestational age of 31 weeks. Additional screening exams are then scheduled as recommended by the ophthalmologist on the basis of retinal findings (Hartnett and Penn, 2012).

Current management of ROP focuses on treating neovascularization. Diode laser photocoagulation is the mainstay of current approaches, which is used to cauterize involved areas of the retina (Sapieha, Joyal et al., 2010). Complications of this procedure include corneal edema, intraocular hemorrhage and cataract formation, all of which may compromise vision (Chen, Stahl et al., 2011). While this prevents further NV, and thus reduces risk of retinal detachment, it permanently destroys the peripheral retina and, with it, a portion of the child's visual field (Hellstrom, Ley et al., 2010).

MAJOR CLINICAL TRIALS

The first multicenter trial investigating a cryotherapy as a potential treatment for ROP began in 1986. Cryotherapy for Retinopathy of Prematurity (CRYO-ROP) showed that ablation of the unvascularized peripheral retina resulted in improved vision in infants with severe ROP. This study additionally investigated the incidence and natural course of disease and set minimum standards for defining disease stages, which have been used in subsequent studies. Preliminary results showed improved clinical outcome, measured as

visual acuity, with use of cryotherapy. This treatment subsequently became the mainstay of treatment for ROP (Diez-Roux, Argilla et al., 1999; Lutty, Chan-Ling et al., 2006; Hartnett and Penn, 2012).

With the development of laser photocoagulation, the Early Treatment for Retinopathy of Prematurity (ETROP) was sponsored by the NIH and begun in 1999. Results from ETROP supported the use of laser therapy to ablate peripheral avascular retina, and supported intervention at earlier stages in ROP pathogenesis. Laser photocoagulation remains the mainstay of treatment today.

Recently, results from the primary completion date of Bevacizumab Eliminates the Angiogenic Threat of Retinopathy of Prematurity (BEAT-ROP, Clinical trial number NCT00622726) were published (Mintz-Hittner, Kennedy et al., 2011). Bevacizumab (trade name Avastin, Genentech/Roche) is a humanized monoclonal antibody targeted to inhibit VEGF function. Anti-VEGF therapies have been used successfully to treat a variety of diseases, including neoplasia and other types of vascular retinopathies (Dorrell, Uusitalo-Jarvinen et al., 2007). BEAT-ROP compared use of bevacizumab as monotherapy to laser photocoagulation. Initial results show that bevacizumab treatment significantly benefited infants with Stage 3 or greater ROP in Zone I, nearest the fovea, but had no benefit for infants with ROP in Zone II. Disadvantages of this treatment identified in BEAT-ROP are primarily related its intravitreal delivery, which can cause ophthalmic inflammation or other complications, and must be repeated for continued efficacy. However, this trial was too small to assess local and systemic toxicity that may be caused by bevacizumab in this patient population, and additional studies are also needed to determine the optimal dose (Mintz-Hittner, Kennedy et al., 2011).

Two additional clinical trials have investigated the regulation of oxygen therapy as a means to prevent ROP development. Supplemental Therapeutic Oxygen for Pre-threshold Retinopathy of Prematurity (STOP-ROP) enrolled infants with prethreshold ROP in at least one eye. Initial data published in 1999 found no differences in rate of ROP development in infants with 96-99% oxygen saturation (SaO_2) versus those with 89-94%. A decade later, the Surfactant, Positive Pressure, and Pulse Oximetry Randomized Trial (SUPPORT) study compared rates of ROP development between premature infants born 24 -26 weeks PMA with 85-89% SaO_2 and those with 91-95%. Lower oxygen saturation was associated with decreased rates of ROP development but increased mortality (Hartnett and Penn, 2012).

RISK FACTORS FOR RETINOPATHY OF PREMATURITY

ROP is a multifactorial disease with several well-characterized risk factors. The first risk factor associated with development of ROP was use of supplemental oxygen therapy. The first epidemic of ROP was primarily due to widespread and unchecked use of oxygen therapy in care for premature infants. Oxygen therapy increases retinal oxygen tension and thus contributes to inhibition of vascular development, and may even contribute to vaso-obliteration of the newly formed vasculature. When Campbell noted the correlation in 1951 and scientific evidence confirmed her observation (Wheatley, Dickinson et al., 2002), more conservative use of oxygen was implemented. This simple change in clinical practice resulted in substantially reduced incidence of ROP (Hatfield, 1972).

Multiple studies have confirmed that short gestational age closely correlates with an infant's risk of developing ROP (Wheatley, Dickinson et al., 2002; Kim, Sohn et al., 2004; Good, Hardy et al., 2005; Bizzarro, Hussain et al., 2006). Because the retinal vasculature

does not reach the most peripheral tissue until almost full term, the gestational age at which a premature infant is born directly correlates with the area of avascular tissue in the peripheral retina (Chen and Smith, 2007). Advances in medicine in the 1970s and 1980s lead to increased survival rates of very premature children, which resulted in a resurgence of ROP despite cautious use of oxygen therapy (Valentine, Jackson et al., 1989; Gibson, Sheps et al., 1990; Wheatley, Dickinson et al., 2002; Coats, 2005; Fleck and McIntosh, 2008).

Reduced gestational weight is an independent risk factor for ROP (Wheatley, Dickinson et al., 2002; Kim, Sohn et al., 2004; Good, Hardy et al., 2005; Bizzarro, Hussain et al., 2006). As many as 68% of infants born weighing less than 1250 g develop ROP; when born at less than 750 g, ROP affects up to 93% (Bizzarro, Hussain et al., 2006). Poor weight gain in the first week of life has also been highly associated with risk of developing ROP (Hellstrom, Ley et al., 2010). Weight is likely related to levels of insulin-like growth factor 1 (IGF-1), an important somatic growth factor produced both by the fetus and by the placenta. Prematurely born infants have reduced serum levels of IGF-1 due to the loss of placental and amniotic sources. *In vitro* studies have shown that sufficient levels of IGF-1 are necessary for VEGF activation of survival pathways in ECs. Reduced IGF-1 levels may therefore contribute to vasoattenuation early in ROP (Hellstrom, Perruzzi et al., 2001).

More recently, risk of ROP development has been associated with reduced serum levels of insulin-like growth factor binding protein 3 (IGFBP3) (Lofqvist, Chen et al., 2007; Fleck and McIntosh, 2008). Produced in the liver, this molecule has several functions including regulating the pro-mitogenic and anti-apoptotic functions of IGFs, as well as additional roles in angiogenic regulation that are still unclear. Lofqvist et al. (2007) showed that IGFBP3 modulates vascular survival in the murine model of ROP using both knockout

models and pharmacological rescue (Lofqvist, Chen et al., 2007). Clinical studies comparing serum levels of IGFBP3 between infants who developed proliferative ROP and those with no ROP showed a statistically significant difference between the 2 groups (Lofqvist, Chen et al., 2007).

A variety of other risk factors have been identified but are less well characterized. Many pulmonary issues increase the risk of developing ROP independently of birth weight and gestational age, including apnea, prolonged use of ventilators, use of surfactant treatment (Kim, Sohn et al., 2004), bronchopulmonary dysplasia, and respiratory distress syndrome (Lad, Nguyen et al., 2008). Additionally, several conditions affecting the overall health of the child have also been found to increase risk. These conditions include intraventricular hemorrhage, cerebral palsy, the number of blood transfusions required in the neonatal period, requirement of parenteral nutrition, hypo- and hypercarbia, early intubation, hypotension, patent ductus arteriosus, necrotizing enterocolitis, poor postnatal weight gain, and sepsis caused by *Candida* yeast. However, no relationships were found between ROP development and factors such as maternal smoking, maternal alcohol consumption, or exposure of retina to light (Wheatley, Dickinson et al., 2002).

HEREDITARY RISK FACTORS

A growing body of evidence suggests that a genetic component may also modulate risk of ROP development. A retrospective twin study published in 2006 found a genetic predisposition to ROP, suggesting that as much as 70% of the variance in susceptibility to ROP is due to a heritable component (Bizzarro, Hussain et al., 2006).

Additionally, epidemiological studies published in the last decade have identified differences in ROP risk between various ethnic groups. CYROP-ROP found that African American infants are at lower risk than Caucasian (Tadesse, Dhanireddy et al., 2002), while Latino Americans are at higher risk than either group (Lad, Nguyen et al., 2008). A small study out of Alaska found that native Alaskan and Asian infants had higher ROP risk than either Caucasian or African American infants (Lang, Blackledge et al., 2005). More recent results indicate that, among US infants, nonblack race and of male gender were predictors of severe ROP, independent of any underlying conditions that might explain the difference in disease severity (Yang, Donovan et al., 2006). Internationally, rates of ROP cases are also disparate between countries in North and South America (Munoz and West, 2002).

Several studies have examined the role of single nucleotide polymorphisms (SNPs) in genes with known roles in angiogenesis (Holmstrom, van Wijngaarden et al., 2007). A clinical investigation comparing infants with and without ROP found that homozygosity of VEGF–634 G allele in the 5' untranslated region served as an independent risk factor for the development of ROP (Cooke, Drury et al., 2004). Another group demonstrated the that the VEGF–634 C allelotype was significantly more common in infants with ROP (Vannay, Dunai et al., 2005). Others have suggested that the polymorphisms in VEGF may be in linkage disequilibrium with polymorphisms in the 5' flanking sequence (Holmstrom, van Wijngaarden et al., 2007). The most recently published analysis suggested no association between ROP development and VEGF-634 C, VEGF-460C, VEGFR-2, hepatocyte growth factor (HGF), or HGF receptor polymorphisms (Kaya, Cokakli et al., 2013). To date our understanding of the role of VEGF polymorphisms on disease development is incomplete. Other SNP analyses found no association between ROP outcome and polymorphisms of IGF-

1 (Balogh, Derzbach et al., 2006) or endothelial nitric oxide synthase (Rusai, Vannay et al., 2008).

Related Ophthalmic Diseases

Several inherited vascular retinopathies share phenotypes with the second phase of ROP. Familial Exudative Vitreoretinopathy (FEVR) (MIM #133780) and Norrie disease (MIM# 310600) are congenital diseases characterized by abnormal vascularization of the peripheral retina, retinal folds, retinal detachment, and the formation of a retrolental fibrovascular membrane (Nikopoulos, Venselaar et al., 2010). Both diseases are caused by mutations in genes that play a role in non-canonical Wnt signaling pathways, which functions in retinal vascular development as previously described (Fruttiger, 2007; Ye, Wang et al., 2009). Because the peripheral retina is incompletely vascularized in these diseases, the resulting tissue ischemia leads to NV, similar to Phase 2 ROP. These neovessels are prone to leakage and rupture, causing exudates and bleeding, which can lead to further complications such as scarring, retinal detachment and blindness (Robitaille, MacDonald et al., 2002).

FEVR is a genetically heterogeneous disease that follows several modes of transmission. Although autosomal dominance is most common, autosomal recessive and X-linked recessive patterns also exist. Mutations in FZD4 (located on 11q14.2), LDP5 (11q13.2) and Norrin disease protein (NDP, the protein produce of *Norrin*, Xp11.3) (Robitaille, MacDonald et al., 2002; Nikopoulos, Venselaar et al., 2010), and TSPAN12 (7q31.31) (Nikopoulos, Gilissen et al., 2010) have all been identified as causative of FEVR. Due to the genetic heterogeneity, cases of FEVR range from mild, with only a small avascular

peripheral retinal zone, to severe, with retinal holes, tears, NV, exudation, vitreal hemorrhage, retinal folding, retinal detachment, and even blindness (Nikopoulos, Venselaar et al., 2010).

Norrie disease is an X-linked disease specifically caused by mutations in NDP. Affected infants present with congenital blindness, and nearly a third also suffer from mental retardation and deafness. Hearing loss in the second decade is common. An intraocular pseudoglioma is often found and can lead to microphthalmia. Other ocular findings include cataract development, alterations in the composition of the vitreous body, vitreoretinal hemorrhage, formation of a retrolental fibrovascular tissue, retinal folding and detachment, and subretinal exudations (Nikopoulos, Venselaar et al., 2010).

A small percentage of infants with severe cases of ROP have been found to have mutations in NDP (Shastry, Pendergast et al., 1997; Hiraoka, Berinstein et al., 2001; Talks, Ebenezer et al., 2001; Haider, Devarajan et al., 2002; Hutcheson, Paluru et al., 2005; Dickinson, Sale et al., 2006; Hiraoka, Takahashi et al., 2010), FZD4 (MacDonald, Goldberg et al., 2005; Ells, Guernsey et al., 2010), and LRP5 (Hiraoka, Takahashi et al., 2010). To date, no mutations in TSPAN12 have been reported in ROP patients, although it is likely that they exist. None of these mutations, however, accounts for a substantial proportion of ROP (Shastry, 2010), and other genes are likely to play a role in ROP development.

ANIMAL MODELS OF ROP

Mouse

Many investigational studies into ROP use a mouse model. Vascularization of the murine retina progresses in a manner similar to humans (Fruttiger, 2007). However, these steps occur post-natally, rather than *in utero*. The retinal vasculature of a newborn mouse is analogous to that of an infant born at 25 weeks PMA (Yanni, McCollum et al., 2008). At postnatal day 2 (P2), budding superficial vessels near the optic disc occupy only a single plane. These vessels extend anteriorly and reach the most peripheral tissue between P7 and P12. The deep plexus forms from the superficial between P8 and P12 (Davies, Eubanks et al., 2003; Gariano and Gardner, 2005; Ritter, Banin et al., 2006; Zhao, Ma et al., 2009). The intermediate plexus forms between P14 and P21 (Ritter, Banin et al., 2006). The retinal vasculature then undergoes remodeling and mature vasculature is created by the end of the first month of life (Ritter, Banin et al., 2006).

The murine model of ROP, termed oxygen-induced retinopathy (OIR) was first established by Smith in 1994 (Smith, Wesolowski et al., 1994). In this protocol, neonatal mice are exposed to 75% oxygen for 96 hours beginning on P7. The hyperoxia induces vaso-attenuation and obliteration of the central vascular bed (Polverini, Cotran et al., 1977; Smith, Wesolowski et al., 1994; Chen and Smith, 2007) and prevents development of intermediate and deep retinal vessels (Davies, Eubanks et al., 2003). Mice are returned to room air (~21% oxygen) on P12. The avascular central retina subsequently becomes ischemic, which leads to vasoproliferation and NV. The development of NV peaks at P17, and generally regresses by 6 months of age (Smith, Wesolowski et al., 1994; Chen and Smith, 2007).

The murine OIR model reliably reproduces Phase 1 of ROP in infants exposed to supplemental oxygen therapy and Phase 2 of ROP in all infants (Polverini, Cotran et al., 1977; Lutty, Chan-Ling et al., 2006). This model is advantageous as mice are relatively inexpensive to purchase and maintain, and they reliably produce large litters. Mice are especially useful for genetic studies as a variety of inbred strains and knock out models are commercially available and have been extensively characterized (Lutty, Chan-Ling et al., 2006).

There are, however, disadvantages to the use of the murine model. The pathology of murine OIR is the reverse of that observed in humans; in mice, the central vasculature undergoes obliteration whereas the peripheral retina is affected in the human condition. Additionally, OIR does not cause some of the complications seen in ROP. Namely, the murine condition does not lead to retinal detachment, the complication most dangerous to vision due to the disproportionately large lens of the murine eye (Polverini, Cotran et al., 1977).

Although the murine OIR model is reliable in its reproduction of ROP, there are known differences in response between inbred strains of mice. The albino BALB/c strain of mice has been shown to be more resistant to NV than the C57BL strain. This was associated with improved survival of astrocytes and microglia immediately following return to normoxia in the BALB/c strain compared to C57BL (Dorrell, Aguilar et al., 2010). Exposure to hyperoxia has also been shown to induce more photoreceptor death in C57BL mice than in BALB/c (Walsh, Bravo-Nuevo et al., 2004). Studies of other angiogenic stimuli have also documented variability in responses between inbred strains of mice (Rohan, Fernandez et al., 2000; Zhu, Iurlaro et al., 2003; Chan, Pham et al., 2005; Liu, Smith et al., 2010), suggesting a genetic component to angiogenesis generally and OIR specifically.

Alternative Animal Models

Other models of ROP have been developed in rats, rabbits, cats, and dogs, all of which undergo retinal vascular development in the post-natal period (Lutty, Chan-Ling et al., 2006; Yanni, McCollum et al., 2008). The most commonly used rat model was developed in 1993 by Penn (Penn, Tolman et al., 1993). In this protocol, newborn rats are exposed to oxygen levels cycled between 10% and 50% oxygen every 24 hours for 14 days. The fluctuations in oxygen levels are thought to reflect the fluctuating lung function and resulting changes in PaO_2 of a preterm infant. Rats subsequently develop central vaso-obliteration, similar to that seen in human ROP (Penn, Tolman et al., 1993). The major disadvantage of the rat model compared to the murine is the increased costs associated with purchase and keep of the larger rodent species. Additionally, there are known differences in susceptibility within the same strain between vendors which may alter experimental results (Yanni, McCollum et al., 2008).

Large animal models – including the canine and feline models – were used in the earliest studies of ROP. Both models involve exposing neonatal animals to hyperoxic conditions (100% oxygen in the canine model, 80% in the feline) for the first 4 days of life to induce vaso-obliteration. Return to normoxia leads to hypoxia in avascular areas and, subsequently, NV. Experiments using the cat model were the first to demonstrate that "physiological" hypoxia drives angiogenesis. The major benefits of using large animal models of ROP over rodent models are the robust NV and associated consequences seen in the large animals. Additionally, the large intravitreal space in eyes of larger animals facilitates studies of therapeutic agents (Lutty, Chan-Ling et al., 2006). The major

disadvantage of these models includes increased gestational periods and the significant increase in cost compared to rodent models.

Recently, a model of ROP has been developed using adult zebrafish model. This model is the only one to date that does not rely on a phase of hyperoxia-induced vaso-obliteration. Rather, adult zebrafish are maintained in hypoxic water (10% air saturation via nitrogen gas perfusion) for 6 to 12 days. This induces retinal NV in regions near the optic disc, which can be quantified by counting the number of sprouts, new branches, and vascularization. Advantages of this model include the relatively cheap cost of zebrafish and ease of maintenance. Similar to the murine model, zebrafish are also relatively easy to manipulate genetically; for example, the fli1:EGFP strain of zebrafish are most often used in this model as they are optically translucent and have green fluorescent vasculature. Disadvantages of this model include the limited number of antibodies available for zebrafish proteins and the requirement of specialized equipment and space for aquariums (Cao, Jensen et al., 2010).

SIGNIFICANCE

ROP is a leading cause of blindness in the pediatric population. A growing body of evidence suggests that there is a heritable component that contributes to disease risk. Identification of genes that modify susceptibility may provide a means to determine which children are at higher risk of developing ROP, which would allow more informed clinical management of premature infants. Furthermore, this work may lead to discovery of pharmacological targets that would promote physiological retinal vascular regeneration. Identification of mechanisms underlying revascularization in ROP would additionally

improve understanding of other diseases of pathological angiogenesis. These diseases include tumor growth and metastasis, atherosclerosis, endometriosis, and other proliferative retinopathies such as diabetic retinopathy, the most common cause of visual loss in adult Americans.

The first study ("The Genetic Control of Avascular Area in Murine Oxygen Induced Retinopathy"), uses forward genetic techniques to identify regions of the genome associated with murine OIR outcome. This study identified 2 quantitative trait loci (QTL) associated with susceptibility to OIR. We additionally found that albino mice generated in the intercross were more resistant to retinopathy than their pigmented littermates.

As albinism in our mapping cross was caused by homozygous loss of function of *Tyrosinase* (*Tyr*), this later finding led to the second study ("Dopaminergic Modulation of Retinal Endothelial Progenitor Cell Recruitment and Revascularization"). This study investigated the candidacy of *Tyr* as a quantitative trait gene using the *Tyr*-null B6(Cg)-*Tyr*$^{c\text{-}2J}$/J ("c-2J") strain of mice. This study confirmed that *Tyr* expression is associated with increased susceptibility to OIR, and identified that this effect is mediated through increased peripheral production of dopamine (DA). DA, signaling through the D1-like family of receptors, inhibited EPC proliferation within the bone marrow, migration to circulation, recruitment to the retina, and revascularization after hyperoxic damage. This study has important clinical implications as DA is used therapeutically in neonatal care.

The third study ("Response of Endothelial Progenitor Cells to Murine Oxygen Induced Retinopathy: A Time Course Study") was conducted in order to better understand the role of EPC recruitment to the retina during revascularization in the OIR model. Using the c-2J and the appropriate control strain, EPCs were quantified in bone marrow, blood,

and retinal samples on P7, prior to exposure to the OIR model; P7.5, 12 hours after exposure to hyperoxia; P8; P9; P9.5; P10; P11; P12; and P13. Avascular area and weight were additionally measured at these same time points. This study identified patterns in EPC numbers that correlate with improved or worsened OIR outcome. Additionally this study suggests that traditional time points used to define stages in this model inaccurately describe the response of the retinal vasculature and of EPCs.

Finally, we performed a microarray analysis ("Microarray-based Identification of Genes and Pathways Associated with Differential Retinal Responses to Hypoxia in the Murine Oxygen Induced Retinopathy Model"). Using samples from susceptible and resistant murine strains, both from normoxic control mice and from mice exposed to the OIR protocol, we identified genes and pathways that are associated with improved or worse OIR outcome. This work was additionally compared to the current body of literature documenting changes in gene expression in the OIR model.

Taken together, these studies seek to identify a genetic component to susceptibility to the murine OIR model of ROP. The work herein describes experiments seeking to identify genes and pathways involved in disease development, as well as to explore a novel mechanism by which *Tyr* regulates retinal angiogenesis.

CHAPTER 2

GENETIC CONTROL OF AVASCULAR AREA IN MOUSE OXYGEN-INDUCED RETINOPATHY

ABSTRACT

The C57BL/6ByJ and BALB/cByJ inbred strains of mice are, respectively, susceptible and resistant to OIR. This work investigates the genetic control of the retinal avascular area in mouse OIR using an inbred mapping cross. The central retinal avascular area was measured on postnatal day 16 in C57BL/6ByJ, BALB/cByJ, 101 (C57BL/6ByJ x BALB/cByJ)F_2, and 116 (BALB/cByJ x C57BL/6ByJ)F_2 mice that had been subjected to the established murine OIR protocol. Genotyping was performed at 856 informative single nucleotide polymorphisms approximately evenly distributed across the genome from each of 85 selected F_2 mice to determine QTLs associated with weight and avascular area. C57BL/6ByJ mice had significantly larger avascular areas than BALB/cByJ ones. Albino mice of the F_2 generation had smaller avascular areas than the non-albino mice. Weight, gender, and the paternal grandmother were found to act as additive covariates associated with the avascular area on P16; mapping analyses that used a model incorporating these covariates found a QTL on chromosome 7 related to avascular area. Analyses that used a model without covariates additionally found a QTL on chromosome 9 related to avascular area. A QTL for bodyweight was mapped to chromosome 5. The data confirm that retinal avascular area in the mouse OIR model is under genetic control, and identified QTLs on chromosomes 7 and 9 that modify susceptibility to OIR.

LIST OF ABBREVIATIONS

ANOVA – analysis of variance
CSPG4 – chondroitin sulfate proteoglycan 4, or NG2
D2 – dopamine receptor 2
DA - dopamine
Dkk3 – Dickkopf 3
EC – endothelial cell
EPO – erythropoietin
F_2 – filial (intercross) 2nd generation
FGF – fibroblast growth factor
FGFr2 – fibroblast growth factor receptor 2
FEVR – familial exudative vitreoretinopathy
FZD4 – Frizzled 4 receptor
ICAM-1 –intracellular adhesion molecule 1
IGF-1 – insulin-like growth factor 1
IGF-2 – insulin-like growth factor 2
IGFBP3 - insulin-like growth factor binding protein 3
ITGAL – integrin alpha L, or CD11a
ITGALM– integrin alpha M, or CD11b
KO – knock-out
LRP5 – low-density lipoprotein receptor-related protein 5
LOD – logarithm of odds
NDP – Norrie disease protein
NV - neovascularization
OIR – oxygen-induced retinopathy
P – post-natal day
QTG – quantitative trait gene
QTL – quantitative trait loci
ROP – Retinopathy of Prematurity
RPE – retinal pigment epithelium
SNP – single nucleotide polymorphism
TH – tyrosine hydroxylase
Tyr – Tyrosinase
VEGF – vascular endothelial growth factor
Xlkd1 – extracellular link domain containing 1

INTRODUCTION

ROP is a significant cause of vision loss in children in both developed and developing countries (Bizzarro, Hussain et al., 2006; Gilbert, 2008; Hartnett, 2010). ROP is a complex disease where disruption of normal developmental angiogenesis initially leads to a persistent avascular phase, which is followed by a phase of pathological NV. Known risk factors include the use of supplemental oxygen therapy, low birth weight, early gestational age at time of birth (Wheatley, Dickinson et al., 2002; Kim, Sohn et al., 2004), and low serum levels of IGF-1 (Perez-Munuzuri, Fernandez-Lorenzo et al., 2010) and IGFBP3 (Lofqvist, Chen et al., 2007). Several clinical investigations have found that rates of severe ROP differ between ethnic groups even after adjusting for socioeconomic factors such as access to health care, suggesting a heritable component to ROP development (Tadesse, Dhanireddy et al., 2002; Lang, Blackledge et al., 2005; Bizzarro, Hussain et al., 2006; Holmstrom, van Wijngaarden et al., 2007). Polymorphisms in the Wnt pathway genes FZD4, LRP5, and NDP have been associated with individual cases of severe ROP (Hiraoka, Berinstein et al., 2001; Hutcheson, Paluru et al., 2005; Ells, Guernsey et al., 2010; Hiraoka, Takahashi et al., 2010). However, as yet there are no genetic factors known to account for a major proportion of variability in severity of ROP (Holmstrom, van Wijngaarden et al., 2007).

OIR in the mouse was developed as a model of ROP (Smith, Wesolowski et al., 1994). In the mouse OIR model, exposure to hyperoxia leads to central vaso-obliteration. When the mice are returned to a normoxic environment, the presence of a region of avascular retina creates a pro-angiogenic milieu, which leads to retinal NV (Polverini, Cotran et al., 1977; Smith, Wesolowski et al., 1994; Lutty, Chan-Ling et al., 2006). The hyperoxic phase of OIR creates somewhat similar conditions to those created in the past by overuse of oxygen in the

treatment of premature infants. However, hyperoxia in the OIR model leads to obliteration of central retinal vessels, while ROP results from the failure of vascularization of the peripheral retina. The neovascular phases of OIR and ROP are broadly analogous. When mice that have been exposed to hyperoxia in the OIR model are returned to normoxia the retina gradually revascularizes with vessels that appear anatomically normal. The initial stages of vascular regeneration are seen before pathological neovascular tufts become evident. The study of the revascularization phase of OIR may be pertinent to understanding retinal angiogenesis in the pre-proliferative phase of ROP. For example, the demonstration that exogenous IGFBP3 increased vessel regrowth in OIR was followed by the observation that serum IGFBP3 correlates with less severe ROP in humans (Lofqvist, Chen et al., 2007).

Inter-strain differences in response to OIR models have been investigated in both mice and rats. Van Wijngaarden *et al.* (van Wijngaarden, Brereton et al., 2007) demonstrated that pigmentation status is associated with retinal avascular area in crosses between Fischer 344 and Dark Agouti rat strains. In crosses between these 2 strains, retinas from albino animals exposed to OIR were found to express lower levels of EPO than retinas from pigmented animals. In further work (van Wijngaarden, Brereton et al., 2007) van Wijngaarden *et al.* found that OIR-susceptible rat strains demonstrated less expression of angiogenesis-related genes in early retinal development than did OIR-resistant rats, but higher expression of these genes in the proliferative phase of OIR. Chan *et al.* performed a similar study comparing gene expression in retinas of different mouse strains exposed to the OIR model (Chan, Pham et al., 2005). Dorrel *et al.* have shown that the astrocytes in the retinas of C57BL/6J mice exposed to the OIR protocol, unlike the astrocytes of BALB/c mice, quickly degenerate after the mice are returned to normoxia (Dorrell, Aguilar et al., 2010).

Although these strain specific differences have been found, no previous study has employed a genome wide approach to investigate genetic differences that modify OIR.

This study uses a known difference between BALB/cByJ and C57BL/6ByJ mice to investigate the genetics of control of the extent of avascular area measured four days after return to normoxia. These strains were used in a mapping cross designed to identify QTL that modify this phenotype. Since C57BL/6 mice exposed to the OIR model develop more severe NV and revascularize more slowly than BALB/c mice, despite having similar vaso-obliterative responses (Dorrell, Aguilar et al., 2010), the phenotype of avascular area measured four days after return to normoxia is likely to be largely a measure of rate of vascular regrowth.

MATERIALS AND METHODS

Animals

All experimental procedures were approved by University of Kansas Medical Center Institutional Animal Care and Use Committee. BALB/cByJ and C57BL/6ByJ mice were purchased from Jackson Laboratories (Bar Harbor, ME). All mice were kept in a 12-hour light, 12-hour dark cycle with ambient room temperature between 19^{o}C and 22^{o}C. Mice were kept on standard diet for breeding pairs (8626 rodent diet, Harlan Laboratories, Indianapolis, IN), with chow and water available ad libitum.

An F_2 intercross population was bred using reciprocal mating strategies (Figure 2.1). Phenotypes were obtained from 116 (BALB/cByJ x C57BL/6ByJ) F_2 and 101

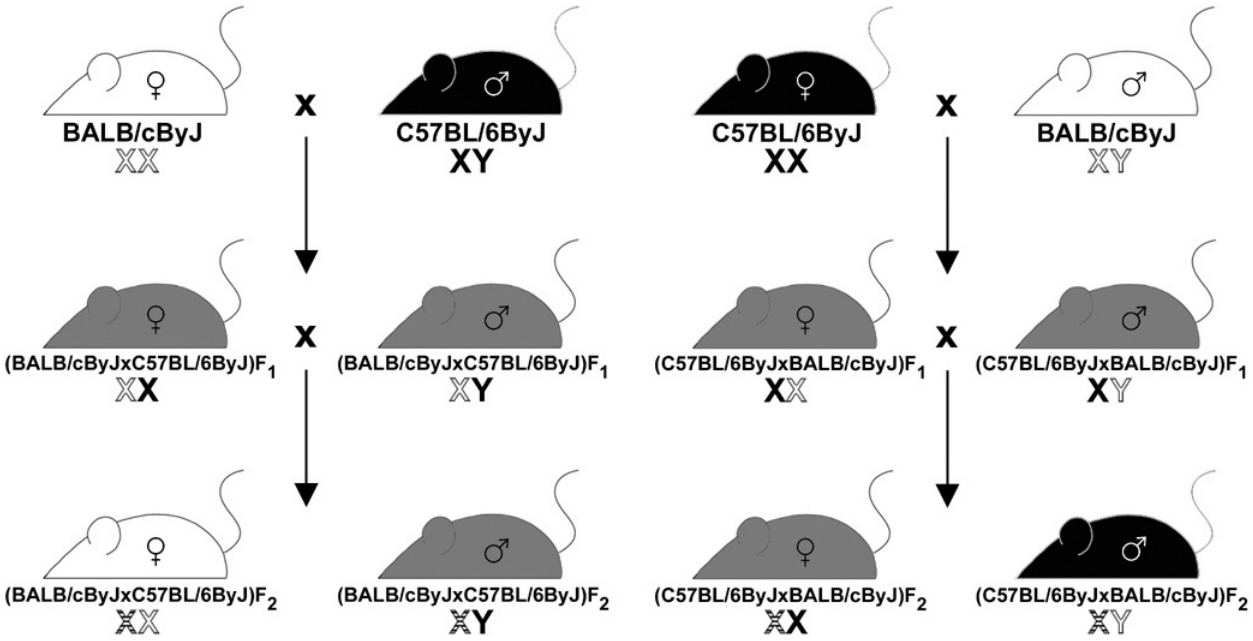
BALB/cByJ
XX
x
C57BL/6ByJ
XY
C57BL/6ByJ
XX
x
BALB/cByJ
XY
(BALB/cByJxC57BL/6ByJ)F1
XX
x
(BALB/cByJxC57BL/6ByJ)F1
XY
(C57BL/6ByJxBALB/cByJ)F1
XX
x
(C57BL/6ByJxBALB/cByJ)F1
XY
(BALB/cByJxC57BL/6ByJ)F2
XX
(BALB/cByJxC57BL/6ByJ)F2
XY
(C57BL/6ByJxBALB/cByJ)F2
XX
(C57BL/6ByJxBALB/cByJ)F2
XY

Figure 2.1. Illustration of the breeding scheme used in the mapping cross.
The BALB/cByJ and C57BL/6ByJ parental strains are crossed in both directions. The resulting F_1 mice are inbred through brother–sister mating to produce the F_2 generation. This figure shows the manner in which the Y chromosomes and recombined (black and white-striped) and unrecombined (solid color) X chromosomes are passed through the generations of the cross. White chromosomes are inherited from the BALB/cByJ albino parent, and black chromosomes are inherited from the C57BL/6ByJ pigmented parent. The different coat colors shown in the F_2 generation are for illustrative purposes only. The color of the F_2 animals is unrelated to either gender or the direction of the cross.

(C57BL/6ByJ x BALB/cByJ) F_2 mice. Values were also obtained from BALB/cByJ and C57BL/6ByJ mice to confirm differential susceptibility to OIR between strains.

Avascular areas in OIR

OIR was induced by exposing pups to 75% oxygen beginning on P7 and returning them to normoxia after 120 hours. O_2 levels in the chambers were continuously controlled using a ProOx portable monitor (Biospherix, Redfield, NY), which was calibrated monthly using room air and 100% O_2. Retinas were analyzed 96 hours after return to hypoxia since previous unpublished observations had suggested that at this time-point the inter strain differences were greatest. This experimental plan allows genetic modifiers of vascular regeneration to be investigated. On P16, mice were weighed, anesthetized with a lethal dose of tribromoethanol delivered by intraperitoneal injection, perfused with high molecular weight fluorescein isothiocyanate labeled-dextran (MW $\geq$ 2,000,000, Sigma, St. Louis, MO, USA) via the left ventricle to visualize patent vessels, and then enucleated. Tail samples were taken and stored at -20^{o}C, and gender was documented.

Retinas were dissected, fixed overnight in 4% paraformaldehyde at 4^{o}C, and flat-mounted using anti-fade medium (Southern Biotech). Immunofluorescent micrographic images of the retinas were taken using an SMZ 1500 microscope (Nikon, Tokyo, Japan) and MagnaFire Camera and software (Optronics, Goleta, CA). ImageJ software (http://rsbweb.nih.gov/ij/) was used to manually trace and measure nonperfused areas. A mean avascular area was calculated for each mouse using data from left and right eyes.

Genotyping Strategy

Selective genotyping methods that decrease the cost of genotyping with only minor loss of information (Darvasi, 1997; Van Gestel, Houwing-Duistermaat et al., 2000; Ayoub and Mather, 2002) were used. For the purpose of selecting the mice to genotype, the avascular area was adjusted for the weight of the animals to account for the effect of weight on response to OIR. To do this, a correlation coefficient of -0.1743 mm^2/g was determined using linear regression and multiplied by the weight to create an adjustment factor for each mouse. The adjustment factor was then subtracted from the measured avascular area to create an adjusted avascular area. Using the adjusted avascular area, mice were selected for genotyping.

Since a significant difference was observed between the avascular areas of albino and non-albino mice, these groups were considered separately when choosing mice to genotype. A group of mice with the smallest adjusted avascular areas (11 albino and 32 non-albino mice) and a group with the largest adjusted areas (11 albino and 32 non-albino mice) were chosen for genotyping.

DNA preparation

DNA was extracted from 0.5 cm tail samples using the DNEasy Blood and Tissue Kit (Qiagen, Valencia, CA); concentration and purity (absorbance ratio at 260/280 nm) were determined using a NanoDrop-1000 spectrophotometer (ThermoFisher Scientific, Waltham, MA). DNA samples were diluted to 25-150 ng/µL.

Genotype Analysis

Genotyping services were provided by the Center for Inherited Disease Research (Johns Hopkins University, Baltimore, MD) using a standard linkage panel containing 856 informative autosomal and X chromosomal SNPs (Mouse Medium Density Linkage Panel, Illumina, San Diego, CA). For each chromosome, except chromosome X, the most proximal marker genotyped was within 13.4 Mbp of the centromere; on chromosome X, the most proximal marker was at 33.5 Mbp from the centromere. The most distal marker was within 5.8Mbp of the telomere for all chromosomes. Internal markers were no more than 24.6 Mbp from each other (chromosome 1) except on chromosome 2, where two markers were spaced 64.4 Mbp apart. Mean spacing was approximately 7.88 Mbp between markers. Physical distances quoted in this paper are taken from mouse genome build 37.2 (http://www.ncbi.nlm.nih.gov/mapview), and SNP data is taken from dbSNP Build 128 (http://www.ncbi.nlm.nih.gov/projects/SNP/). DNA samples from each parental strain and one F_1 mouse produced from each direction were used as control samples. Data checking analyses as suggested by Broman *et al.* (Broman, Sen et al., 2009) were run prior to mapping analysis to ensure quality and integrity of both phenotype and genotype data. Due to inconsistencies in genotyping results, an albino female mouse from the low avascular area group was excluded from subsequent analysis.

The genotype of the tyrosinase locus of the mice not selected for genotyping was inferred from coat color. In this cross, albinism is conferred by homozygosity for the BALB/c allele of tyrosinase. The genotype of albino mice at the tyrosinase locus was encoded as $A^{B/c}A^{B/c}$. For all non-albino mice, a code indicating "not- $A^{B/c}A^{B/c}$" was used.

QTL Mapping

Identification of covariates Coat color, paternal grandmother, gender, and albinism were tested using analysis of variance (ANOVA) models to identify traits that are associated with the primary phenotypes of interest (weight and unadjusted avascular area). Inclusion of covariates in mapping analysis reduces residual variation and enhances QTL detection (Broman, Sen et al., 2009). Any variable found to have a statistically significant association was included in mapping models, as described below.

Linkage analysis The data were analyzed using R/qtl software (Broman, Wu et al., 2003). Initial linkage analysis was performed using standard interval mapping to determine logarithm of odds (LOD) score correlating genotype with phenotype for each marker. Weight and unadjusted avascular area were analyzed separately as primary phenotypes. Analyses were also performed using gender, paternal grandmother, pigmentation, and weight as covariates. All covariates were compared as additive and interactive covariates in separate models to determine best fit. To account for the multiple testing inherent in genome-wide QTL studies, and control the type I error rate such that the probability of a false positive over all tests is below some value, significance thresholds were determined empirically via permutation testing (Churchill and Doerge, 1994). We estimated the experiment-wise significance thresholds using 1,000 permutations of each data set, defining the LOD thresholds for highly-significant QTL (at $P < 0.05$) and significant QTL (at $P < 0.1$). One thousand permutation replicates has been shown to be adequate to estimate critical thresholds (Churchill and Doerge, 1994), and is the number routinely employed in QTL mapping studies.

Gene-gene interactions Secondary analyses included composite interval mapping to determine influence of markers near QTL on other loci (i.e. gene-gene interactions). Additionally, two dimensional, two-QTL scans were performed to consider linked or interacting QTL.

Estimating QTL Effects To estimate the contribution of QTL identified in the linkage analysis, the allelic effects were calculated and compared between mice categorized by genotype ($A^{B/c}A^{B/c}$, $A^{B/c}A^{C57}$, $A^{C57}A^{C57}$). Additive and dominance effects were also considered in calculations. The QTL effects were assumed to correspond to the SNP marker nearest the peak LOD score.

RESULTS

Differences in Response to OIR Between Strains

In order to confirm response of parental strains to the OIR model, 15 BALB/cByJ offspring from 3 litters and 10 C57BL/6ByJ mice from 3 litters were exposed to hyperoxia as described. Typical flat-mounted fluorescein-dextran perfused retinas are shown in Figure 2.2. Measurement of mean retinal avascular area showed C57BL/6ByJ mice to have a 2.9-fold greater unadjusted area than did the BALB/cByJ mice at P16 (1.55 mm^2 versus 0.53 mm^2, Student's t-test, $p < 0.0005$, Figure 2.2).

Weight ranged from 4.15 – 10.95 g. BALB/cByJ mice weighed more at P16 than did their C57BL/6ByJ counterparts (with means of 7.64 g and 6.05 g respectively, ANOVA, $p = 0.009$). After adjusting avascular area for weight as described above, the C57BL/6ByJ mice were still found to have greater avascular areas than did BALB/cByJ mice (2.60 mm^2 versus

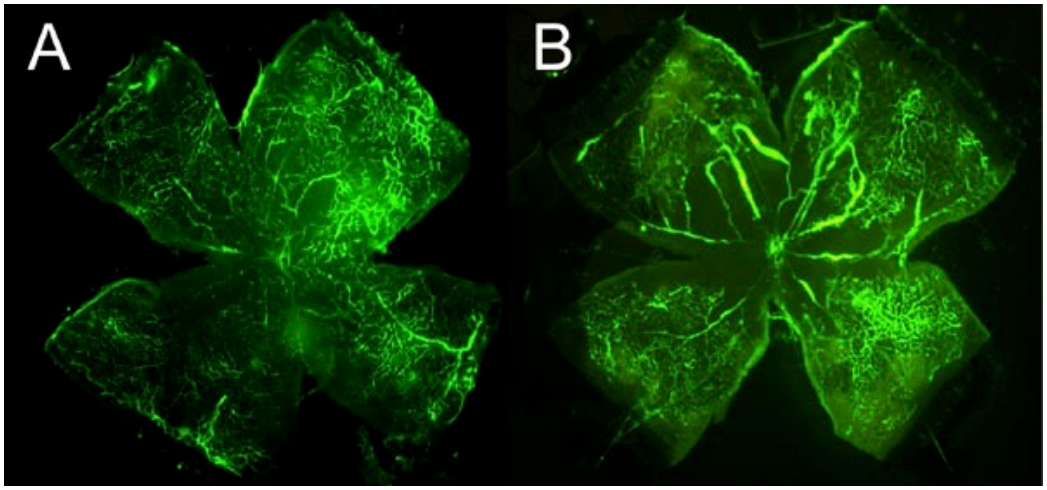
A
B

Figure 2.2. Retinas after OIR protocol.
(**A**) Flatmounted retina of a BALB/cByJ mouse on P16 after exposure to the OIR protocol. The retina is relatively well vascularized at this time point. (**B**) A retina from a C57BL/6ByJ mouse at the same time point after exposure to the OIR protocol. The central retina has large avascular areas.

1.86 mm^2, ANOVA, p = 0.0002, Figure 2.3), suggesting that the difference in avascular area is not due to differences in weight alone.

No difference in unadjusted avascular area was found between male and female mice, either within each strain or across strains (ANOVA, BALB/cByJ – p = 0.4, C57BL/6ByJ – p = 0.5; Student's t-test, all mice - p = 0.06). The same was true when comparing adjusted avascular area between mouse genders (ANOVA, BALB/cByJ – p = 0.07, C57BL/6ByJ – p = 0.15; Student's t-test, all mice - p = 0.08).

Effect of Covariates on Phenotypes in F_2 Population

Weight was investigated as a primary phenotype to identify potential QTL related to body mass at P16. ANOVA tests were performed to investigate the correlation of secondary phenotypes with weight, but no statistically significant association between weight and gender, strain of paternal grandmother, or coat color was found.

F_2 mice had unadjusted avascular areas ranging from 0.013 to 2.76 mm^2, with a mean of 1.06 mm^2. Mean weight at P16 was 6.70 g, with a range from 3.56 g to 11.77 g. Linear regression analysis showed that avascular area was inversely associated with weight (ANOVA, $p < 10^{-8}$, Figure 2.4).

Coat color pigmentation correlated with adjusted retinal avascular area. Albino F_2 mice exposed to the OIR model had smaller adjusted avascular areas than did pigmented mice (ANOVA, $p < 5 \times 10^{-8}$, Figure 2.5). No association between avascular area and any of the individual non-albino coat colors was found (ANOVA, p = 0.39).

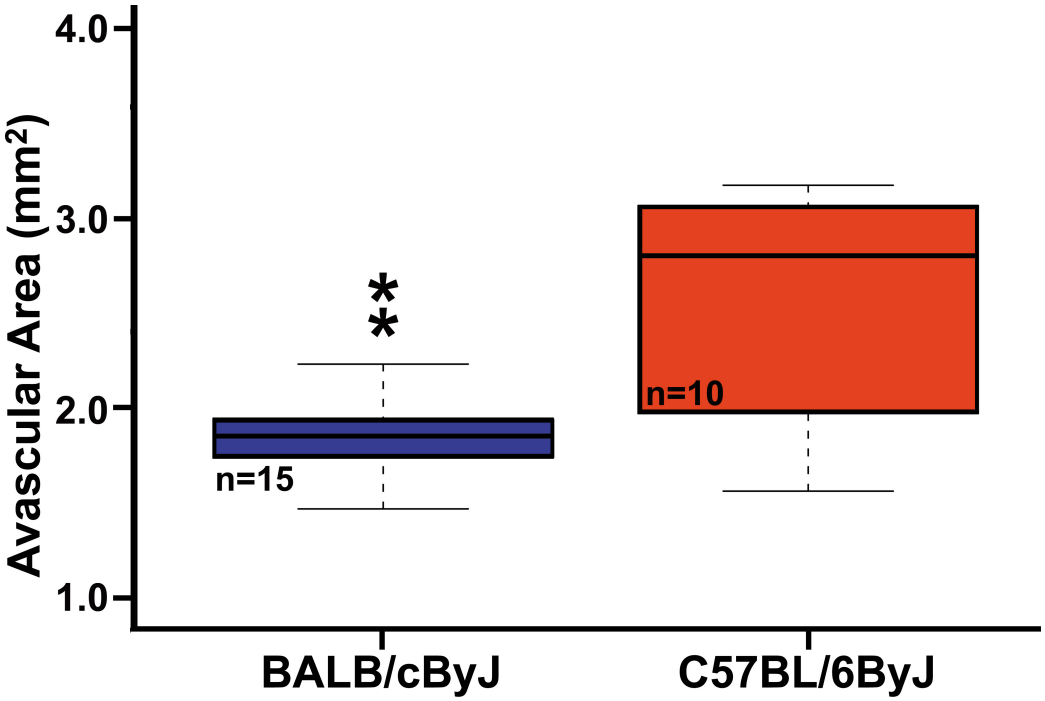
4.0
3.0
2.0
1.0
Avascular Area (mm²)
**
n=15
n=10
BALB/cByJ
C57BL/6ByJ

Figure 2.3. Mean avascular areas of parental strains after adjusting for the influence of weight.
The BALB/cByJ strain has smaller areas of avascular retina in response to hyperoxia than the C57BL/6ByJ strain (ANOVA, p=0.0002).

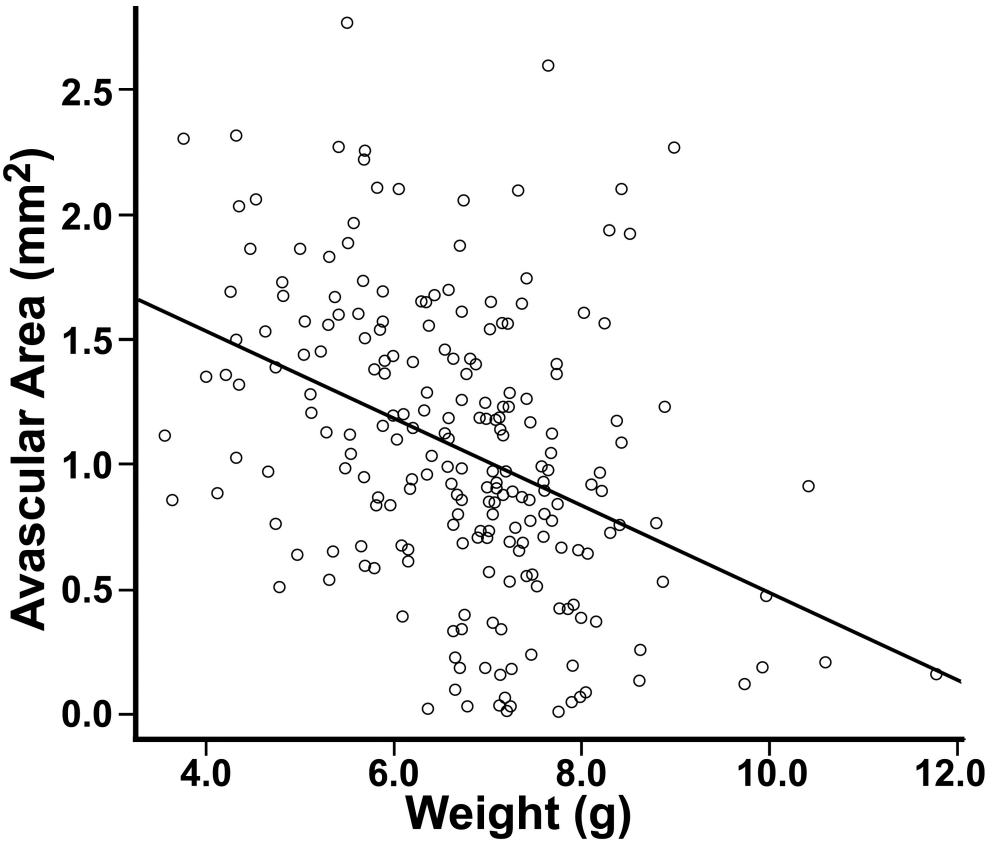
Avascular Area (mm2)
2.5
2.0
1.5
1.0
0.5
0.0
4.0
6.0
8.0
10.0
12.0
Weight (g)

Figure 2.4. The inverse association between avascular area and weight of F_2 mice at P16 after exposure to OIR.
The avascular area was shown to correlate with weight with a coefficient of −0.1743. This association was shown to be statistically significant (ANOVA, $p<10^{-8}$).

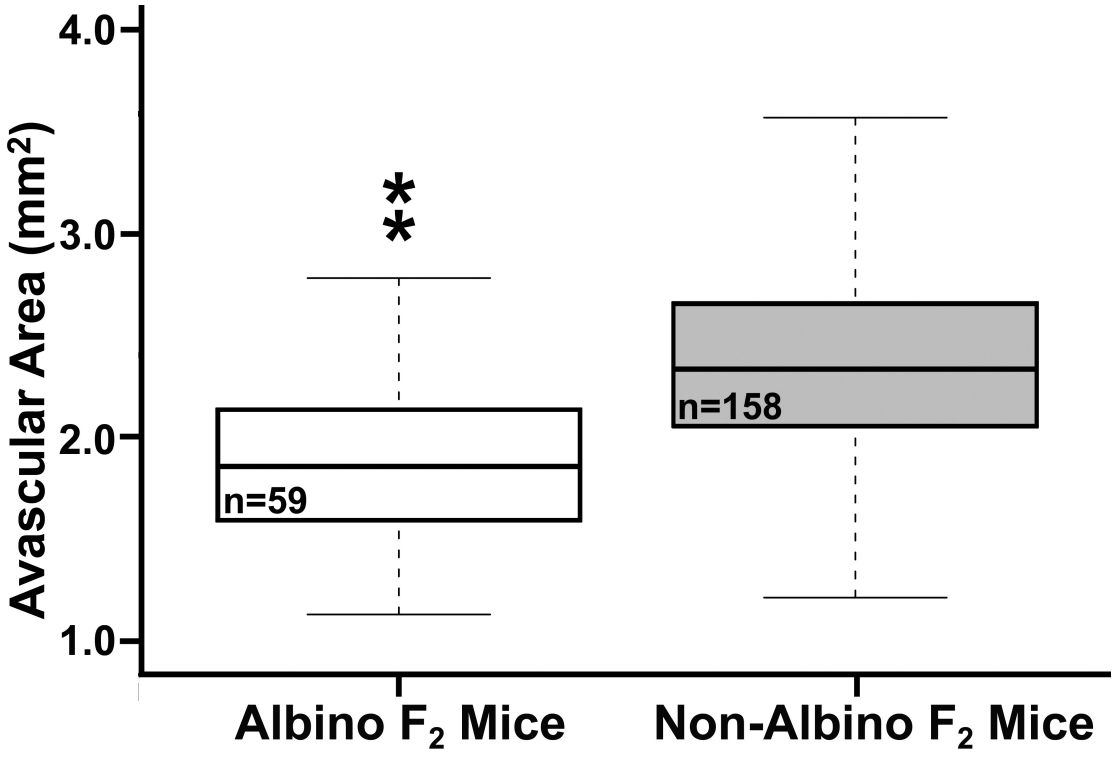
4.0
3.0
2.0
1.0
Avascular Area (mm²)
**
n=59
n=158
Albino F2 Mice
Non-Albino F2 Mice

Figure 2.5. Comparison of avascular areas for albino and non-albino F_2 mice.
The mean avascular area of albino mice was found to be 0.67 mm^2 versus 1.20 mm^2 for non-albino mice, a statistically significant difference (ANOVA, $p<0.0001$).

Strain of the paternal grandmother was associated with adjusted avascular area in the F_2 generation (ANOVA, $p = 0.0004$). F_2 mice produced from inbreeding (BALB/cByJ x C57BL/6ByJ)F_1 parents had smaller avascular areas than those produced from the reciprocal cross (2.12 mm^2 versus 2.34 mm^2). Paternal grandmother was included in the mapping analysis as an additive covariate. Segregating F_2 mice by both paternal grandmother and gender did not show any statistically significant differences (ANOVA, $p = 0.41$), suggesting that the two covariates did not interact.

In the F_2 mice, unlike in the parental generation, gender was associated with avascular area (avascular area 2.16 mm^2 for males, 2.28 mm^2 for females, ANOVA, $p = 0.02$). Gender was not found to interact with other secondary phenotypes such as weight, coat color, or paternal grandmother (ANOVA, $p = 0.08$, 0.52, and 0.40, respectively) in the F_2 generation.

ANOVA testing of weight, paternal grandmother and gender did not show any statistically significant interaction between the covariates ($p > 0.05$). Therefore they were included as additive covariates in mapping analyses.

Analyses were performed to identify potential QTL related to body mass at P16. ANOVA tests were run to consider candidature of secondary phenotypes as covariates, but no statistically significant association between weight and gender, strain of paternal grandmother, or coat color was found.

Identification of QTLs Related to OIR Response

Mapping without covariate inclusion: Initial QTL analysis employed a covariate-free model. This analysis identified 2 LOD score peaks associated with avascular area that

reached the genome-wide threshold of $\alpha = 0.05$. These peaks occurred on chromosomes 7 and 9 (Table, Figure 2.6A). On chromosome 9, the peak LOD score (3.75, $p = 0.05$, Figure 2.6B) occurred at SNP rs4135590, located 42.8 Mbp distal from the centromere. Genotype at this QTL explained 6.5% of the variance in avascular area ($p = 0.0007$, Table), with each BALB/cByJ allele having an additive protective effect (Figure 2.6C). The 1.8-LOD support interval was found to be 12.4– 96.0 Mbp distal from the centromere.

The peak on chromosome 7 was located at SNP rs13479427, 107.2 Mbp distal from the centromere. The LOD score of this peak was 8.90 ($p < 0.004$). The QTL on chromosome 7 explained 17.5% of the phenotypic variance (Table, $p < 0.004$). At this locus, the BALB/cByJ allele had a recessive protective effect. A 1.8-LOD support interval was determined to lie 81.2-146.5 Mbp distal from the centromere. The marker at 146.5 Mbp was the most telomeric marker included in the SNP panel, therefore we cannot exclude the possibility that the support interval may extend as far as the telomere.

A 2 QTL model including the peaks on chromosome 7 and 9 found that these loci explain 23.2% of the phenotypic variance ($p = 1.8 \times 10^{-11}$), with a combined LOD score of 12.4.

Mapping with Covariates. Using weight, the strain of the paternal grandmother, and gender as additive covariates, a single LOD score peak associated with unadjusted avascular area was identified on chromosome 7 at a genome-wide threshold of $\alpha = 0.05$ (Table, Figure 2.6D). This QTL is located at 134.2 Mbp, between SNPs rs13479506 and CEL-7_115892950. The LOD score of this peak was 9.83 ($p < 0.004$). The QTL on chromosome 7 in conjunction with the covariates explained 34.2% of the phenotypic variance (Table, $p < 0.004$). At this locus, the BALB/cByJ allele had an additive protective effect (Figure 2.6E)

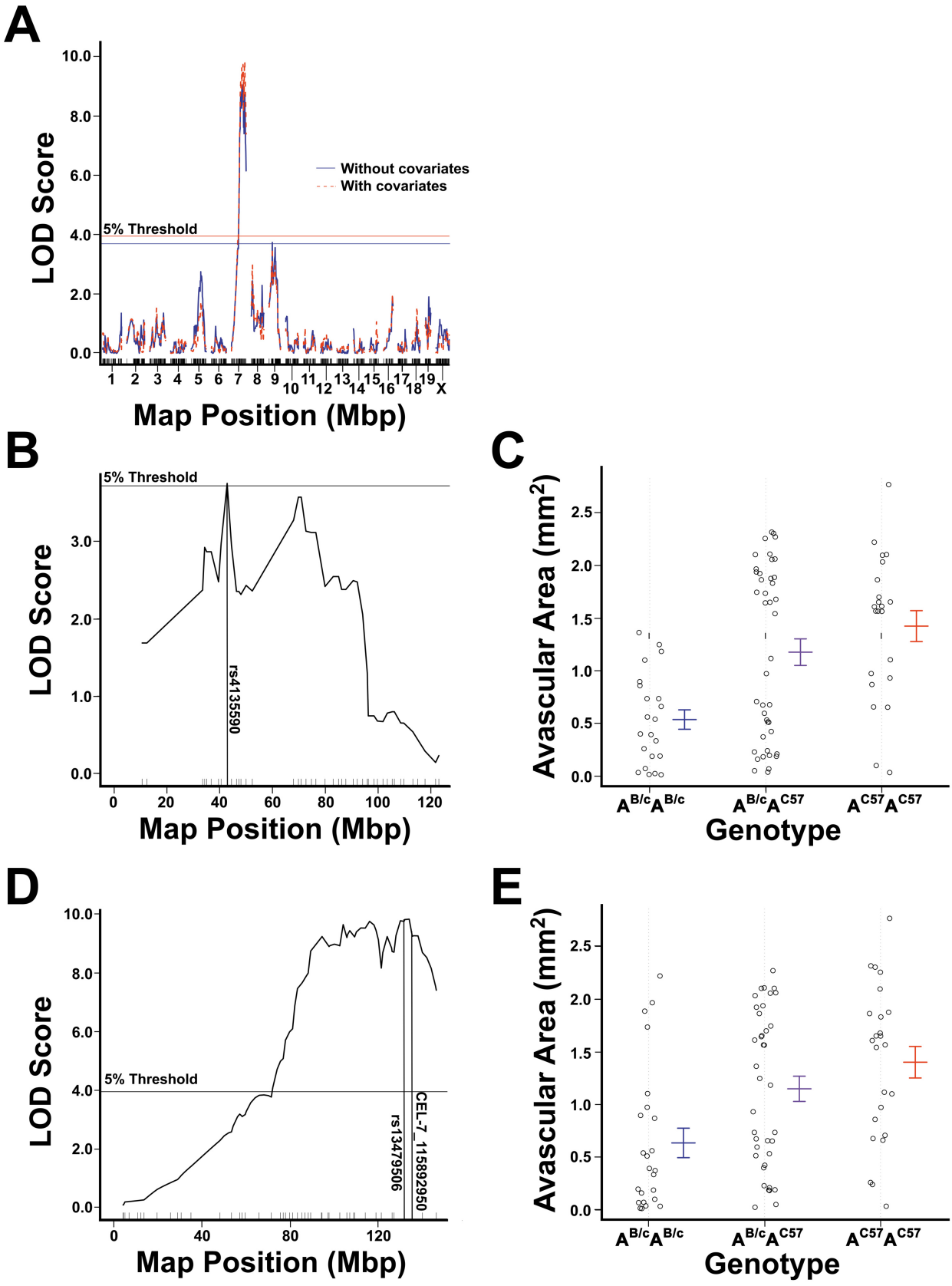
A
LOD Score
Without covariates
With covariates
5% Threshold
Map Position (Mbp)
B
LOD Score
5% Threshold
rs4135590
Map Position (Mbp)
C
Avascular Area (mm2)
Genotype
D
LOD Score
5% Threshold
rs13479506
CEL-7_115892950
Map Position (Mbp)
E
Avascular Area (mm2)
Genotype

Figure 2.6. The results of genetic linkage mapping using central retinal avascular area as the phenotype.

(**A**) Linkage map of avascular area across the whole genome created using no covariates (blue) and using weight, paternal grandmother, and gender as additive covariates in the analysis (red). Empirically derived genome-wide ($\alpha = 0.05$) thresholds of significance are shown as horizontal lines. For mapping without covariates the threshold of significance was a LOD score of 3.75. For mapping with covariates, the threshold of significance LOD score of 3.81. Mapping without covariates identified peaks on chromosomes 7 (LOD = 8.90) and 9 (LOD = 3.75). Mapping with covariates identified a peak on chromosome 7 (LOD = 9.83). (**B**) Linkage map of avascular area across chromosome 9 created without inclusion of covariates, showing a peak at SNP rs4135590 (LOD=3.75, p=0.05). (**C**) Effect plots of primary peak on chromosome 9. The BALB/cByJ allele is designated $A^{B/c}$, and the C57BL/6ByJ alleles is designated A^{C57}. The BALB/cByJ allelotype was found to be additively protective against the development of OIR. (**D**) Linkage map of avascular area across chromosome 7 created by including weight, paternal grandmother, and gender as additive covariates, showing a peak between SNPs rs13479506 and CEL-7_115892950 (LOD = 9.83, $p < 0.004$). (**E**) Effect plot of the peak on chromosome 7 at the nearest marker, CEL-7_115892950. The BALB/cByJ allelotype at this locus is shown to have a protective effect in a recessive manner.

Significance	Chr.	Phenotype	LOD Score	Markers at or flanking QTL	Marker position (Mbp)	LOD support interval (Mbp)	Effect on Phenotype
p < 0.004	7	Avascular area (P16)	8.90†	rs13479427	107.2	81.2 – 146.5	17.5%
			9.83*	rs13479506 CEL-7_115892950‡	131.8 135.8	88.2 – 146.5	34.2%
p = 0.05	9	Avascular area (P16)	3.75	rs4135590	42.8	12.4 – 96.0	6.5%
p = 0.05	5	Weight (P16)	3.91	CEL-5_93945748	97.1	52.8 – 133.6	4.1%

† Mapping analysis excluded covariates; * Mapping analysis included weight, sex, and paternal grandmother as covariates. ‡ Two markers flanking the LOD score peak are reported.

Table. 2.1 QTL associated with retinal avascular area in oxygen-induced retinopathy.
† mapping analysis excluded covariates; * mapping analysis included weight, gender, and paternal grandmother as covariates. ‡ the two markers flanking the LOD score peak are reported.

The 1.8-LOD support interval was calculated to extend from 88.2 to 146.2 Mbp distal from the centromere. The distal boundary of this interval coincided with the most distal marker tested. Therefore it is possible that if a marker at the telomere had been tested it would have been found that the interval extends as far as the telomere.

Locus-Locus Interactions: Composite interval mapping was conducted using genotype at the putative QTL on chromosome 7 as an additive or interactive covariate with other loci; this model reduces residual variation in order to clarify evidence for further QTL, allowing detection of background loci with weak main effects (Broman, Sen et al., 2009). No additional loci were discovered. A two-dimensional, two-QTL scan was conducted to identify any epistatic interactions. No statistically significant linked or multiple QTL were found.

Identification of a QTL Related to Weight

Standard interval mapping identified a LOD score peak on chromosome 5 that reached the genome-wide threshold for high significance ($\alpha = 0.05$, as determined by permutation tests). The peak occurred at the SNP CEL-5_9395748, approximately 97.1 Mbp distal from the centromere (LOD = 3.91, p = 0.024, Figure 2.7). At this locus, the C57BL/6ByJ allele was found to be associated with greater weight at P16 in a dominant fashion. Using this single-QTL model, genotype at this locus was estimated to explain 4.1% of the variance in weight (p = 0.01). A 1.8-LOD support interval was derived using an algorithm in R/qtl by interpolating between markers on the basis of recombination frequency and was found to be 52.8 – 133.6 Mbp distal from the centromere.

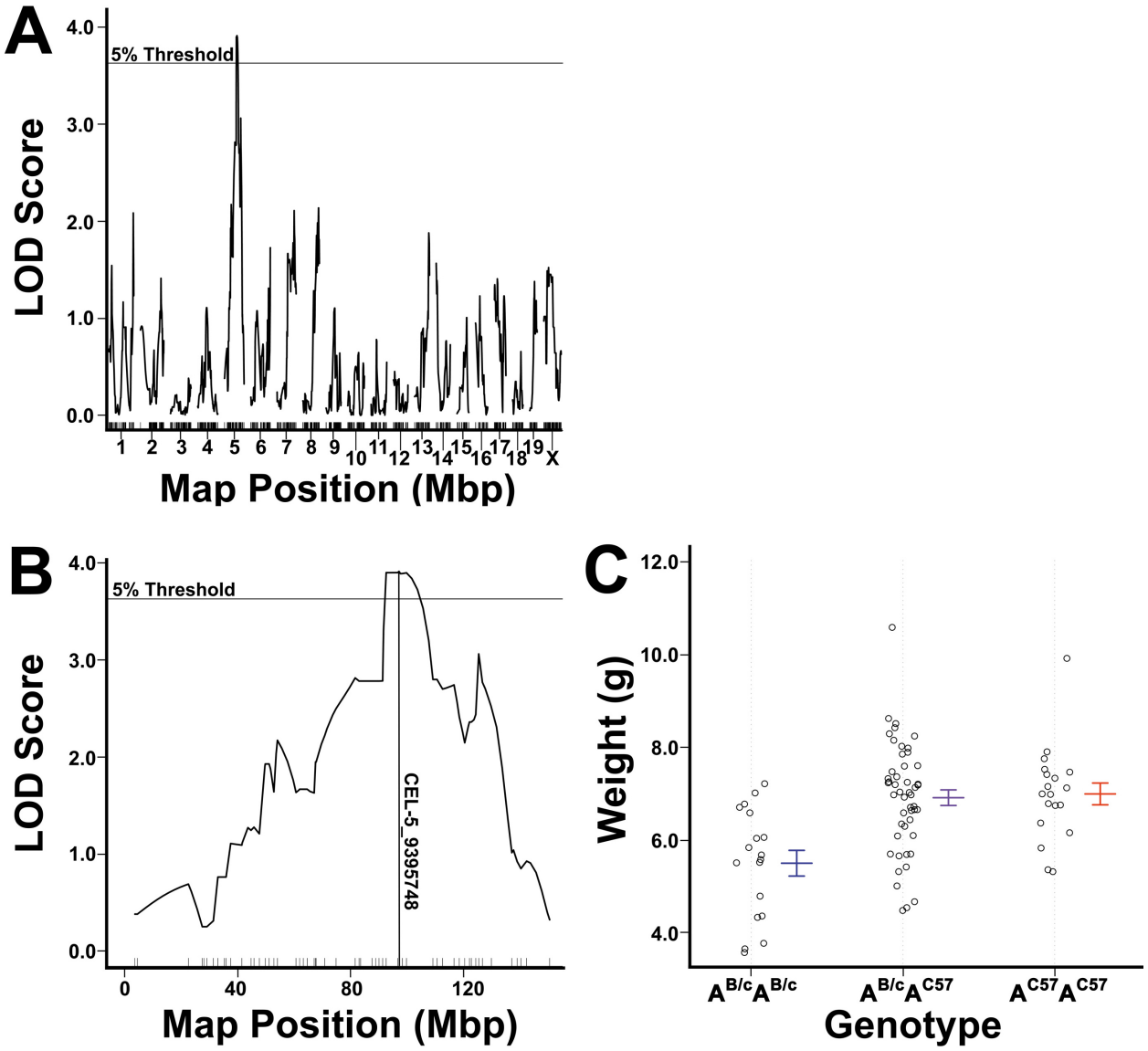
A
LOD Score
4.0
3.0
2.0
1.0
0.0
5% Threshold
1 2 3 4 5 6 7 8 9 10 11 12 13 14 15 16 17 18 19 X
Map Position (Mbp)
B
LOD Score
4.0
3.0
2.0
1.0
0.0
5% Threshold
CEL-5_9395748
0 40 80 120
Map Position (Mbp)
C
Weight (g)
12.0
10.0
8.0
6.0
4.0
A^B/c A^B/c
A^B/c A^C57
A^C57 A^C57
Genotype

Figure 2.7. The results of genetic linkage mapping using bodyweight at P16 after exposure to hyperoxia as the phenotype.
(**A**) A genome-wide linkage map of weight on postnatal day 16 after exposure to the OIR model. The threshold of significance was found to be 3.86 ($\alpha = 0.05$), as determined by permutation tests. (**B**) Shows linkage across chromosome 5, with significant linkage at marker CEl-5_93945748 (LOD = 3.91, p = 0.024). (**C**) Effect plot of genotypes at this marker on postnatal day 16; homozygosity for the BALB/cByJ allelotype at this locus is associated with reduced weight in a recessive manner (ANOVA, $p < 0.001$). The BALB/cByJ allele is designated $A^{B/c}$, and the C57BL/6ByJ alleles is designated A^{C57}.

Identification of Candidate Genes

A list of candidate genes located within the 1.8 LOD support intervals for the QTLs was created using a web-based virtual positional cloning program, Positional Medline (Yoshida, Makita et al., 2009 Database queried March 15, 2011). The program identifies candidate genes for the LOD support interval of putative QTLs related to keywords (Yoshida, Makita et al., 2009). The search region on chromosome 7 was extended to the telomere (152 Mbp); 160 candidate genes were identified in this interval using "retina AND angiogenesis" as keywords in the query. The 10 genes most correlated with the search terms were *mitogen-activated protein kinase 3, antigen KI-67, fibroblast growth factor 4, fibroblast growth factor receptor 2, insulin-like growth factor 2, tyrosine hydroxylase, fibroblast growth factor 3, extra cellular link domain-containing 1, BCL2/adenovirus E1B interacting protein 3,* and *cyclin D1*. Using "oxidative stress" as keywords in the query over the same interval to identify potential candidate genes related specifically to vaso-obliteration, Positional Medline identified 231 genes; the top 10 included: *mitogen-activated protein kinase 3, tyrosine hydroxylase, antigen KI-67, cytochrome P450 2E1, amyloid beta A4, parathyroid hormone, integrin alpha M, integrin alpha L, integrin-linked kinase,* and *insulin-like growth factor 2*.

Twenty-five genes were found within the support interval of the QTL on chromosome 9 using "retina AND angiogenesis", including *alpha disintegrin and metallopeptidase domain 10, chondroitin sulfate proteoglycan 4, alpha crystallin B, sphingosine-1-phosphate receptor 2, Pbx/knotted 1 homeobox 2, erythropoietin receptor, dopamine receptor 2, heat shock protein 2, cytochrome P450 family 1 subfamily a polypeptide 2,* and c*ytochrome P450 family 1 subfamily a polypeptide 1*; "oxidative stress" identified 246

candidates, including *kelch-like ECH-associated protein 1*, *apolipoprotein A-I, beta-site APP cleaving enzyme 1*, *dopamine receptor 2*, *low density lipoprotein receptor, intercellular adhesion molecule 1, cytochrome P450 family 19 subfamily a polypeptide 1, amyloid beta (A4) precursor-like protein 2, cytochrome P450 family 1 subfamily a polypeptide 2,* and c*ytochrome P450 family 1 subfamily a polypeptide 1.*

For the support interval found on chromosome 5 using weight as the primary phenotype, "birth weight" was used as the keyword in the query to derive 101 candidate genes, including *scavenger receptor class B, member 1*, *alpha fetoprotein, group specific component, chemokine (C-X-C motif) ligand 2*, *heparanase, chemokine (C-X-C motif) ligand 1, casein beta, amphiregulin, chemokine (C-X-C motif) ligand 4,* and *chemokine (C-X-C motif) ligand 10.*

DISCUSSION

ROP remains a significant cause of vision loss in the pediatric population. Although some risk factors have been identified, its development is complex and involves both environmental and genetic factors. This study aimed to initiate the identification of genes that may play a role in ROP susceptibility. Using the murine OIR model, we developed a mapping cross between C57BL/6ByJ and BALB/cByJ inbred mouse strains. These mice were confirmed to have significantly different vascular responses to OIR at P16, with the BALB/cByJ strain having smaller avascular areas than the C57BL/6ByJ strain. These results support those published by Dorrell, et al. (Dorrell, Aguilar et al., 2010), which found that while both strains have similar vaso-obliterative areas upon return to normoxia at P12, the BALB/cByJ strain revascularizes more rapidly than the C57BL/6J strain.

Genetically determined differences in retinal ocular morphology between the strains may play a role in response to OIR. Recent reports using confocal scanning laser ophthalmoscopy confirm physiological differences in retinal structure between adult C57BL/6J and BALB/c mice, with BALB/c mice having significantly thinner central retinas (211 μm versus 237 μm) (Huber, Beck et al., 2009). The differences between C57BL/6J and BALB/c mice are at least partially related to C57BL/6J being a pigmented strain while BALB/c is an albino strain (Jeffery, 1997; Ilia and Jeffery, 1999; Rachel, Dolen et al., 2002), and this issue is discussed further below.

The mapping cross revealed QTL associated with susceptibility to OIR on chromosomes 7 and 9. The BALB/cByJ allele of the chromosome 7 QTL was found to be protective in a recessive manner. In a mapping model that includes weight, gender, and paternal grandmother as additive covariates, allelotype at this marker is estimated to explain 34% of the phenotypic variation. The BALB/cByJ allele of the chromosome 9 QTL was also found to be protective in a recessive manner; this peak only reached statistical significance when covariates were excluded from the model. In a single QTL model, this allele was estimated to explain 7% of the variation in phenotype.

No QTL was identified on the X chromosome, despite evidence that the strain of the paternal grandmother was associated with avascular area. It was noted that, when initially performing mapping analyses with single covariates to confirm their inclusion in the final model, inclusion of paternal grandmother alone caused a loss of the peak on chromosome 9. This suggests that directionality of the cross may influence susceptibility via an epigenetic effect on a gene or genes within this locus, rather than through a modifier gene on the X chromosome.

A QTL related to weight at P16 was identified on chromosome 5. The C57BL/6ByJ allele was found to be associated with greater weight in a dominant manner; genotype at this locus was estimated to explain 4.1% of the variance in weight at this time point. The selective genotyping model based on avascular area, rather than weight, may have introduced bias in estimating the effect of this QTL on weight and avascular area. In both human ROP and murine OIR, increased birth weight and subsequent weight gain are protective against NV (Coats, 2005; Chen and Smith, 2007); although C57BL/6ByJ mice have larger avascular areas at P16 than their BALB/cByJ counterparts, the data suggest that the C57BL/6ByJ genome does contain an allele related to weight that serves to protect against OIR.

Initial analysis of F_2 mice revealed significantly different retinal avascular areas in albino and non-albino mice. This result supports findings from a rat backcross (van Wijngaarden, Brereton et al., 2007) as well as across different strains of rats (van Wijngaarden, Coster et al., 2005). As albinism in this cross is caused by homozygous loss of function of *Tyr*, the rate-limiting enzyme in the biosynthesis of melanin (Jeffery, 1997), these data suggest that *Tyr* or a linked gene might play a role in disease susceptibility. The QTL identified on chromosome 7 by mapping analysis includes *Tyr* (located 94.58-94.64 Mbp) within the 1.8-LOD support interval. The association between albinism and avascular area demonstrated here supports a similar observation in rats (van Wijngaarden, Brereton et al., 2007). An intriguing possibility is that *Tyr* itself is a modifier of the area of avascular retina in rodent OIR. The *Tyr* gene has various roles in ocular physiology. There are numerous morphological differences between the retinas of albino and non-albino mice, and it is not clear whether these may be associated with responses to hyperoxia. It is possible that the

thicker C57BL/6 retina becomes more hypoxic than the BALB/c retina, and that this leads to greater astrocyte degeneration and slower revascularization (Jeffery, 1997; Ilia and Jeffery, 1999; Rachel, Dolen et al., 2002). The absence of melanin in the RPE may alter the response of the retina to oxidative stress (van Wijngaarden, Brereton et al., 2007). Alternatively, since the absence of melanin in the iris increases the amount of light reaching the retina (Summers, 1996), it is possible that greater retinal light exposure affects the revascularization process, even though light has not previously been demonstrated to play a role in modifying the severity of OIR (Wesolowski and Smith, 1994). Furthermore, *Tyr* can form L-3,4-dihydroxyphenylalanine (L-dopa), the immediate precursor of DA (Ito, Kato et al., 1984). The role of dopamine metabolism in OIR is currently unknown, but DA is known to modulate tumor angiogenesis (Chakroborty, Sarkar et al., 2009) and may play a role in angiogenesis in OIR. However, neither our experiment nor the work that found an association between albinism and OIR in rats (van Wijngaarden, Brereton et al., 2007) were designed to test the candidature of any particular gene.

Positional Medline identified several other interesting candidate genes located within the support interval of the QTL on chromosome 7 using the keywords "retina AND angiogenesis". MAPK3, or ERK-1, is a mitogen-activated kinase that is activated by fibroblast growth factor (FGF) to induce EC proliferation in retinal angiogenesis (Zubilewicz, Hecquet et al., 2001) and has been shown to play a role in regulating VEGF expression in response to oxidative stress (Klettner and Roider, 2009). FGF4, a member of the FGF family, is a mitogen that is involved in development and morphogenesis of various cell and tissue types (Kosaka, Sakamoto et al., 2009). Over-expression of FGFR2, a receptor for FGF, has been demonstrated in several types of neoplasia, including breast cancer, prostate cancer

(Schwertfeger, 2009), renal cell carcinoma (Tsimafeyeu, Demidov et al., 2011), and gastric cancer (Katoh, 2009). Within the retina, insulin-like growth factor 2 (IGF-2) is present almost exclusively in the photoreceptors and vasculature, where it is the major locally expressed growth factor. However, it is not expressed in the vascular ECs in neovascular tufts formed in response to OIR (Lofqvist, Willett et al., 2009). Tyrosine hydroxylase, TH, is the enzyme primarily responsible for dopamine production in the central nervous system and retina; in the eye, it is found primarily in amacrine cells in the inner plexiform layer (Reis, Ventura et al., 2007). *Xlkd1*, or extra-cellular link domain containing 1, encodes a hyaluronan receptor expressed on lymphatic endothelium in both adult and embryonic vessels and XLKD1 positive cells were recently identified in the hyaloid vascular system of the developing murine eye (Zhang, Tse et al., 2010).

Four of the top 10 putative genes identified using the key terms "oxidative stress" (*Mapk3, Th, Mki67,* and *Igf2*) were also identified in the prior search. Integrin alphas L, and M (ITGAL, or CD11a, and ITGAM, or CD11b, respectively) are expressed on neutrophils and, when complexed with beta 2 integrin CD18, function to modulate migration of the cells to the site of injury by binding ICAM-1 on ECs (Mazzone and Ricevuti, 1995). VEGF-A has been shown to stimulate neutrophil and T cell recruitment in an Itgal- and Itgam-dependent manner (Chidlow, Glawe et al., 2010). Integrin linked kinase signaling has been shown to mediate production of brain-derived neurotrophic factor by ECs (Guo, Kim et al., 2008), and oxidative stress disrupts this signaling pathway (Saito, Hayashi et al., 2004).

Although ranked less highly by the Positional Medline algorithm, 3 genes related to Wnt signaling pathways were included in the list of candidate genes. Wnt signaling plays an essential role in cell survival, proliferation, and migration, and has an important role in

controlling retinal angiogenesis (Ye, Wang et al., 2009). Mutations in genes related to this pathway have been implicated in several ocular neovascular diseases with phenotypic similarities to ROP, including FEVR and Norrie disease (Nikopoulos, Venselaar et al., 2010). Mutations in FZD4 have been identified as a cause of familial FEVR (Robitaille, MacDonald et al., 2002) and have been confirmed in cases worldwide (Nallathambi, Shukla et al., 2006; Jia, Li et al., 2010). More recently, FZD4 mutations have been found in a small number (3%) of a cohort of infants with severe ROP (Ells, Guernsey et al., 2010). Interestingly the mouse *Fzd4* gene lies within the QTL found on chromosome 7. Wnt11 is another gene involved in Wnt signaling that is encoded within the QTL on chromosome 7; WNT11 is a non-canonical ligand in the pathway. Within the retina specifically, mutations in Wnt11 have been shown to result in increased angiogenesis and branching (Stefater, Lewkowich et al., 2011). Dickkopf 3 (DKK3) belongs to a family of secreted glycoproteins that act as regulators of Wnt signaling. In the retina, *Dkk3* is expressed by Muller glia and retinal ganglion cells and is a cell-type specific positive regulator of Wnt signaling. In response to photoreceptor death in a murine model of retinal degeneration, *Dkk3* expression is up-regulated and inhibited caspase activation in Muller glia (Nakamura, Hunter et al., 2007).

The LOD support interval on chromosome 9 also contains several interesting candidates identified by Positional Medline related to retina and angiogenesis. CSPG4, or chondroitin sulfate proteoglycan 4, also known as NG2, is expressed by nascent pericytes early in angiogenesis. Studies of ischemic retinal NV have shown decreased ectopic vessel protrusion into the vitreous and decreased proliferation of both pericytes and ECs in NG2 knock-out (KO) mice (Ozerdem and Stallcup, 2004). Similarly to MAPK3, MAP2K1 (MEK1) mediates FGF-stimulated EC proliferation in tumor models (Zubilewicz, Hecquet et al.,

2001). IL18 has been shown to play a role in regulating regression of pathological NV in mice after exposure to the OIR model (Qiao, Sonoda et al., 2007); additional studies using KO mice suggest that IL18 plays a role in regulation of retinal vessel formation (Qiao, Sonoda et al., 2004). CRYAB, or crystalline alpha B, is a chaperone within the small heat shock protein family and has been shown using KO mouse models to play a role in intraocular angiogenesis by acting as a chaperone for VEGF-A (Kase, He et al., 2010). EPO has been linked to both ROP and diabetic retinopathy. Local tissue EPO levels are suppressed during retinal vessel loss in OIR and elevated during NV, and pharmacological use of EPO was shown to protect against hypoxia-induced apoptosis (Chen, Connor et al., 2008). siRNA inhibition of EPO expression during the neovascular phase successfully inhibited NV (Chen, Connor et al., 2009). Human and murine studies have both found that vitreal EPO expression was associated with proliferative diabetic retinopathy (Watanabe, Suzuma et al., 2005).

Candidates derived using the key terms “oxidative stress” included several adhesion molecules. ICAM1 is expressed by ECs and plays a critical role in leukocyte stasis and migration to the site of injury (Long, 2011). D2 (dopamine receptor 2) acts as an antioxidant in physiological conditions; it has been found to regulate the production of reactive oxidative species, and KO mice have higher blood pressure in part due to the increased oxidative damage in the kidney (Armando, Wang et al., 2007). LDLR is also involved in mediating oxidative stress; KO mouse models have increased oxidative stress, inflammation, and atherosclerosis (Holvoet, 2008). Furthermore, oxidative modification of this receptor has been associated with EC dysfunction (Sakurai and Sawamura, 2003). Three different cytochrome P450 genes were also found to be candidates by the Positional

Medline program; however, this may be a spurious result due to the large amount of data published regarding oxidative stress generated in the metabolism of various drugs.

The support interval of the QTL on chromosome 5 associated with weight includes 101 candidate genes related to "birth weight." Low maternal serum α-fetoprotein (AFP) levels have been shown in humans to be associated with large birth weight infants (Baschat, Harman et al., 2002). Heparanase, HPSE, plays a role in placental development and affects both structure and nutrient transport (Vallet, Miles et al., 2009). CXCL1, 2, 4, and 10 are chemokines that have been studied extensively in regards to their role in inflammation (Horuk and Peiper, 1996; Romagnani, Lasagni et al., 2004), development, angiogenesis (Romagnani, Lasagni et al., 2004; Strieter, Belperio et al., 2004), and neoplasia (Strieter, Belperio et al., 2004).

CONCLUSIONS

Revascularization in OIR is related to weight, strain of paternal grandmother, gender, and albinism. Our data support the existence of a QTL on chromosome 5 that influences weight after exposure to hyperoxia, as well as QTLs on chromosomes 7 and 9 that modify susceptibility to OIR. Ongoing studies are investigating the role of candidate QTGs as modifiers of the progression of OIR. It is hoped that investigation of QTGs will help to elucidate the pathogenesis of ROP. These modifier genes may also be candidates for susceptibility genes in other complex ocular diseases involving aberrant angiogenic responses, such as diabetic retinopathy and neovascular age-related macular degeneration.

CHAPTER 3

DOPAMINERGIC MODULATION OF RETINAL ENDOTHELIAL PROGENITOR CELL RECRUITMENT AND REVASCULARIZATION

ABSTRACT

ROP is a leading cause of vision loss in the pediatric population. ROP has a phase of arrest of vascularization of the peripheral retina followed by a stage of pathological angiogenesis. Our prior work identified *Tyr* as a candidate QTG associated with revascularization of the retina after hyperoxic vaso-obliteration in the murine model of ROP, OIR. This study tests the candidature and mechanism of action of *Tyr* in modulating retinal revascularization and investigates a putative mechanism. Compared with *Tyr* wild-type mice, *Tyr*-null mice have lower serum DA higher levels of CD45- and lo/CD34+/CD133+ endothelial progenitor cells in their bone marrow and blood, greater recruitment of CD34+/CD133+ cells to the revascularizing retina, and faster retinal revascularization. Pharmacological administration of DA inhibits endothelial progenitor cell recruitment to the retina and revascularization in both *Tyr* null and wild-type animals. Real-time PCR analysis of DA receptor expression and experiments using receptor agonists suggest D1-like family of receptors mediates these effects. The suggested role of dopaminergic inhibition of retinal revascularization and of endothelial progenitor cell recruitment has important implications for ROP and other diseases of premature infants, and potentially for the pathophysiology of other retinal vasculopathies.

LIST OF ABBREVIATIONS

ANOVA – analysis of variance
BM – bone marrow
c-2J – B6(Cg)-*Tyr*$^{c-2J}$/J
D2 – dopamine receptor 2
DA - dopamine
EC – endothelial cell
EPC – endothelial progenitor cell
HPLC–ED – high performance liquid chromatography with electrochemical detection
ISHAGE - International Society for Hematotherapy and Graft Engineering
N_2 – backcross 2nd generation
OIR – oxygen-induced retinopathy
P – post-natal day
QTG – quantitative trait gene
QTL – quantitative trait loci
ROP – Retinopathy of Prematurity
RPE – retinal pigment epithelium
rt-PCR – real time polymerase chain reaction
TH – tyrosine hydroxylase
Tyr – Tyrosinase

INTRODUCTION

ROP is a leading cause of blindness in children in the US (Gilbert, 2008). ROP is a complex disease where a phase of arrest of peripheral retinal vascularization is followed by a phase of pathological neovascularization. OIR in the mouse was developed as a model of ROP (Smith, Wesolowski et al., 1994). In the mouse OIR model, exposure to hyperoxia leads to central vaso-obliteration. When mice are returned to a normoxic environment, the presence of a region of avascular retina creates a pro-angiogenic milieu, which leads to retinal NV (Polverini, Cotran et al., 1977; Smith, Wesolowski et al., 1994; Lutty, Chan-Ling et al., 2006). The current study used the OIR model to investigate the genetics of retinal vascular regeneration in the aftermath of hyperoxia-induced central retinal vaso-obliteration. Retinal vascular regeneration was studied in order to find pathways that potentially may be therapeutically modulated to improve retinal vascularization in ROP, and which may play a role in other retinal vasculopathies and vascular regeneration in other organs.

Our previous work used an inter-strain difference between C57BL/6ByJ and BALB/cByJ mice to map QTL controlling retinal revascularization. C57BL/6ByJ mice have larger avascular areas in response to hyperoxic vaso-obliteration in the OIR model than do BALB/cByJ at both P12 (Symons, Swaim et al., 2009) and P16 (O'Bryhim, Radel et al., 2012). *Tyr* is located at 94.5 Mbp on chromosome 7, within a significant QTL identified in a mapping study (O'Bryhim, Radel et al., 2012), with albino mice in this cross exhibiting smaller vaso-obliterative areas than non-albino mice. A similar association between albinism and decreased retinal avascular area in OIR has been found in rats (van Wijngaarden, Coster et al., 2005; van Wijngaarden, Brereton et al., 2007). Albinism in the

BALB/cByJ strain is caused by homozygous loss of function of *Tyr*, the rate-limiting enzyme in the biosynthesis of melanin (Jeffery, 1997). Therefore, these data suggest that *Tyr* or a linked gene might play a role in disease susceptibility.

Tyr has been shown by independent groups to contribute to production of DA in peripheral tissues (i.e., outside of the central nervous system). Pigmented TH-null transgenic mice produced 18% more catecholamines than did albino littermates (Rios, Habecker et al., 1999). Additionally, pigmented mice have been shown to have significantly higher levels of DA specifically compared to albino mice regardless of presence or absence of functional TH (Eisenhofer, Tian et al., 2003). In the eye specifically, L-dopa produced by TYR can be secreted from the RPE and converted into DA by amacrine cells, and DA receptors are expressed as early as embryonic day 14 in gestation (Reis, Ventura et al., 2007). Both DA and L-dopa are thought to influence retina differentiation in early development (Kralj-Hans, Tibber et al., 2006).

Outside of the eye, DA is known to inhibit angiogenesis. Several studies in tumor models showed that DA signaling through D2 inhibits angiogenesis (Basu, Nagy et al., 2001; Gomez R Fau - Gonzalez-Izquierdo, Gonzalez-Izquierdo M Fau - Zimmermann et al., 2006; Chakroborty, Chowdhury et al., 2008). DA can influence angiogenesis through its actions on both EPCs and vascular ECs (Chakroborty, Sarkar et al., 2009).

This study was conducted to explore the role of *Tyr* as a modifier gene in revascularization following hyperoxic vaso-obliteration induced by the OIR model. Given the evidence for *Tyr*'s candidature, the series of experiments here investigate the mechanism of action by which *Tyr* modulated revascularization, in particular testing the hypothesis that modulation of dopaminergic pathways may influence retinal revascularization.

MATERIALS AND METHODS

Animals

All experimental procedures were approved by University of Kansas Medical Center Institutional Animal Care and Use Committee. c-2J mice are a substrain of the C57BL/6J mouse strain that has a spontaneous loss of function mutation in *Tyr* that was bred to homozygosity. Both C57BL/6J and c-2J mice were purchased from Jackson Laboratories (Bar Harbor, ME). All mice were kept in a 12-hour light, 12-hour dark cycle with ambient room temperature between 19°C and 22°C. Breeding pairs were maintained on a higher-fat diet (8626 rodent diet, Harlan Laboratories, Indianapolis, IN), with chow and water available ad libitum. All experiments except described used mice from a minimum of 3 litters to avoid strain-specific bias.

Oxygen-Induced Retinopathy

OIR was induced according to protocol (Smith, Wesolowski et al., 1994) by exposing pups to 75% oxygen beginning on P7 and returning them to normoxia after 120 hours. O_2 levels in the chambers were continuously controlled using a ProOx portable monitor (Biospherix, Redfield, NY), which was calibrated monthly using room air and 100% O_2. Mice were weighed, anesthetized with a lethal dose of tribromoethanol via intraperitoneal injection, and sacrificed at P12, P13, or P16.

Avascular Areas in OIR

After induction of anesthesia, C57BL/6J, c-2J, and backcross animals were perfused with high-molecular weight fluorescein isothiocyanate-labeled dextran (MW≥2,000,000;

Sigma, St. Louis, MO) via the left ventricle to visualize patent vessels and enucleated. Retinas were fixed overnight in 4% paraformaldehyde, dissected, and flat-mounted using anti-fade medium (Southern Biotech, Birmingham, AL). Immunofluorescent micrographic images were taken using an SMZ 1500 microscope (Nikon, Tokyo, Japan) and MagnaFire Camera and software (Optronics, Goleta, CA). ImageJ (http://rsbweb.nih.gov/ij/) was used to manually trace and measure avascular areas.

Backcross Breeding Strategy

An N_2 backcross population was bred by mating female C57BL/6J mice to male c-2J mice to derive a (C57BL/6J x c-2J)N_1 generation. Female N_1 mice were bred with male c-2J mice to create the N_2 generation (Figure 3.1). N_2 mice were exposed to the OIR model and sacrificed on P13 for enucleation as described above.

Flow Cytometry

After induction of anesthesia on P13, blood samples from C57BL/6J and c-2J mice were taken via cardiac puncture. Samples were incubated in 3x volume of RBC lysis buffer (Biolegend, San Diego, CA) according to instructions, centrifuged at 300 g, and re-suspended in 1 mL 1% BSA in PBS. BM was harvested by aspiration from the same mice from both femurs and tibias.

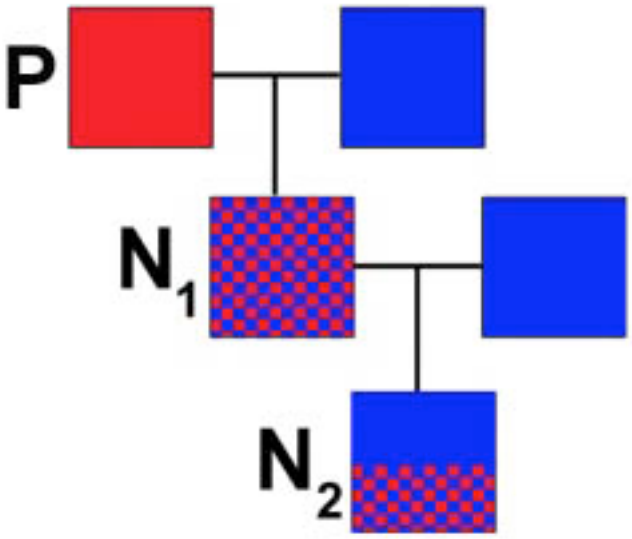
P
N1
N2

Figure 3.1 Illustration of the breeding scheme used in the backcross.
Female C57BL/6J mice, represented in red, were bred to male c-2J mice, represented in blue, to derive a (C57BL/6J x B6(Cg)-*Tyr*$^{c\text{-}2J}$/J)N_1 generation. Female N_1 mice were bred with male c-2J mice to create the N_2 generation. N_2 mice were exposed to OIR, and avascular area was compared between albino and non-albino (black) littermates.

BM and blood samples were filtered through a 70 μM mesh filter and centrifuged at 300 g for 10 minutes at 4°C. Given the rarity of EPCs, bone marrow and blood samples were stained for flow cytometric analysis of EPCs using modifications of the International Society for Hematotherapy and Graft Engineering (ISHAGE) protocol as described previously (Balasubramaniam, Mervis et al., 2007). This procedure has been used to successfully isolate CD133+ progenitor cells from small samples of both BM and blood. Samples were incubated in CD45-FITC, CD34-APC, CD133-PE (Biolegend, San Diego, CA) for 30 minutes on ice. Cells were washed with 1% BSA, centrifuged at 300 g for 10 minutes, and re-suspended in DAPI (Invitrogen, Grand Island, NY) for 10 minutes to differentiate live cells. After a final wash and spin, samples were re-suspended in 1% BSA and analyzed at the University of Kansas Medical Center Flow Cytometry Core with a Beckman LSRII Flow Cytometer (Miami, FL). Single-stain positive controls and negative controls were used to set the gates and determine voltage compensation for fluorescent intensity. A minimum of 1,000,000 cells was counted from each sample, and samples were run until 3,000,000 cells were counted or the sample was exhausted. Cells were gated to exclude DAPI positive dead cells, and then gated to select for the CD45-negative and -lo population. Of these, CD133 and CD34 double positive cells were counted as a percentage of all live, CD45-/lo cells.

Immunofluorescent Staining

Retinae were permeablilized overnight in 0.5% Triton X-100, washed, and incubated in 20 μg/mL *Griffonia simplicifolia* isolectin B4 (Sigma, St. Louis, MO) in PBLec (PBS, pH 6.8, 1% Triton X-100, 0.1 mM $CaCl_2$, 0.1 mM $MgCl_2$, 0.1 mM $MnCl_2$) overnight. After blocking, retinae were incubated in hamster anti-murine CD34 (1:100, Biolegend, San Diego, CA) or

rabbit anti-Ki67 (1:50, Abcam, Cambridge, MA), and rat anti-murine CD133 (1:200, Biolegend, San Diego, CA) overnight. Retinae were subsequently stained with Texas Red anti-rat IgG (1:400, Abcam, Cambridge, MA) or Texas Red anti-rabbit (1:200, Abcam, Cambridge, MA) and Dylight 649 anti-hamster IgG (1:200, Biolegend, San Diego, CA) for 1 hour at room temperature, washed, and flatmounted using anti-fade medium (Southern Biotech, Birmingham, AL). Two micrographic images of each retina was taken using a Nikon Digital Eclipse C1Si confocal microscope (Tokyo, Japan) and Nikon EZC1 software (Tokyo, Japan). The number of CD34+/CD133+ cells were counted and averaged for each retina.

Quantification of dopamine concentration in serum

Peripheral blood samples were collected by cardiac puncture on P13, allowed to sit at room temperature for 10-15 minutes, and centrifuged at 2,200 g for 10 minutes. The supernatant serum was collected, snap frozen on dry ice, and stored at -80^{o}C until further processing. Samples were thawed on ice and catecholamines were extracted using ESA Catecholamine Analysis Kits (ESA, Chelmsford, MA) according to protocol. DA concentrations were determined using an isocratic high performance liquid chromatography system (ESA Coulochem III, Chelmsford, MA) coupled to a Coulochem III dual-channel electrochemical array detector (HPLC-ED) (E1 + 0.35 mV and E2 – 0.25 mV using a 5011 dual analytical cell ESA Model 5100A). DA was separated with a C18 reverse phase column (ESA HR-80 C18, 4.6 mm × 80 mm, 3 μm) with a pH 4.0 citrate-acetate mobile phase containing 4.0% methanol and ~0.35 mM 1-octane-sulfonic acid at a flow rate of 1.8 ml/min. 3,4-dihydroxy-benzylamine was used as the internal standard. Plasma DA concentrations were expressed as pg/mL serum.

Gene expression studies

Tyr and DA receptor expression were determined using real-time PCR (rt-PCR) expression analysis. BM and blood samples from 3 litters were harvested as described and pooled for each litter. BM samples from an additional litter were pooled, incubated in antibodies as described above to allow sorting of CD45-/CD34+/CD133+ and Cd45-/CD34-/CD133- cells on a BD FACSAria IIu (San Jose, CA) at the University of Kansas Medical Center Flow Cytometry Core.

For all samples, RNA was isolated using an RNEasy Mini Kit (Qiagen, Valencia, CA) according to the manufacturer's protocol. Extracted RNA was reverse-transcribed in 20 μL reactions using an iScript cDNA synthesis kit (Bio-Rad, Hercules, CA); negative controls used nuclease-free H_2O in place of reverse transcriptase. Primers were designed to flank an intron using Primer3 software and tested for specificity using BLAST software (NCBI, Bethesda, MD). Primers were then commercially synthesized (IDT Technology, Skokie, IL) (Table 3.1). S16 was used as an endogenous control from which relative level of mRNA expression was estimated.

Each 20 μL reaction mixture contained 10 μL 2x SYBR Green master-mix (Applied Biosystems, Foster City, CA), 1 μL each of forward and reverse primers (0.5 μM final concentration), and 2 μL cDNA sample diluted 1:2 with nuclease-free H_2O. An Eco Real-Time PCR System (Illumina, San Diego, CA) was used to run the reactions. Cycling

Gene Name	Forward Primer	Reverse Primer
Dopamine receptor 1	TCC AAG TCA TAG CCT GGA CTG CAA	GCA GCT GCT TCC AAA GAA CAC CTT
Dopamine receptor 2	TCT TCT GGT GGC CAC ACT GGT TAT	GCA CAC AGG TTC AAG ATG CTT GCT
Dopamine receptor 3	TGG CAG GTT ATC CAC ATC CCT GAA	TGG CAT GCC TGA CAG TGG GTA TTA
Dopamine receptor 4	TGC AGA CAC CCA CCA ACT ACT TCA	AGT AGA CAA AGA GAG GCA GCA CCA
Dopamine receptor 5	GCT GCT GCT TTA GTG CAG GTT GAA	AAC ACT GAG CAC CAA CTG GCA AAG
S16	AGG AGC GAT TTG CTG GTG TGG ATA	TTT GAG ATG GAC TGT CGG ATG GCA

Table 3.1. Primer sequences used in rt-PCR gene expression analyses.
Primers were designed using Primer3 software and tested for specificity using BLAST software. Sequences expressed as 5' to 3'.

conditions included an initial denaturation (95°C, 10 minutes) followed by 40 cycles of denaturation (95°C, 15 seconds), annealing (60°C, 10 minutes), and extension (72°C, 35 seconds). Samples were tested in duplicate for each candidate gene, as were standard cDNA pool and water samples to provide positive and negative controls, respectively. Melting curves were analyzed to confirm amplicon specificity. A threshold was established for each plate of reactions, and the cycle number where the fluorescence curve intersected with the threshold was calculated (Ct). The Ct values for the genes of interest were compared with the Ct for the transcripts of the ribosomal S16 protein (ΔCt).

Pharmacological Studies

All pharmacological agents used in these studies were dissolved in saline and administered by intraperitoneal injection on P11. We chose this time point since retinal revascularization starts prior to the customary end-point of exposure to hyperoxia in the OIR model (Lange, Ehlken et al., 2009) and our additional work suggests that the greatest influx of EPCs into the retina occurs at this time point. Drugs assessed in this study included DA hydrochloride (50mg/kg) (Sigma, St. Louis, MO), D2 antagonist eticlopride (1mg/mL) (Sigma, St. Louis, MO), D1/5 antagonist SCH39166 (3mg/kg) (Tocris, Ellisville, MO), and D4 antagonist L745,870 (3mg/kg and 6mg/kg) (Tocris, Ellisville, MO). Receptor-specific antagonists were tested in C57BL/6J mice. Each litter was divided into 2 groups, which received either drug or a corresponding volume of vehicle control (saline). Mice were sacrificed 24 hours after injection and enucleated for retinal flat-mounting and Immunofluorescent staining as described previously.

Statistical Analysis

The data are presented as means. Statistical analyses were performed using R software package, using Student's t-test and ANOVA tests where appropriate. $P < 0.05$ was considered statistically significant.

RESULTS

Tyr *function inhibits retinal revascularization after OIR-induced vascular damage*

Retinal avascular area from C57BL/6J and c-2J mice were measured upon return to normoxia, at P12, and 96 hours after return, on P16. We found that the c-2J retinae had 10% smaller avascular areas than C57BL/6J mice at P12 that just reached the threshold of significance (2.80 mm^2 vs. 3.12 mm^2, $p = 0.05$, Student's t-test). Four days later, there was a nearly 50% difference in mean avascular areas between strains (0.94 mm^2 vs. 1.81 mm^2, $p = 2.5 \times 10^{-10}$, Student's t-test) (Figure 3.2A).

We performed a (C57BL/6J x c-2J) x c-2J backcross to ascertain whether the difference in revascularization was related to *Tyr* function or another, unknown mutation carried by the c-2J strain. Albino N_2 mice produced in this cross had a mean avascular area of 2.54 mm^2. Pigmented littermates had mean avascular area of 3.30 mm^2 ($p = 0.0005$, Student's t-test, Figure 2.B), demonstrating that avascular area segregated with albinism. Therefore the gene causing altered retinal avascular area is *Tyr* or is tightly linked to *Tyr*.

Tyr *function alters EPC recruitment to the retina but not EC proliferation*

To determine whether the difference in avascular area related to *Tyr* function was due to increased proliferation of existing retinal ECs or was related to differences in EPC

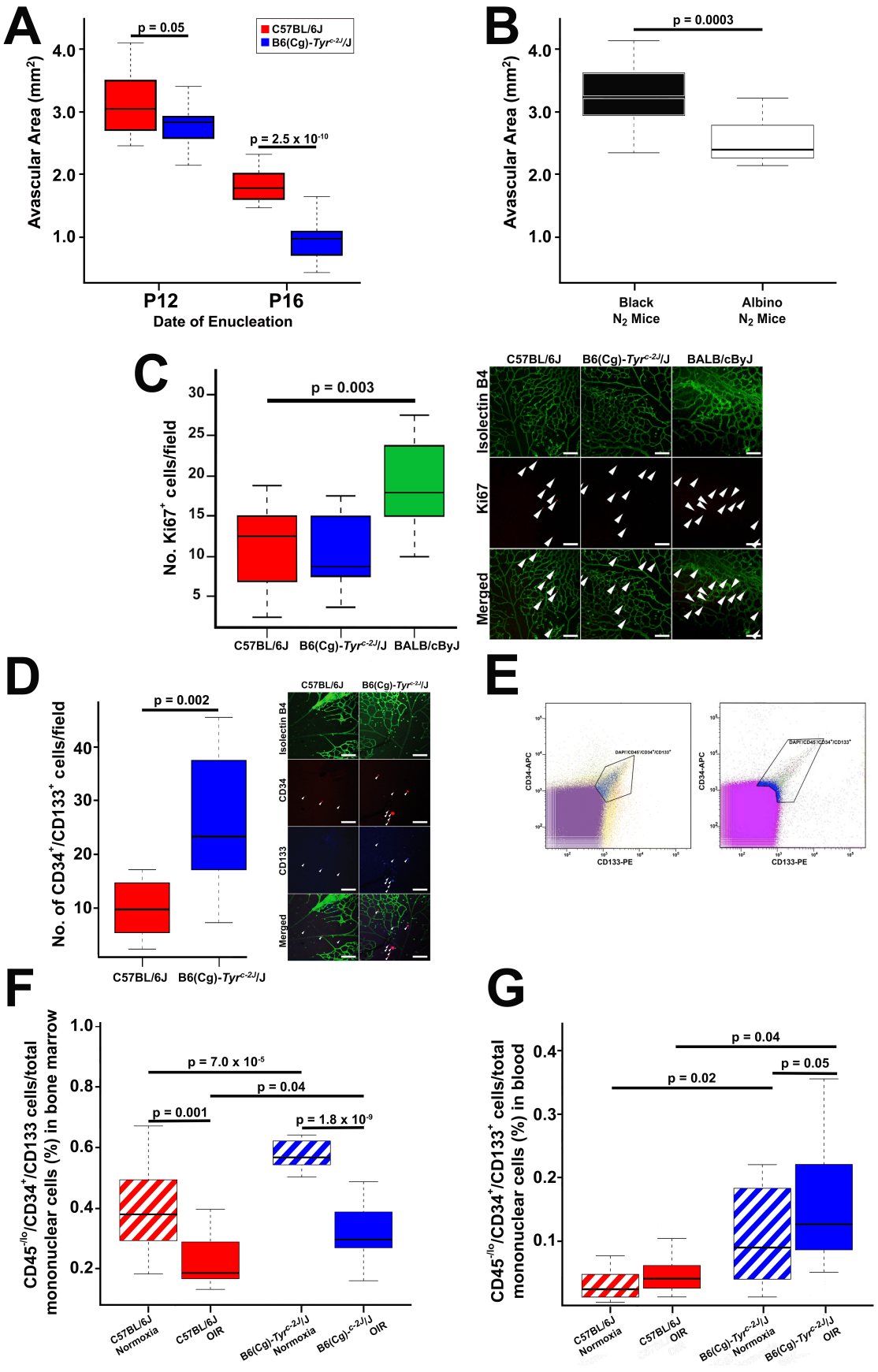
A
p = 0.05
C57BL/6J
B6(Cg)-Tyrc-2J/J
p = 2.5 x 10-10
Avascular Area (mm2)
4.0
3.0
2.0
1.0
P12
P16
Date of Enucleation
B
p = 0.0003
Avascular Area (mm2)
4.0
3.0
2.0
1.0
Black
N2 Mice
Albino
N2 Mice
C
p = 0.003
No. Ki67+ cells/field
30
25
20
15
10
5
C57BL/6J
B6(Cg)-Tyrc-2J/J
BALB/cByJ
C57BL/6J
B6(Cg)-Tyrc-2J/J
BALB/cByJ
Isolectin B4
Ki67
Merged
D
p = 0.002
No. of CD34+/CD133+ cells/field
40
30
20
10
C57BL/6J
B6(Cg)-Tyrc-2J/J
C57BL/6J
B6(Cg)-Tyrc-2J/J
Isolectin B4
CD34
CD133
Merged
E
CD34-APC
CD133-PE
CD34-APC
CD133-PE
F
p = 7.0 x 10-5
p = 0.04
p = 0.001
p = 1.8 x 10-9
CD45-/lo/CD34+/CD133 cells/total mononuclear cells (%) in bone marrow
1.0
0.8
0.6
0.4
0.2
C57BL/6J Normoxia
C57BL/6J OIR
B6(Cg)-Tyrc-2J/J Normoxia
B6(Cg)-c-2J/J OIR
G
p = 0.04
p = 0.05
p = 0.02
CD45-/lo/CD34+/CD133+ cells/total mononuclear cells (%) in blood
0.4
0.3
0.2
0.1
C57BL/6J Normoxia
C57BL/6J OIR
B6(Cg)-Tyrc-2J/J Normoxia
B6(Cg)-Tyrc-2J/J OIR

Figure 3.2. *Tyr* function is associated with reduced retinal revascularization and EPC recruitment.

(**A**) Avascular area in the central retina on P12 and P16. C57BL/6J mice (n =15 and 18, respectively) had larger avascular areas than *Tyr*-null c-2J (n =19 at both time points). The difference was greater and more significant at P16 (Student's t-test), suggesting *Tyr* modifies revascularization. (**B**) N_2 albino mice (n = 13) created in a (C57BL/6J x c-2J) x c-2J backcross had smaller avascular areas than pigmented littermates (n = 12). (**C**) No difference in number of proliferating ECs was found between C57BL/6J (n = 16) and c-2J retina (n = 10). (**D**) C57BL/6J mice (n = 7) had fewer CD34+/CD133+ cells recruited to the retina than c-2J (n = 11), with representative photomicrographs (arrowheads indicated double-positive cells). (**E**) Flow cytometry gates used to quantify DAPI-/CD34+/CD133+ EPCs as a fraction of all live, CD45-/lo/CD34+/CD133+ EPCs from BM (upper) and blood (lower). (**F**) C57BL/6J mice had fewer CD45-/lo/CD34+/CD133+ cells in the BM, both in normoxic and OIR conditions (n = 18 and 12, respectively) than c-2J (n = 13 and 18). (**G**) C57BL/6J mice have fewer circulating CD45-/dim/CD34+/CD133+ cells, both in normoxic and OIR conditions (n = 14 and 18, respectively) than c-2J mice (n = 16 and 19). Scale Bar: 100μm.

recruitment, we performed confocal microscopy. We co-stained with GS isolectin B4 and Ki-67 to quantify proliferation in ECs, or with isolectin, CD34 and CD133 to identify putative EPCs. No differences were found in frequency of EC proliferation between c-2J and C57BL/6J strains (10.4 vs. 11.4 cells/field, $p = 0.73$, Student's t-test). Interestingly, BALB/c mice have higher numbers of both EPCs and proliferating ECs than C57BL/6J (Figure 3.2C). However, c-2J mice have higher numbers of putative EPCs than C57BL/6J (27.0 vs. 10.0 cells/field, $p = 0.002$, Student's t-test) (Figure 3.2D).

Flow cytometric quantification of EPCs

We performed flow cytometry to detect DAPI-/CD45-/CD34+/CD133+ EPCs in bone marrow and in peripheral blood. In BM samples, c-2J mice had higher proportions of EPCs amongst their total mononuclear cells than did C57BL/6J mice both in normoxic conditions (0.61% vs. 0.40%, $p = 7 \times 10^{-5}$, Student's t-test) and after exposure to OIR (0.28% vs. 0.20%, $p = 0.04$, Student's t-test) (Figure 3.2E). Mice exposed to OIR had reduced fraction of EPCs in BM samples compared to normoxic controls in both strains (C57BL/6J – $p < 1 \times 10^{-4}$, Student's t-test; c-2J – $p < 1 \times 10^{-7}$, Student's t-test).

Similarly, c-2J mice had increased fraction of circulating EPCs compared to C57BL/6J both in normoxia (0.10% vs. 0.040%, $p = 0.02$, Student's t-test) and after OIR exposure (0.17% vs. 0.090%, $p = 0.04$, Student's t-test) (Figure 3.2F). However, OIR exposure led to an increase in the number of circulating EPCs compared to normoxic controls in both strains that did not reach statistical significance.

Serum DA concentration

Using HPLC-ED, c-2J mice were found to have approximately 75% lower serum concentration of DA than C57BL/6J (0.75 ng/mL vs. 2.92 ng/mL, p = 0.01, Student's t-test) (Figure 3.3A), confirming data from other studies suggesting that *Tyr* contributes to peripheral DA production early in murine life.

DA receptor expression

Whole (unsorted) BM samples expressed gene transcripts for D1, D4, and D5 (Table 3.2). Sorted CD45-/CD34+/CD133+ EPCs from mice of both strains also expressed these receptors, and had greater expression of these DA receptors than did non-hematopoietic, non-EPC BM cells. Expression of D2 and D3 was very low or undetectable in all sample types from mice of both strains.

Inhibition of revascularization by DA through Drd1/5

Intraperitoneal DA administration reduced retinal revascularization in both the C57BL/6J (3.71 vs. 3.43 mm^2, p = 0.01, Student's t-test) and c-2J strains (3.28 vs. 2.96 mm^2, p = 0.006, Student's t-test) (Figure 3.3B). DA treatment was additionally associated with reduced EPC recruitment to the retina in both strains (C57: 7.7 vs. 14.4 cells/field, p = 0.008, Student's t-test; c-2J: 12.9 vs. 29.3 cells/field, p = 0.005, Student's t-test) (Fig. 2C).

Administration of SCH39166, a D1 and D5 antagonist, in C57BL/6J mice resulted in improved resistance to OIR. Retinal avascular area 24 hours after administration was significantly smaller than in control saline-treated littermates (3.69 mm^2 vs. 4.04 mm^2, Student's t-test, p = 0.029, Figure 3.4A). This finding was associated with improved

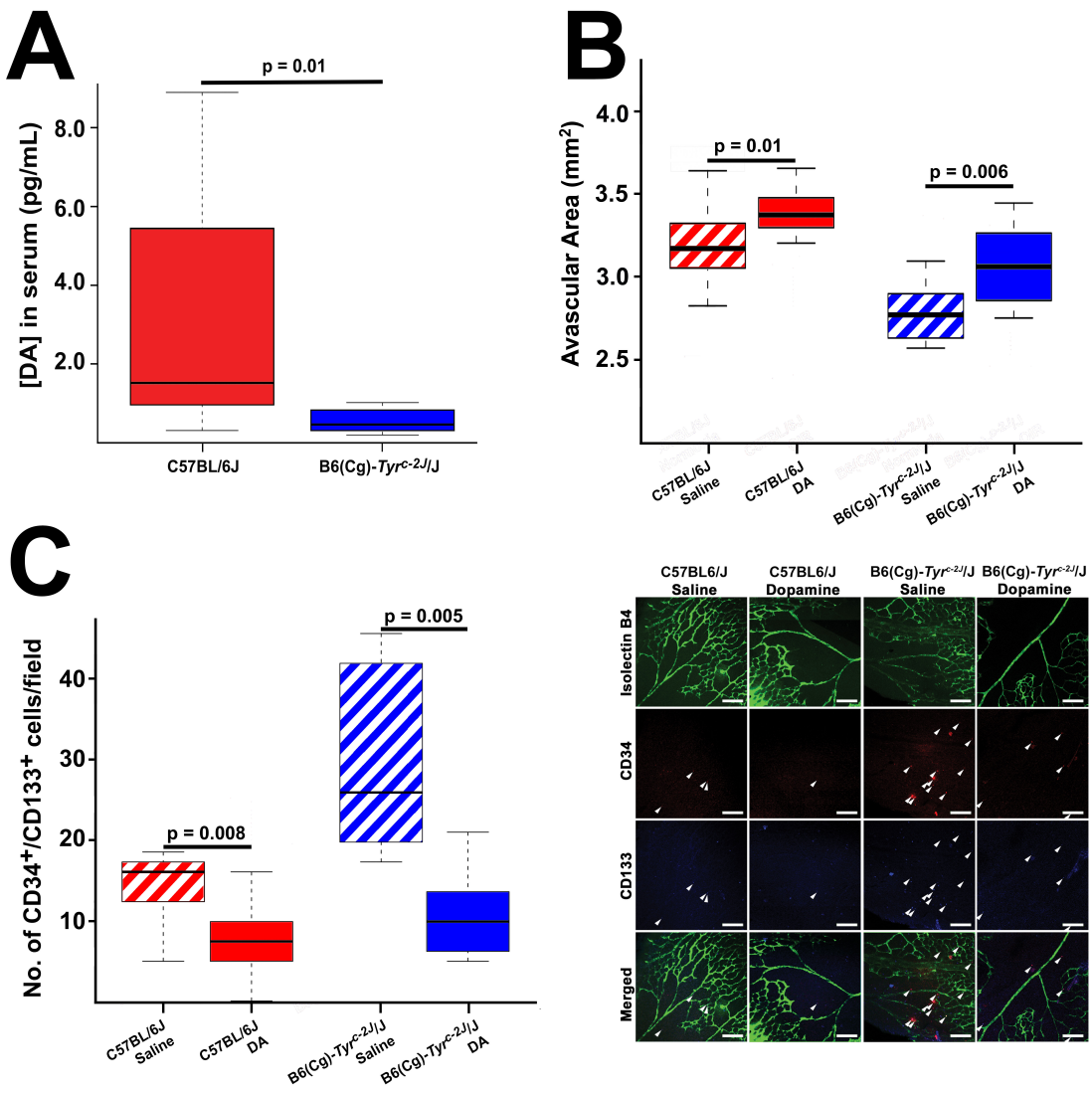
A
p = 0.01
[DA] in serum (pg/mL)
8.0
6.0
4.0
2.0
C57BL/6J
B6(Cg)-Tyrc-2J/J
B
Avascular Area (mm2)
4.0
3.5
3.0
2.5
p = 0.01
p = 0.006
C57BL/6J Saline
C57BL/6J DA
B6(Cg)-Tyrc-2J/J Saline
B6(Cg)-Tyrc-2J/J DA
C
No. of CD34+/CD133+ cells/field
40
30
20
10
p = 0.005
p = 0.008
C57BL/6J Saline
C57BL/6J DA
B6(Cg)-Tyrc-2J/J Saline
B6(Cg)-Tyrc-2J/J DA
C57BL6/J Saline
C57BL6/J Dopamine
B6(Cg)-Tyrc-2J/J Saline
B6(Cg)-Tyrc-2J/J Dopamine
Isolectin B4
CD34
CD133
Merged

Figure 3.3 DA inhibits EPC recruitment and retinal revascularization.
(**A**). C57 mice (n = 15) had greater levels of serum DA than *Tyr*-null c-2J mice (n = 8). (**B**) Intraperitoneal injection of DA (50mg/kg) was associated with increased avascular area compared to vehicle control mice for both the C57BL/6J strain (control, n = 15; DA, n = 12) and the c-2J (control, n = 11; DA, n = 12). (**C**) DA administration was also associated with decreased recruitment of CD34+/CD133+ EPCs to the retina for both the C57BL/6J (control, n = 13; DA, n = 9) and the c-2J strains (n = 9 for both groups), with representative photomicrographs (arrowheads indicated double-positive cells). Scale Bar: 100μm.

Δ Ct (Ct_{gene} - C_{S16})

	C57BL/6J			**B6(Cg)-*Tyr^{c-2J}*/J**		
	Unsorted Bone Marrow	**Sorted Bone Marrow**		**Unsorted Bone Marrow**	**Sorted Bone Marrow**	
		CD45-/ CD34+/ CD133+	CD45-/ CD34-/ CD133-		CD45-/ CD34+/ CD133+	CD45-/ CD34-/ CD133-
Dopamine receptor 1	1.63	-1.98	0.35	4.39	-1.87	-1.72
Dopamine receptor 2	16.08	ND	ND	17.24	ND	ND
Dopamine receptor 3	14.04	ND	ND	ND	ND	ND
Dopamine receptor 4	2.32	-3.42	-0.84	4.91	-5.31	1.77
Dopamine receptor 5	2.27	-1.32	-0.68	5.62	-4.04	3.20
Tyrosinase	1.31			1.94		

Table 3.2. rt-PCR results of DA receptor gene expression in 3 BM cell populations.
BM from an entire litter was pooled to generate individual samples. Data from unsorted, whole BM was derived from 3 litters per strain. Data from sorted cells were collected from one litter of each strain. The data presented are ΔCt values. EPCs from both strains demonstrate greater expression of D1, D4, and D5 compared to non-hematopoietic, non-EPC BM cells. Expression of D2 and D3 was very low or undetectable in all sample types, and is indicated as "ND" . Blank cells indicate that the test was not performed on the given sample.

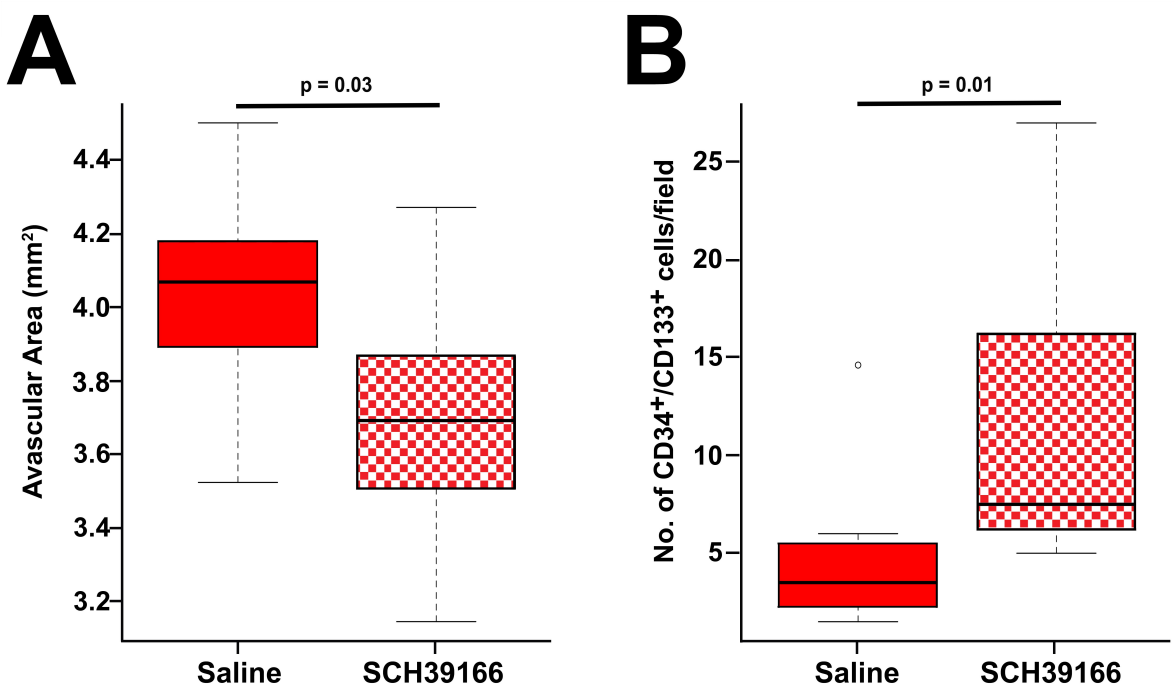
A
p = 0.03
Avascular Area (mm²)
4.4
4.2
4.0
3.8
3.6
3.4
3.2
Saline
SCH39166
B
p = 0.01
No. of CD34⁺/CD133⁺ cells/field
25
20
15
10
5
Saline
SCH39166

Figure 3.4. DA signals through D1/5 to inhibit retinal revascularization and EPC recruitment.
(**A**) Treatment of C57BL/6J mice with D1/5 antagonist SCH39166 (n = 10) resulted in improved retinal revascularization compared to saline-treated controls (n = 8). (**B**) Administration of SCH39166 in C57BL/6J mice was also associated with increased recruitment of CD34+/CD133+ EPCs to the retina compared to vehicle-treated control littermates (n = 11, both groups).

recruitment of CD34+/CD133+ EPCs to the retina at this time point (11.55 vs. 4.55 cells/field, Student's t-test, p = 0.01, Figure 3.4B). Testing of D2 and D4 antagonists in C57BL/6J mice showed no difference in avascular area compared to control-treated littermates (data not shown).

DISCUSSION

ROP is a significant and growing cause of vision loss in children. The etiology and pathophysiology of ROP are complex and incompletely understood. In particular, the factors that determine whether ROP in an individual patient will spontaneously resolve or progress to severe, vision-threatening vasoproliferation are only partially determined (Coats, 2005; Lofqvist, Hansen-Pupp et al., 2009). We performed genome wide mapping using murine OIR, a model of ROP, in order to identify pathways that may influence the rate of physiological retinal vascularization after an oxidative insult. In our earlier genetic work, we mapped loci that influenced the extent of central retinal vaso-obliteration 4 days after mice were removed from the normoxic environment (O'Bryhim, Radel et al., 2012). Since the mouse strains that we used, C57BL/6J and BALB/cByJ, show only small differences in vaso-obliteration immediately after removal from the hyperoxic environment (Dorrell, Aguilar et al., 2010), we anticipated that any genetic loci found would predominantly affect the revascularization process. The principal QTL identified in this experiment, with a LOD score of 9.83, was on chromosome 7 and included the *Tyr* gene. This result supported experiments in the rat model (van Wijngaarden, Brereton et al., 2007) that identified *Tyr* or a linked gene as a modifier of avascular area in OIR. The studies described here confirm the role of *Tyr* in modulation of OIR and demonstrate a mechanism by which it alters disease susceptibility.

We compared B6(Cg)-*Tyr*$^{c-2J}$/J *Tyr* null mice with C57BL/6J, the appropriate *Tyr* wild-type background strain, to demonstrate that *Tyr* inactivity was associated with increased retinal revascularization. A backcross confirmed that the genetic locus surrounding *Tyr* was responsible for this effect. It is possible but unlikely that a further spontaneous mutation has arisen that is linked to *Tyr* and has an effect on revascularization.

Experiments using proliferation markers suggested that *Tyr* exerted an effect independent of vascular EC proliferation. Therefore we sought differential effects on EPCs using CD34, which has previously been used to identify this cell population in murine retinae (Lofqvist, Chen et al., 2007) and in mice identifies a population that includes highly functional EPCs (Yang, Ii et al., 2011), and CD133 which identifies tissue EPCs in mice (Balasubramaniam, Mervis et al., 2007; Suriano, Chaudhuri et al., 2008; Zeng, Li et al., 2012). Confocal microscopy found a significant difference in CD34+/CD133+ EPCs between *Tyr* wild-type and null retinae. Subsequent investigations found that CD45-/CD34+/CD133+ cells were also more common in BM and peripheral blood of *Tyr* null mice than wild-type mice. Further experiments will demonstrate whether there are also differences in retinal recruitment of other BM-derived angiogenic cells, and whether there are functional differences in circulating EPCs that can be demonstrated in tissue culture.

Previously published studies (Rios, Habecker et al., 1999; Eisenhofer, Tian et al., 2003), show that *Tyr* function in the C57BL/6J strain contributes to increased serum DA concentration compared to *Tyr*-null c-2J mice. We confirmed that this effect is also seen after mice are exposed to hyperoxia in the OIR model. Administration of exogenous DA in c-2J mice inhibits recruitment of EPCs and decreases revascularization compared to vehicle-

treated controls, such that their response to OIR is similar to that of C57BL/6J mice. Treatment in the C57BL/6J strain further delayed vascular regeneration.

Subsequent pharmacological studies suggest that dopaminergic regulation of this process occurs via the D1-like family of receptors. This family includes D1 and D5. SCH39166 is an antagonist of both receptors; administration of this drug in C57BL/6J mice resulted in increased recruitment of EPCs and decreased avascular area 24 hours later. Due to the large amount of sequence homology between D1 and D5, currently available pharmacological agents have limited selectivity between the receptors.

Studies in an adult murine tumor model have suggested that DA inhibits CD45-/VEGFR2+/CD34+ EPC recruitment via D2 (Chakroborty, Chowdhury et al., 2008). Work by Spiegel, *et al.* indicated that EPC receptor expression was dynamic, and that expression of D3 and 5 on EPCs was up-regulated after stimulation with granulocyte colony stimulating factor (Spiegel, Shivtiel et al., 2007). It is possible that the presence of cytokines or other growth factors in young mice may influence DA receptor expression and therefore their response to DA.

The possibility that DA may inhibit recruitment of EPCs to the retina in human neonates requires further investigation in order to determine DA's safety in the setting of neonatal intensive care units. Intravenous infusion of DA is used pharmacologically to treat systemic hypotension that is resistant to volume expansion. An association between DA treatment and increased risk of ROP in premature infants has been found (Mizoguchi, Chu et al., 1999). However, multivariate analysis suggested that the apparent effect of DA in univariate analyses was explained by other known risk factors for ROP (Allegaert, Cossey et al., 2004). In light of the current data, further investigation of the impact of DA on EPCs in

premature neonates is required, and increased screening efforts for infants who receive DA infusions may be warranted.

CONCLUSIONS

This study is the first to demonstrate that that dopaminergic signaling modulates retinal revascularization, and is the first evidence that *Tyr* modifies this system. Further research will determine whether these findings have relevance to the control of vascular regeneration in other retinal vasculopathies, and especially in diabetic retinopathy. Further studies will be required to determine whether selective DA antagonists may improve EPC function and recruitment in premature human neonates, thus mitigating the arrest of retinal vascular development in early ROP, consequently leading to reduced vascular proliferation and improved visual outcomes.

CHAPTER 4

TIME COURSE ANALYSIS OF ENDOTHELIAL PROGENITOR CELL RECRUITMENT IN OXYGEN INDUCED RETINOPATHY

ABSTRACT

New evidence suggests that EPCs contribute to the development of ROP, a leading cause of blindness in infants. This study seeks to characterize their involvement in ROP using C57BL/6J and *Tyr*-null c-2J mice in the murine OIR model. The number of live, CD45-/CD34+/CD133+ putative EPCs was quantified in BM and blood using flow cytometry. CD34+/CD133+ cells in retina were measured using confocal microscopy. Avascular area was measured from GS isolectin B4-stained retinal flat-mounts. Data was collected on P7, P7.5, P8, P9, P9.5, P10, P11, P12, and P13. In the C57BL/6J strain, overall numbers of CD45-/CD34+/CD133+ cells increase in the bone marrow by P9 and then gradually decline through P13. Circulating cells follow a sinusoidal pattern, whereas recruitment of this population to the retina does not greatly vary from normoxic numbers. c-2J mice have increased numbers of CD45-/CD34+/CD133+ cells in the bone marrow through P11. The number of cells in circulation increases significantly upon exposure to hyperoxia but drop to normoxic baseline levels by P8, and subsequently increase throughout the remainder of the study. Recruitment of CD34+/CD133+ cells to the retina peaks at P9 and stabilizes at lower levels through the remainder of the study. Avascular area increases from P7 through P9 and then plateaus. CD34+/CD133+ putative EPCs are a dynamic population of cells that appear to initially respond to hyperoxia from P7 through P9. Retinal vascularization and EPCs patterns change at approximately P9 in the c-2J strain and P11 in the C57BL/6J strain. This suggests that the traditional time points used to characterize OIR should be reconsidered, especially in the context of delivering pharmacological agents to modify EPC response.

LIST OF ABBREVIATIONS

ANOVA – analysis of variance
BM – bone marrow
c-2J – B6(Cg)-*Tyr*$^{c-2J}$/J
D2 – dopamine receptor 2
DA - dopamine
EC – endothelial cell
EPC – endothelial progenitor cell
ISHAGE - International Society for Hematotherapy and Graft Engineering
OIR – oxygen-induced retinopathy
NV – neovascularization
P – post-natal day
ROP – Retinopathy of Prematurity
Tyr – Tyrosinase
VEGFR2 – vascular endothelial growth factor 2

PURPOSE

ROP is a leading cause of visual impairment in the pediatric population (Hartnett, 2010). This disease occurs when an infant is born prior to the completion of the retinal vascular system. The relative hyperoxia of the extrauterine environment arrests further vascular development, the first stage of ROP. As the child matures and the retina becomes more metabolically active, the resulting avascular areas subsequently become ischemic and can lead to the second stage of ROP, which is characterized by pathological NV.

Processes in the pathogenesis of ROP can be investigated using a mouse OIR model (Smith, Wesolowski et al., 1994; Lutty, Chan-Ling et al., 2006). Our prior work (O'Bryhim, Radel et al., 2012) and that by others (Dorrell, Aguilar et al., 2010) have documented differences in response to OIR between inbred strains of mice. Notably, we identified an association between *Tyr* function in the C57BL/6J strain and increased susceptibility to OIR compared to *Tyr*-null c-2J mice of the same genetic background, as described. These findings are in line a backcross in rats that found *Tyr*-null albino N_2 rats to be more resistant to OIR compared to pigmented littermates (van Wijngaarden, Brereton et al., 2007). The responses of these strains may serve as a model for differences in susceptibility to ROP in humans.

EPCs contribute to post-natal angiogenesis in wound healing (Asahara, Murohara et al., 1997), tumor metastases (Asahara, Masuda et al., 1999), and in tissue remodeling (e.g. diabetes mellitus) (Fadini, Agostini et al., 2005; Gallagher, Liu et al., 2007). EPCs are BM-derived cells that constitute a subpopulation of mononuclear cells (Case, Ingram et al., 2008). Murine EPCs are commonly defined as cells that express surface markers CD34 (Asahara, Masuda et al., 1999; Sekiguchi, Ii et al., 2011; Yang, Ii et al., 2011), CD133 (Balasubramaniam, Mervis et al., 2007; Zeng, Li et al., 2012; Zeng, Ding et al., 2012), VEGFR2

(Sekiguchi, Ii et al., 2011), and Sca-1 (Nakagawa, Masuda et al., 2011; Yang, Ii et al., 2011). As no EPC-specific markers have been identified to date, there is considerable discrepancy over the exact definition of this cell population (Case, Ingram et al., 2008)

Recent evidence suggests that this cell population also plays a role in the development of ROP. Work by Ligi and colleagues suggests that EPCs isolated from very-low birth weight infants have altered gene expression and functional changes that discourage angiogenesis, although no statistically significant difference were found in the quantity of circulating CD34+ EPCs (Ligi, Simoncini et al., 2011). Machalinska, *et al.,* however, found an increase in number of circulating CD144 (VE-Cadherin)+/CD133+/CD34+ EPCs in infants with Phase 2 ROP compared to premature infants without ROP and compared to term infants (Machalinska, Kotowski et al., 2011).

It is likely that differences in the various sets of published results are related to the time at which EPCs are examined in relation to the stage of disease. Therefore, we sought to characterize changes in EPC recruitment and angiogenesis over the course of OIR. We additionally examined EPC patterns in both resistant and susceptible strains of mice to compare patterns that contribute to a more or less successful vascular response. This allows for a comprehensive assessment of the dynamic role of EPCs in OIR, which will both elucidate their role in disease progression and will also serve to optimize time points for future studies targeting this cell population.

MATERIALS AND METHODS

Animals

All experimental procedures were approved by University of Kansas Medical Center Institutional Animal Care and Use Committee. C57BL/6J and B6(Cg)-*Tyr*$^{c-2J}$/J mice were purchased from Jackson Laboratories (Bar Harbor, ME). All mice were kept in a 12-hour light, 12-hour dark cycle with ambient room temperature between 19°C and 22°C. Mice were kept on standard breeding pair diet (8626 rodent diet; Harlan Laboratories, Indianapolis, IN), with food and water available ad libitum.

Oxygen-Induced Retinopathy

OIR was induced according to established protocols (Smith, Wesolowski et al., 1994) by exposing pups to 75% oxygen beginning on P7. Mice were returned to normoxia either immediately prior to sacrifice, or after 120 hours of exposure (P12). O_2 levels in the chambers were continuously controlled using a ProOx portable monitor (Biospherix, Redfield, NY), which was calibrated monthly using 100% O_2 and room air (~21%).

Tissue Harvest

Mice were weighed and anesthetized with a lethal dose of tribromoethanol delivered by intraperitoneal injection at the following time points: P7 (prior to exposure to hyperoxia), P7.5, P8, P9, P9.5, P10, P11, P12, and P13 (24 hours after return to normoxia). After induction of anesthesia, blood samples were collected by puncturing the left ventricle with 27 G needle; samples were incubated in 3x volume of RBC lysis buffer (Biolegend, San Diego, CA) according to instructions, centrifuged at 300 g, and resuspended in 1 mL 1% BSA

in PBS (Balasubramaniam, Mervis et al., 2007). BM was harvested from both femurs and tibias by removing the ends of each bone and aspirating the contents with 200 μL of Hank's Balanced Salt Solution (Sigma, St. Louis, MO, USA). Mice were subsequently enucleated and eyes were stored overnight in 4% PFA at 4°C.

Flow Cytometry

Bone marrow and blood samples were filtered through a 70 μM mesh filter and subsequently centrifuged at 300 g for 10 minutes at 4°C. Given the rarity of EPCs, BM and blood samples were stained for flow cytometric analysis of EPCs using modifications of the ISHAGE protocol as previously described (Balasubramaniam, Mervis et al., 2007). This procedure has been used to successfully isolate $CD133^+$ progenitor cells from small (100 μL) samples of both BM and blood. Samples were incubated in CD45-FITC (Biolegend, San Diego, CA), CD34-APC (Biolegend, San Diego, CA), CD133-PE (Biolegend, San Diego, CA) for 30 minutes on ice. Cells were washed with 1% BSA, centrifuged at 300 g for 10 minutes, and resuspended in DAPI (Sigma, St. Louis, MO) for 10 minutes to detect dead cells. After a final wash and spin, samples were resuspended in 1% BSA and analyzed at the University of Kansas Medical Center Flow Cytometry Core with a Beckman LSRII Flow Cytometer (Miami, FL). Single-stain (positive) controls and negative controls were used to set the gates and determine voltage compensation for fluorescent intensity. A minimum of 1,000,000 cells was counted from each sample, and samples were run until 3,000,000 cells were counted or the sample was exhausted. As previously described (Balasubramaniam, Mervis et al., 2007), cells were gated to exclude DAPI positive dead cells, and then gated to select for the non-

hematopoietic CD45-/dim population. Of these, CD133 and CD34 double positive cells were counted as a percentage of all live, non-hematopoietic cells.

Retinal Avascular Area and Immunofluorescent Staining

Retinas from both eyes were dissected and stained with *Griffonia simplicifolia* isolectin B4 (Sigma, St. Louis, MO) according to established protocols (Gerhardt, Golding et al., 2003). Briefly, retinae were permeablilized overnight in 0.5% Triton X-100, 1% BSA at 4°C. After washing, retinae were incubated in 20 μg/mL isolectin in PBLec (PBS, pH 6.8, 1% Triton X-100, 0.1 mM $CaCl_2$, 0.1 mM $MgCl_2$, 0.1 mM $MnCl_2$) overnight at 4°C.

Retinae from left eyes of each mouse were then washed and flat-mounted using anti-fade medium (Southern Biotech, Birmingham, AL). Immunofluorescent micrographic images of the retinas were taken using an SMZ 1500 microscope (Nikon, Tokyo, Japan) and MagnaFire Camera and software (Optronics, Goleta, CA). ImageJ software (http://rsbweb.nih.gov/ij/) was used to manually trace and measure avascular areas.

Retinae from right eyes were washed and blocked with Superblock (ThermoScientific, Rockford, IL) for 1 hour at room temperature, followed by incubation in 1:100 hamster anti-murine CD34 and 1:200 rat anti-murine CD133 (Biolegend, San Diego, CA) ON at 4°C. After washing with PBS, retinae were incubated with 1:200 Dylight 649 anti-hamster IgG and 1:400 Texas Red anti-rat IgG for 1 hour at room temperature, washed, and flat-mounted.

Statistical Analysis

Analyses were performed using R software package. Statistical comparisons between time points were made using Two-Way ANOVA tests with pairwise comparisons; comparisons between strains were made using Student's t-test at each time point. $P < 0.05$ was considered statistically significant. Data are expressed graphically as modified boxplots, where the box represents the median, first and third quartiles. The "whiskers" represent 1.5 times the interquartile range, and data points outside of this range are denoted as open circles. Asterisks indicate statistically significant differences in value compared to the value observed on P7.

RESULTS

BM CD45-/CD34+/CD133+ Cells

At all time points examined, c-2J mice had more BM EPCs than did C57BL/6J mice (Figure 4.1A). This difference reached significance at all time points except P7.5 and P9. In the C57BL/6J strain, CD45-/CD34+/CD133+ numbers initially increased within 12 hours of exposure to hyperoxia but subsequently declined to below normoxic levels by P8. The number of putative EPCs increased 2.5-fold from P8 to P9 and then declined through P13.

The response of the bone marrow CD45-/CD34+/CD133+ population to hyperoxia differed between C57BL/6J and c-2J mice; in c-2J the fraction of putative EPCs gradually increased 30% from P7 through P9. After a slight decrease over the next 12 hours, the number of EPCs then rose to a maximum on P11, but, similar to patterns in C57BL/6J BM, declined significantly in the last days of the experiment.

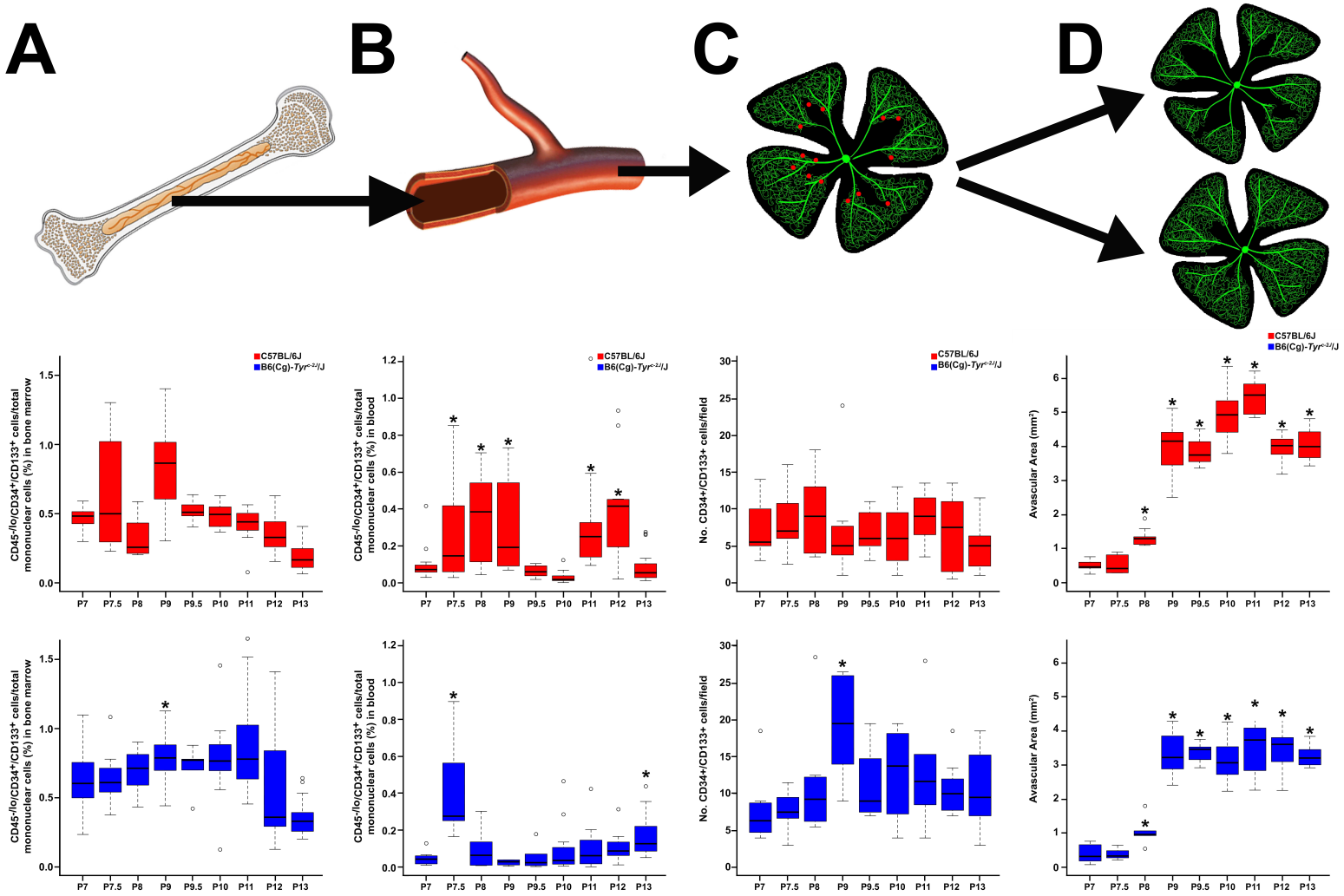
A
B
C
D
C57BL/6J
B6(Cg)-Tyrc-2J/J
CD45-/loCD34+/CD133+ cells/total mononuclear cells (%) in bone marrow
CD45-/loCD34+/CD133+ cells/total mononuclear cells (%) in blood
No. CD34+/CD133+ cells/field
Avascular Area (mm2)
P7
P7.5
P8
P9
P9.5
P10
P11
P12
P13

Figure 4.1. Response of EPCs in BM, blood and retina and changes in avascular area during OIR in C57BL/6J and c-2J mice.
(**A**) Patterns of CD34+/CD133+ EPCs present in the BM of C57BL/6J ad c-2J mice during the OIR model. c-2J mice had more BM putative EPCs than did C57BL/6J mice at all time points except P7.5 and P9. (**B**) Patterns of CD34+/CD133+ EPCs present in the blood of C57BL/6J and c-2J mice during the OIR model. Cells in circulation of C57BL/6J mice followed a sinusoidal pattern; in the c-2J strain, cell numbers increased significantly in response to exposure to hyperoxia, declined to a minimum and then rose during the remainder of the study. (**C**) Patterns of CD34+/CD133+ EPCs recruited to the retina of C57BL/6J mice during the OIR model. The number of recruited cells did not vary greatly from values seen on P7 in the C57BL/6J strain. The c-2J strain had a significant increase in cells on P9. (**D**) Central avascular area of C57BL/6J and c-2J mice during the OIR model. C57BL/6J mice had greater avascular area at all time points. Both strains respond to initial exposure to hyperoxia similarly. Differences in avascular area do not reach statistical significance until P9. Data are presented as modified box plots; open circles represent outlying data points. Asterisks denote statistically significant differences compared to values at P7 (Two-way ANOVA with pair wise comparison, $p < 0.05$).

Circulating CD45-/CD34+/CD133+ Cells

The size of the circulating CD45-/CD34+/CD133+ cell population was volatile in both strains (Figure 4.1B). In C57BL/6J mice, the cell fraction increased from P7 through P8 and then declined to a minimum on P10. The number of cells increased to a maximum 48 hours later, on P12. One day after return to normoxia, however, the number of EPCs dropped 80%. In the c-2J strain, the number of circulating cells increased 10-fold in the first 12 hours of exposure to hyperoxia but dropped by P8 and continued to decline to a minimum on P9. The number steadily rose during the last 4 days of the study.

In the c-2J strain, the number of circulating CD45-/CD34+/CD133+ cells substantially increased upon exposure to hyperoxia, but then subsided by P8 and dropped further by P9. After P9, the number of circulating cells increased steadily through the rest of the study. c-2J mice had fewer circulating cells compared to C57BL/6J mice at most time points tested, except at P7.5, P10, and P13. This difference between strains reached statistical significance at all time points except P7.5 and P10.

Retinal CD34+/CD133+ Cells

The pattern of CD34+/CD133+ cell recruitment to the retina varied largely between the strains of mice (Figure 4.1C). In the C57BL/6J strain, there were no statistically significant differences in cell numbers over time, although a small increase was seen from P10 to P11. In c-2J mice significant recruitment occurred between P8 and P9, and thereafter CD34+/CD133+ cell numbers subsided to near the level seen on P8. c-2J mice had more EPCs in the retina at all time points except P7.5. The difference reached significance on P9, P9.5, P10, and P13.

Avascular Area

The initial vaso-obliterative response was nearly identical in the two strains. There was no significant difference in avascular area between un-exposed mice at P7 (Figure 4.1D). No vaso-obliteration was apparent in either strain 12 hours after exposure to hyperoxia. In the following 36 hours, however, the central avascular area had increased approximately 8 times compared to the area at P7 in both strains. This difference reached statistical significance on P9, and avascular areas then diverged between the strains. In the C57BL/6J mice, the central avascular area continued to increase peripherally to a maximum on P11. The retina began to revascularize after this time point as avascular area decreased 27% by P12. In the c-2J strain, the central area increased only until P9. After P9, the avascular area remained relatively stable with a small increase (10%) between P10 and P11 and subsequent decrease following return to normoxia.

Weight

The patterns of change in weight over the time course of the experiment were very similar in C57BL/6J and c-2J mice (Figure 4.2). By P11, both strains gained approximately 150% of their weight at P7. Weight plateaued from P11 to P12 and then decreased significantly upon return to normoxia. At all time points except P9.5, the C57BL/6J mice weighed more than their c-2J counterparts. However, this difference was statistically significant only on P8; it is likely that the significance of this is related to the use of a c-2J litter that contained 12 pups, all of which were of small size.

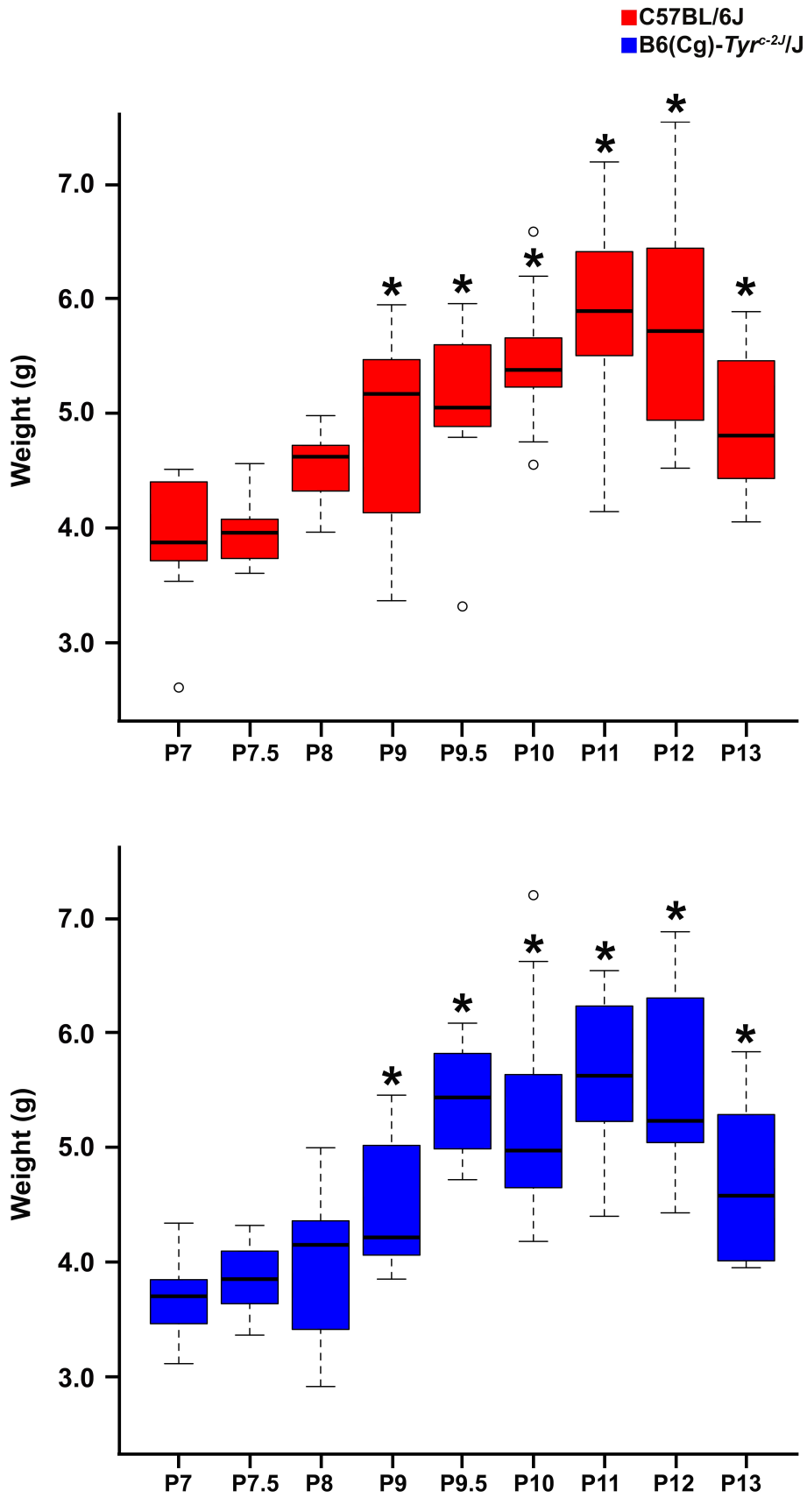
C57BL/6J
B6(Cg)-Tyr^c-2J/J
Weight (g)
7.0
6.0
5.0
4.0
3.0
P7
P7.5
P8
P9
P9.5
P10
P11
P12
P13

Figure 4.2 Weight of mouse pups throughout the OIR model.
Weight gain of C57BL/6J and c-2J mice from P7 through P13. Mice of both strains gained weight in a similar manner. Although C57BL/6J mice weighed more at every time point in the study, this difference was statistically significant only on P8. Data are expressed as modified box plots, and open circles denote outlying observations. Asterisks denote statistically significant differences compared to weight at P7 (Two-way ANOVA with pair wise comparison, $p < 0.05$).

DISCUSSION

EPCs play an important role in post-natal angiogenesis in both pathological and physiological processes (Asahara, Murohara et al., 1997). Recent reports suggest that EPC function is altered in pre-term and low-birth weight infants (Balasubramaniam, Mervis et al., 2007; Ligi, Simoncini et al., 2011; Machalinska, Kotowski et al., 2011; Safranow, Kotowski et al., 2012). As these infants are at risk of developing ROP (Good, Hardy et al., 2005), it is likely that alteration in EPCs function contributes to disease development. Early evidence in the murine OIR model of ROP supports this hypothesis (Lofqvist, Chen et al., 2007; Nakagawa, Masuda et al., 2011), but their role and significance have not been established. As these cells offer a potential pharmacological target for improving ROP outcome, a better understanding of their recruitment and participation in revascularization will allow more precise targeting. For these reasons, this observational study seeks to characterize EPC recruitment from the bone marrow to the retina as well as to compare patterns between susceptible and resistant strains of mice.

The C57BL6/J and c-2J mice were chosen for use in this study as they represent strains that are more or less susceptible to OIR, respectively. Our prior work indicated that c-2J mice revascularize more rapidly after exposure to hyperoxia compared to C57BL/6J, and that this improved response is associated with increased numbers of EPCs in the BM, blood, and retina at P13. This suggests that recruitment of these cells playa a role in improving outcomes after exposure to OIR.

Systemic differences in EPC mobilization may have consequences outside of the retina For example, data in a murine model of bronchopulmonary dysplasia suggests that EPCs are recruited to the developing lung (Balasubramaniam, Mervis et al., 2007). Effects on

other organ systems should therefore be evaluated when testing pharmacological agents that are designed to alter EPC proliferation, mobilization, or retinal recruitment.

The murine OIR model was developed by Smith and colleagues (Smith, Wesolowski et al., 1994) is traditionally divided into 2 phases: hyperoxia-induced vaso-obliteration from P7 to P12, and subsequent revascularization and NV upon return to normoxia on P12 until resolution, at approximately P25 (Smith, Wesolowski et al., 1994). However, our data measuring avascular area, in conjunction with a previously published report (Lange, Ehlken et al., 2009), suggest that the vaso-obliterative phase terminates several days prior to the customary endpoint. Moreover, changes in CD34+/CD133+ cells in the bone marrow, circulating blood, and retina related to recovery from hyperoxic stress and vascular regeneration also start to occur prior to removal of the mice from the hyperoxic environment.

In the c-2J strain, the shift from vaso-obliteration to vascular regrowth occurs between P8 and P9. After P9, putative EPC numbers increase in blood and BM, while in the retina both avascular area and the number of retinal CD34+/CD133+ cells plateaus. The inhibition of further vaso-obliteration is possibly due to protection by the recruited cells, or may represent a balance between continued vessel destruction and newly initiated vascular regeneration, with the recruited cells likely playing a role.

In the C57BL/6J strain, the transition from the acute response to hyperoxia to a recuperative response occurs later, and the timing varies between the tissues studied. Peripherally, EPCs appear to undergo a shift in behavior at P9.5 or P10. In the BM, this change from a volatile pattern to one of gradual and steady decline occurs at P9.5. The number of mobilized EPCs follows a sinusoidal pattern that reaches a minimum at P10.

Within the retina specifically, this transition appears to occur when the avascular area reaches its maximum at P11, which coincides with the maximal recruitment of CD34+/CD133+ cells to the retina. As in the c-2J strain, it is likely that avascular area begins to decline as recruited cells contribute to the developing vessels in the revascularizing retina.

Retinal avascular area data from Lange, *et al*. show that revascularization commences at P10 for C57BL/6J mice (Lange, Ehlken et al., 2009), a day earlier than found in our study. It is likely that subtle differences in the execution of the OIR model between different laboratories are responsible for this difference. It is also possible that genetic differences responsible for this change in phenotype have arisen between the C57BL/6J strains held by Charles River and the Jackson Laboratories, respectively the sources of Lange's and our mice.

It is difficult to draw conclusions regarding the role of EPC mobilization on OIR outcome due to the volatility of this population during the 6-day period of study. The number of circulating EPCs increases within 12 or 24 hours after exposure to hyperoxia in both strains of mice. This finding supports previous reports from mice exposed to hyperbaric oxygen chamber (Gallagher, Liu et al., 2007). As there are no other published reports characterizing EPCs over time in response to a disease, no comparisons between changes in this population in OIR and other disease models can be made.

Our prior work performed at P13 and two additional reports (Rios, Habecker et al., 1999; Eisenhofer, Tian et al., 2003) indicate that *Tyr* function contributes to peripheral production of dopamine (DA). Studies on the role of DA on EPC function have been conflicting; in tumor models, administration of high doses of DA resulted in reduced

numbers of circulating CD45-/CD34+/CD133+ EPCs in adult C57BL/6J mice (Chakroborty, Chowdhury et al., 2008). Conversely, circulating EPCs stimulated with cytokines prior to collection had increased proliferative capacity when subsequently treated with DA *in vitro,* suggesting that receptor expression by EPCs is dynamic and influenced by cytokines (Spiegel, Shivtiel et al., 2007). It is feasible that consistent exposure of cells to physiological levels of DA as opposed to a short course of DA administered at supraphysiological doses alters the ability of EPCs to be recruited from the circulation into vascularizing tissues. This may explain the reduced recruitment of CD34+/CD133+ cells to the retina despite greater number of circulating cells compared to the c-2J strain. Alternatively, the growth factors present in developing mice may alter EPC mobilization. As the growth factor milieu would change both as the mouse grows and in response to hyperoxic stress, this may account for variability in the number of circulating EPCs over time.

Birth weight and post-natal growth are known risk factors of ROP (Chen and Smith, 2008), and we were therefore interested to see if weight contributed to differences in susceptibility between strains. However, mice gained weight in a very similar pattern, indicating that weight was not responsible for differences in avascular area seen between C57BL/6J and c-2J mice. In both strains, pups lost a significant amount of weight upon return to normoxia. This change may be related to alterations in eating patterns of the pups or feeding behavior by the dam induced by the stress of returning to normoxia after 5 days at hyperoxic conditions.

CONCLUSIONS

This study describes a particular cell population that likely contains EPCs and characterizes their response to the OIR model in relation to changes in retinal avascular area. Our results have a number of lessons for further studies in OIR:

i) there appears to be an early phase of hyperoxic vaso-obliteration that is identical between C57BL/6J and c-2J mice, followed by a later phase of vaso-obliteration that our other work suggests can be protected against by a more adequate EPC response.

ii) OIR can no longer be considered a 2-stage process with vaso-obliteration followed by regeneration and revascularization in normoxia. Rather, there are several stages: early vaso-obliteration, late vaso-obliteration, EPC response in the presence of hyperoxia, EPC response in the presence of normoxia, and pathological vascularization. The duration of exposure to hyperoxia can be varied with a view to the phenomena being investigated. The timing of interventions can also be planned with this sequence in mind.

As improving retinal vascularization will decrease retinal hypoxia and subsequent NV, EPC recruitment may serve as a novel target for treatment for the prevention of ischemic retinopathies such as ROP.

CHAPTER 5

IDENTIFICATION OF GENES AND PATHWAYS ASSOCIATED WITH DIFFERENTIAL RETINAL RESPONSES TO HYPOXIA IN THE MURINE OXYGEN INDUCED RETINOPATHY MODEL

ABSTRACT

Using microarray analysis, this study compares the retinal transcriptional response of BALB/cByJ and C57BL/6ByJ mice exposed to OIR. These strains were chosen to identify gene expression patterns associated with OIR resistance or susceptibility, respectively. Total retinal RNA was isolated at P13 from mice from 3 different litters of each strain from both normoxic control mice and mice exposed to the OIR model. The expression of 69 gene transcripts was significantly altered in C57BL/6ByJ mice exposed to OIR compared to normoxic controls. Sixty-five were significantly altered in BALBC/cByJ experimental mice. Comparison of experimental mice between strains identified significant alteration in expression of 55 genes. Gene set enrichment analysis (GSEA) of KEGG-defined pathways revealed up-regulation of genes related to various neoplastic diseases, cell communication, and extracellular matrix receptor interaction in C57BL/6ByJ mice exposed to OIR compared to BALB/cByJ; BALB/cByJ mice up-regulated expression of genes related to metabolic pathways. Quantitative rt-PCR results were in agreement with the microarray. These data were similar to those published by others profiling gene expression of C57BL/6N mice exposed to hyperoxia at P12. Alterations in gene expression may determine the differential response between these strains to murine OIR, and these data contribute to our understanding of pathways involved in this process.

LIST OF ABBREVIATIONS

Ccl3 - chemokine (C-C motif) ligand 3, or *Mip-1a*
Ctgf – connective tissue growth factor
Cxcr4 - chemokine (C-X-C motif) receptor 4, or SDF-1
EPC – endothelial progenitor cell
GSEA – gene set enrichment analysis
HIF-1α – hypoxia-inducible factor 1 α
IGFBP3 – insulin-like growth factor binding protein 3
KEGG – Kyoto Encyclopedia of Genes and Genomes
MHC – major histocompatibility complex
Mip-1a – macrophage inhibitory protein 1 alpha, or Ccl3
NV - neovascularization
OIR – oxygen-induced retinopathy
P – post-natal day
PPAR – peroxisome proliferator-activated receptor
rt-PCR – real time polymerase chain reaction
ROP – Retinopathy of Prematurity
SDF-1 – stromal cell-derived factor 1, or Cxcr4
Tnfrsf12a – Tumor necrosis factor receptor superfamily member 12A, or Fn14
VEGF – vascular endothelial growth factor

INTRODUCTION

As described in chapter 1, ROP is a leading cause of blindness in the pediatric population (Gilbert, 2008). The murine model, called oxygen-induced retinopathy (OIR), is the most commonly used animal model for the study of ROP (Smith, Wesolowski et al., 1994). In this model, hyperoxic conditions result in central retinal vaso-obliteration that is later followed by revascularization and NV.

There are known differences in susceptibility to OIR between inbred strains of mice. Specifically, the BALB/c strain responds more favorably than does the C57BL/6J strain (Dorrell, Aguilar et al., 2010; O'Bryhim, Radel et al., 2012). While both strains respond to hyperoxia with similar degree of vaso-obliteration measured on P12 after exposure to the OIR model (Ritter, Banin et al., 2006) (Dorrell, Aguilar et al., 2010), BALB/cByJ mice have smaller avascular areas at P16 (O'Bryhim, Radel et al., 2012) and P17 (Dorrell, Aguilar et al., 2010). To date, several microarray studies examining gene expression profiles in murine OIR have been published, but all use sub-strains of the more susceptible C57BL strain (Sato, Kusaka et al., 2009; Ishikawa, Yoshida et al., 2010; Recchia, Xu et al., 2010). No genes expression assays have been reported using the resistant BALB/c strain.

Here we report the results of a microarray analysis designed to compare gene expression of whole retinal RNA from C57BL/6ByJ and BALB/cByJ mice. For each strain, samples were taken from animals raised in normoxia and from animals exposed to OIR. This allowed for four comparisons: i) C57BL/6ByJ control versus OIR, ii) BALB/cByJ control versus OIR, iii) C57BL/6ByJ control versus BALB/cByJ control, and iv) C57BL/6ByJ OIR versus BALB/cByJ OIR. We used GSEA to describe the pathways and processes that differed

between experimental groups and strains. This approach allowed us to identify factors and pathways that are associated with susceptibility to OIR.

MATERIALS AND METHODS

Animals

All experimental procedures conformed to the ARVO Statement for the Use of Animals in Ophthalmic and Vision Research and were approved by the University of Kansas Medical Center Institutional Animal Care and Use Committee. BALB/cByJ and C57BL/6ByJ were purchased from Jackson Laboratories (Bar Harbor, ME). All mice were kept in a 12-hour light, 12-hour dark cycle with ambient room temperature between 19^{o}C and 22^{o}C. Mice were fed a standard diet for breeding mice (8626 rodent diet; Harlan Laboratories, Indianapolis, IN), with chow and water available *ad libitum*.

Oxygen-induced retinopathy

OIR was induced in experimental mice according to standard protocol (Smith, Wesolowski et al., 1994); briefly, pups were exposed to 75% oxygen beginning on P7 to induce central vaso-obliteration and returned to normoxia after 120 hours. Age-matched normoxic control mice were not exposed to the hyperoxic environment.

Tissue preparation and retinal vascular analysis

Mice were anesthetized with a lethal dose of tribromoethanol and enucleated on P13. Retinae were isolated and snap frozen on dry ice prior to storage in -80^{o}C. Mice were

weighed prior to anesthetization and gender was documented; only male mice in the median range of weight of their respective litter were used in the microarray study.

Microarray Analysis

RNA extraction from collected retinal tissue was performed using RNEasy Mini Kit (Qiagen, Valencia, CA). Two retinae from one mouse were pooled to create one sample; one sample from 3 different litters was used for each OIR group, and one sample from 3 different litters was used for each control group for a total of 12 samples. Concentration and quality of each sample was determined using a NanoDrop-1000 Spectrophotometer (Thermo Scientific, Wilmington, DE). All samples were kept at -80^{o}C until use for microarray hybridization or rt-PCR analysis.

Samples were analyzed at the University of Kansas Medical Center Microarray Facility. Affymetrix GeneChip Mouse Genome 430 2.0 Arrays (Affymetrix, Santa Clara, CA) covering 39,000 gene transcripts using 45,000 probe sets were used for gene expression analysis. Sequence clusters used in the design of the GeneChip were created using Mouse Build 107. Data were normalized using Linear Models for Microarray Data (LIMMA) (Smyth, 2003). Genes for which any change with a genome-adjusted $P < 0.05$ were considered significant. GSEA (Subramanian, Tamayo et al., 2005) (http://www.broadinstitute.org/gsea/) was used to identify Kyoto Encyclopedia of Genes and Genomes (KEGG) biological pathways that showed differential regulation between the strains.

Confirmation of changes in gene expression using rt-PCR

Genes of interest were studied using rt-PCR expression analysis to confirm changes in expression. Retinal RNA samples from different mice in the same litters as those tested in the microarray analysis were extracted using an RNEasy Mini Kit (Qiagen). Both retinae from the same mouse were pooled to create one sample; 3 samples from 3 different litters were created for each strain/treatment condition for a total of 12 samples. The extracted RNA was then reverse-transcribed in 20 μL reactions using an iScript cDNA synthesis kit (Bio-Rad, Hercules, CA), using nuclease-free H_2O in place of reverse transcriptase for a negative control. Primers were designed to flank an intron using Primer3 software (Rozen and Skaletsky, 2000) and tested for specificity against sequences for *Mus musculus* using BLAST software (NCBI, Bethesda, MD). Primers were then commercially synthesized (IDT Technology, Skokie, IL) (Table 5.1). S16 was used as an endogenous control from which relative level of mRNA expression was estimated.

Each 20μL reaction mixture contained 10 μL 2x SYBR Green master-mix (Applied Biosystems, Foster City, CA), 1 μL each of forward and reverse primers (0.5 μM final concentration), and 2 μL cDNA sample diluted 1:2 with nuclease-free H_2O. Reactions were run on an HT 7900 Real-Time PCR System (Applied Biosystems). Cycling conditions included an initial denaturation (95^{o}C, 10 minutes) followed by 40 cycles of denaturation (95^{o}C, 15 seconds), annealing (60^{o}C, 10 minutes), and extension (72^{o}C, 35 seconds). Samples were tested in duplicate for each candidate gene, as were standard cDNA pool and water samples to provide positive and negative controls, respectively. Melting curves were analyzed to confirm amplicon specificity. PCR products were run a 2% agarose gel to identify bands and compare to the predicted amplicon size to confirm identity. A threshold

Gene Name	Forward Primer	Reverse Primer
Ltbp2	CATCAAACAGCACCAACCAC	GACTTCCTCTGGCCTCACTG
Il1b	GCCCATCCTCTGTGACTCAT	AGGCCACAGGTATTTTGTCG
Col18a1	ACAGTTGCTGCCTCAGACCT	CAGTCAGGAGAGCTGGTTCC
Sfrp1	CCTGGCTCTGTTCCTACAGC	CGGCCAACATTTTCTGTTTT
Fzd5	AGCCAAATGAGGCACATACC	TCTCCTTTTGCGAGCGTTAT

Table 5.1 Sequence of primers used in rt-PCR gene expression analysis experiment. Primers were designed using Primer3 software and tested for specificity using BLAST software. Sequences expressed as 5' to 3'.

was established for each plate of reactions, and the cycle number where the fluorescence curve intersected with the threshold was calculated (Ct). The Ct values for the genes of interest were compared with the Ct for the transcripts of the ribosomal S16 protein ($^{\Delta}$Ct). The relative gene expression levels were calculated by using the comparative Ct ($^{\Delta\Delta}$Ct).

RESULTS

Changes in gene expression

We report the results of our microarray data as 4 two-way comparisons: 1) response to OIR (compared with normoxia) in C57BL/6ByJ mice, 2) response to OIR in BALB/cByJ mice, 3) C57BL/6ByJ mice vs. BALB/cByJ mice in normoxia, 4) C57BL/6ByJ mice vs. BALB/cByJ mice in response to OIR. Genes were broadly classified into groups according to their Gene Ontology classifications. In all 4 comparisons, both up-regulated and down-regulated groups contained genes classified as being related to **Angiogenesis, Metabolism** and **Transport**. However, different genes in these groups were differentially expressed in different comparisons. Additionally, in most groups, some of the differentially expressed genes are still of unknown function.

Response to hyperoxia

In both C57BL/6ByJ and BALB/cByJ, genes related to **Apoptosis, Cellular Adhesion, Cell Cycle, Development, Inflammation, Mitochondria** and **Stress Response** were up-regulated (Table 5.2). In C57BL/6ByJ, but not in BALB/cByJ, genes classified as being related to **Cellular Component, Chemotaxis** and **Coagulation** were up-regulated in

Gene symbol	Gene Function	C57BL/6ByJ P13 hyperoxic vs. normoxic	p
Cxcr4	*Angiogenesis*	-0.87	0.01
Tek	*Angiogenesis*	-0.73	0.02
Cldn5	*Cell adhesion*	-1.47	0.00
Vtn	*Cell adhesion*	-0.58	0.02
Lrrc66	*Cell component*	-1.44	0.01
Vwf	*Coagulation*	-1.34	0.00
Pdgfrb	*Development*	-0.45	0.02
Gstt1	*Metabolism*	-1.21	0.02
Pla2g4b	*Metabolism*	-0.50	0.04
Ckmt1	*Metabolism*	-0.40	0.01
Mpi	*Metabolism*	-0.32	0.01
Rimkla	*Metabolism*	-0.56	0.00
Mrpl36	*Mitochondrial*	-0.31	0.01
Rdm1	*Stress response*	-0.48	0.03
Slco1c1	*Transport*	-1.78	0.00
Slc38a5	*Transport*	-1.17	0.00
Slc40a1	*Transport*	-1.06	0.01
Abca8a	*Transport*	-0.91	0.00
Ramp2	*Transport*	-0.58	0.04
Rangrf	*Transport*	-0.52	0.00
Vps45	*Transport*	-0.23	0.01
Higd1b	*Unknown*	-1.70	0.00
Ccdc24	*Unknown*	-0.71	0.00
2310003L22Rik	*Unknown*	-0.32	0.05
Arr3	*Vision*	-1.43	0.01
Guca1b	*Vision*	-0.79	0.01

Gene symbol	Gene Function	C57BL/6ByJ P13 hyperoxic vs. normoxic	p
Tgfb2	*Angiogenesis*	0.59	0.04
Thbs1	*Angiogenesis (anti)*	0.66	0.03
Emcn	*Angiogenesis*	0.72	0.05
Plxnd1	*Angiogenesis*	0.74	0.01
Serpinf1	*Angiogenesis (anti)*	0.80	0.04
Ctgf	*Angiogenesis*	0.90	0.01
Igfbp3	*Angiogenesis*	1.01	0.01
Vegfa	*Angiogenesis*	1.06	0.00
Pf4	*Angiogenesis (anti)*	1.24	0.01
Tnfrsf12a	*Angiogenesis*	1.60	0.01
Serpine1	*Angiogenesis*	2.35	0.00
Adm	*Angiogenesis*	2.48	0.00
Unc5b	*Apoptosis*	0.31	0.03
Bag3	*Apoptosis (anti)*	1.75	0.00
Cerkl	*Angiogenesis*	0.76	0.00
Icam1	*Cell adhesion*	0.50	0.02
Mcam	*Cell adhesion*	1.05	0.00
Col2a1	*Cell adhesion*	1.26	0.00
Col18a1	*Cell adhesion*	1.60	0.01
Hist1h2bp	*Cell component*	0.16	0.03
Rhbdf1	*Cell component*	0.51	0.04
Cks1b	*Cell cycle*	0.73	0.04
Cdkn1a	*Cell cycle*	1.32	0.00
Cmtm3	*Chemotaxis*	1.01	0.00
Plaur	*Coagulation*	0.64	0.01
Egln1	*Development*	0.97	0.00
Lgals3	*Development*	2.05	0.01
H2-Q8	*Inflammation*	0.26	0.03
Ccl3	*Inflammation*	0.44	0.00
Ly86	*Inflammation*	0.47	0.02
Zfp36	*Inflammation*	0.70	0.00
C3	*Inflammation*	1.35	0.00
H2-Ab1	*Inflammation*	2.19	0.00
Timp1	*Inflammation*	2.42	0.00
H2-Q7	*Inflammation*	3.17	0.00
Gpi1	*Metabolism*	0.59	0.00
Hk2	*Metabolism*	0.65	0.01
Gls2	*Metabolism*	1.28	0.00
Pfkp	*Metabolism*	1.81	0.00
Bnip3	*Mitochondrial*	1.27	0.00
Serpina3n	*Stress response*	2.57	0.00
Selenbp1	*Stress response*	1.60	0.00
Ltbp2	*Unknown*	1.52	0.01

Table 5.2 Differential gene expression of C57BL/6ByJ mice in response to hyperoxia.
Genes are organized by functional category. Down-regulated genes are listed in the left-hand table; up-regulated genes are listed on the right. Data are expressed as **ΔΔ**Ct values.

hyperoxia. Categories containing genes up-regulated in hyperoxia in BALB/cByJ but not in C57BL/6ByJ were **Signal Transduction, Transcription,** and **Vision** (Table 5.3).

Some of the genes that were down-regulated in hyperoxia fell into the classifications of **Cellular Adhesion, Cellular Component, Development, Mitochondrial, Stress Response** and **Vision** in both C57BL/6ByJ and BALB/cByJ. Additionally, BALB/cByJ had genes that were down-regulated that fell into the category of **Signal Transduction**.

Differential gene expression between C57BL/6ByJ and BALB/cByJ Mice.

In both normoxia and hyperoxia (Tables 5.4 and 5.5, respectively), the classifications **Cellular Adhesion** and **Cellular Component** described some of the genes that were more highly expressed in C57BL/6ByJ and some of the genes that were more highly expressed in BALB/cByJ. The classifiers **Cell Cycle, Development, Inflammation, Signal Transduction,** and **Vision** were used to describe some of the genes that were more highly expressed in C57BL/6ByJ in both normoxia and hyperoxia. **Inflammation, Signal Transduction, Stress Response** and **Transcription** classifiers were used to describe some of the genes that were more highly expressed in BALB/cByJ in both normoxia and hyperoxia. Some genes that were more highly expressed in BALB/cByJ in normoxia fell into the **Development** and **Mitochondria** classifications. The **Apoptosis** classification applied to some genes that were more highly regulated in C57BL/6ByJ and some that were more highly regulated in BALB/cByJ in hyperoxia. Some of the genes that were more highly expressed in C57BL/6ByJ in hyperoxia fell into the **Chemotaxis, Coagulation** and **Mitochondrial** groups.

Gene symbol	Gene Function	BALB/6ByJ P13 hyperoxic vs. normoxic	p
Tek	*Angiogenesis*	-1.57	0.00
Ptprb	*Angiogenesis*	-1.16	0.01
Il1b	*Angiogenesis*	-0.75	0.00
Gja4	*Angiogenesis*	-0.59	0.01
Kdr	*Angiogenesis*	-0.31	0.05
Tie1	*Angiogenesis (anti)*	-0.42	0.04
Cldn5	*Cell adhesion*	-1.21	0.00
Lrrc66	*Cell component*	-1.03	0.04
Rexo4	*Cell cycle*	-0.24	0.04
Vcam1	*Development*	-0.66	0.02
Sema3E	*Development*	-0.33	0.01
Mpi	*Metabolism*	-0.27	0.02
Mrpl36	*Mitochondrial*	-0.38	0.00
Mrpl15	*Mitochondrial*	-0.19	0.05
Eltd1	*Signal transduction*	-1.07	0.00
Arap3	*Signal transduction*	-1.00	0.01
Gpx8	*Stress response*	-0.53	0.03
Slco1c1	*Transport*	-2.12	0.00
Slco2b1	*Transport*	-0.98	0.00
Slc40a1	*Transport*	-0.92	0.01
Slc38a5	*Transport*	-0.75	0.01
Ramp2	*Transport*	-0.69	0.02
Pltp	*Transport*	-0.56	0.05
Abca8a	*Transport*	-0.39	0.05
Eps15l1	*Transport*	-0.28	0.02
Rangrf	*Transport*	-0.26	0.02
Vps45	*Transport*	-0.16	0.03
Higd1b	*Unknown*	-1.05	0.01
Ccdc24	*Unknown*	-0.39	0.05
Arr3	*Vision*	-0.97	0.01

Gene symbol	Gene Function	BALB/6ByJ P13 hyperoxic vs. normoxic	p
Fzd5	*Angiogenesis*	0.05	0.04
Plxnd1	*Angiogenesis*	0.75	0.01
Vegfa	*Angiogenesis*	0.84	0.00
Igfbp3	*Angiogenesis*	1.90	0.00
Adm	*Angiogenesis*	1.56	0.02
Ercc3	*Apoptosis*	0.33	0.02
Col2a1	*Cell adhesion*	0.48	0.02
Mcam	*Cell adhesion*	0.59	0.02
Mns1	*Cell cycle*	0.44	0.05
Plat	*Coagulation*	0.30	0.03
Egln1	*Development*	0.73	0.00
Mgp	*Development*	0.76	0.02
H2-D1	*Inflammation*	0.52	0.01
H2-Q7	*Inflammation*	0.66	0.01
H2-Ab1	*Inflammation*	0.82	0.00
H2-K1	*Inflammation*	1.02	0.01
C4b	*Inflammation*	1.16	0.03
C3	*Inflammation*	0.82	0.01
Gls2	*Metabolism*	1.21	0.00
Gpi1	*Metabolism*	0.65	0.00
Hk2	*Metabolism*	0.57	0.01
Pfkfb3	*Metabolism*	0.60	0.00
Pfkp	*Metabolism*	1.12	0.00
Shmt2	*Metabolism*	0.67	0.02
Bnip3	*Mitochondrial*	1.22	0.00
Camkk1	*Signal transduction*	0.22	0.05
Arrdc3	*Signal transduction*	0.55	0.04
Osmr	*Signal transduction*	1.15	0.02
Mt1	*Signal transduction*	1.16	0.00
Atg9b	*Stress response*	0.20	0.03
Med14	*Transcription*	0.20	0.02
Sox30	*Transcription*	1.19	0.03
Selenbp1	*Stress response*	0.94	0.00
Samd7	*Unknown*	0.99	0.00
Rp1l1	*Vision*	0.23	0.00

Table 5.3 Differential gene expression of BALB/6ByJ mice in response to hyperoxia.
Genes are organized by functional category. Down-regulated genes are listed in the left-hand table; up-regulated genes are listed on the right. Data are expressed as **ΔΔ**Ct values

Gene symbol	Gene Function	C57 normoxic vs. BALB normoxic	p
Serpine1	*Angiogenesis*	-1.32	0.03
Mmp2	*Angiogenesis*	-0.76	0.01
Il1b	*Angiogenesis*	-0.76	0.00
Fgfr1	*Angiogenesis*	-0.51	0.01
Gja4	*Angiogenesis*	-0.49	0.02
Efna1	*Angiogenesis*	-0.49	0.04
Efnb2	*Angiogenesis*	-0.47	0.05
Pgf	*Angiogenesis*	-0.43	0.04
Cav1	*Angiogenesis*	-0.36	0.05
Serpinf1	*Angiogenesis (anti)*	-1.25	0.00
Thbs1	*Angiogenesis (anti)*	-0.57	0.05
Col18a1	*Cell adhesion*	-1.65	0.01
Cerkl	*Apoptosis*	-3.93	0.00
H1f0	*Cell component*	-0.59	0.01
Rexo4	*Cell Cycle*	-1.12	0.00
Rnase4	*Cell Cycle*	-0.60	0.05
Lgals3	*Development*	-2.34	0.00
Tgfb3	*Development*	-0.29	0.03
EphB2	*Development*	-0.20	0.00
H2-Ab1	*Inflammation*	-3.18	0.00
H2-K1	*Inflammation*	-1.49	0.00
Ly86	*Inflammation*	-0.59	0.01
Zfp36	*Inflammation*	-0.49	0.02
Ephx2	*Metabolism*	-0.44	0.04
Gstt3	*Metabolism*	-0.31	0.03
9630033F20Rik	*Metabolism*	-1.07	0.00
Mrpl15	*Mitochondrial*	-0.41	0.02
Tirap	*Signal transduction*	-0.63	0.00
Pdgfc	*Signal transduction*	-0.51	0.04
Kcnip3	*Signal transduction*	-0.93	0.00
Serpina3n	*Stress response*	-1.86	0.02
Gpx8	*Stress response*	-0.66	0.01
Hspb8	*Stress response*	-0.35	0.05
Sox30	*Transcription*	-1.42	0.02
Eps15l1	*Transport*	-0.54	0.00
3110070M22Rik	*Unknown*	-1.36	0.00
Ltbp2	*Unknown*	-1.23	0.02

Gene symbol	Gene Function	C57 normoxic vs. BALB normoxic	p
Fzd5	*Angiogenesis*	0.00	0.00
Flt4	*Angiogenesis*	0.00	0.01
Fgfr2	*Angiogenesis*	0.05	0.05
Flt1	*Angiogenesis*	0.53	0.05
Cxcr4	*Angiogenesis*	0.60	0.04
Igfbp3	*Angiogenesis*	0.62	0.00
Ctgf	*Angiogenesis*	0.61	0.04
Itga9	*Cell adhesion*	0.00	0.00
Itga5	*Cell adhesion*	0.00	0.02
Vtn	*Cell adhesion*	0.55	0.02
Gas7	*Cell component*	0.09	0.01
Dnahc9	*Cell component*	0.75	0.00
Hist1h2bc	*Cell component*	0.78	0.00
Cables2	*Cell cycle*	0.19	0.05
Mcm6	*Cell cycle*	0.89	0.00
Mns1	*Cell cycle*	4.22	0.00
Vwf	*Coagulation*	3.35	0.00
Egln1	*Development*	0.18	0.00
Egfr	*Development*	0.80	0.00
Mgp	*Development*	0.81	0.01
Mmp9	*Development*	0.99	0.01
H2-D1	*Inflammation*	0.47	0.00
Ly96	*Inflammation*	0.64	0.01
Ckmt1	*Metabolism*	0.38	0.02
Gpi1	*Metabolism*	0.47	0.01
Hk2	*Metabolism*	0.64	0.01
Pla2g4b	*Metabolism*	0.65	0.01
Dusp11	*Signal transduction*	0.50	0.00
Mt1	*Signal transduction*	0.79	0.02
Eltd1	*Signal transduction*	1.11	0.00
Cnksr1	*Signal transduction*	4.26	0.00
Cyth1	*Signal transduction*	7.06	0.00
Abca8a	*Transport*	0.51	0.02
Slc38a5	*Transport*	0.53	0.04
Slco1c1	*Transport*	1.43	0.01
Samd7	*Unknown*	0.42	0.04
Gnat1	*Vision*	0.52	0.03
Guca1b	*Vision*	1.94	0.00

Table 5.4 Differential gene expression between strains of mice raised in normoxia.
Genes are organized by functional category. Down-regulated genes are listed in the left-hand table; up-regulated genes are listed on the right. Data are expressed as **ΔΔ** Ct values.

Gene symbol	Gene Function	C57 hypoxic vs. BALB hypoxic	p
Fzd5	*Angiogenesis*	-0.05	0.04
Cerkl	*Apoptosis (anti)*	-3.47	0.00
Ercc3	*Apoptosis*	-0.35	0.02
Itga9	*Cell adhesion*	-0.57	0.03
H1f0	*Cell component*	-0.63	0.01
Rexo4	*Cell cycle*	-1.27	0.00
Rnase4	*Cell cycle*	-1.13	0.00
H2-Ab1	*Inflammation*	-1.81	0.00
9630033F20Rik	*Metabolism*	-0.77	0.04
Ephx2	*Metabolism*	-0.40	0.05
Shmt2	*Metabolism*	-0.29	0.04
Rimkla	*Metabolism*	-0.42	0.00
Tirap	*Signal transduction*	-0.60	0.02
Frmpd1	*Signal transduction*	-0.54	0.00
Pdgfc	*Signal transduction*	-0.48	0.05
Kcnip3	*Signal transduction*	-0.65	0.01
Rdm1	*Stress response*	-0.64	0.01
Sox30	*Transcription*	-2.44	0.00
Rangrf	*Transport*	-0.33	0.01
3110070M22Rik	*Unknown*	-0.73	0.04
Ccdc24	*Unknown*	-0.60	0.01

Gene symbol	Gene Function	C57 hypoxic vs. BALB hypoxic	p
Vegfc	*Angiogenesis*	0.29	0.05
Tgfb2	*Angiogenesis*	0.74	0.01
Edn1	*Angiogenesis*	0.79	0.01
Emcn	*Angiogenesis*	0.91	0.02
Tek	*Angiogenesis*	1.08	0.00
Adm	*Angiogenesis*	1.26	0.04
Pf4	*Angiogenesis (anti)*	1.31	0.01
Ctgf	*Angiogenesis*	1.21	0.00
Bag3	*Apoptosis (anti)*	1.04	0.00
Icam1	*Cell adhesion*	0.41	0.04
Col2a1	*Cell adhesion*	0.46	0.03
Hist1h2bp	*Cell component*	0.17	0.02
Hist1h2bc	*Cell component*	0.94	0.00
Synm	*Cell component*	2.18	0.01
Cdkn1a	*Cell cycle*	0.97	0.02
Mns1	*Cell cycle*	3.41	0.00
Cmtm3	*Chemotaxis*	0.75	0.01
Plaur	*Coagulation*	0.48	0.03
Vwf	*Coagulation*	2.20	0.00
Igf1	*Development*	0.39	0.02
Mmp9	*Development*	0.80	0.03
Egln1	*Development*	1.18	0.00
H2-Q8	*Inflammation*	0.26	0.03
Ccl3	*Inflammation*	0.43	0.00
H2-Q7	*Inflammation*	2.62	0.00
Gpi1	*Metabolism*	0.38	0.03
Hk2	*Metabolism*	0.72	0.00
Pfkp	*Metabolism*	1.14	0.04
Bnip3	*Mitochondrial*	0.30	0.03
Arap3	*Signal transduction*	1.19	0.00
Cnksr1	*Signal transduction*	3.63	0.00
Selenbp1	*Transport*	0.44	0.03
Slco1c1	*Transport*	1.77	0.00
Guca1b	*Vision*	1.34	0.00

Table 5.5 Differential gene expression between strains of mice exposed to OIR.
Genes are organized by functional category. Down-regulated genes are listed in the **ΔΔ** Ct values.

Gene set enrichment analysis results

Using the expression profiles of both experimental and control C57BL/6ByJ and BALB/cByJ mice, GSEA was performed to reveal functional gene sets associated with our data using a false discovery rate of < 0.25 as our cut-off. Seventeen KEGG-defined gene sets were found to be up-regulated in the retina of C57BL/6ByJ mice exposed to OIR compared to normoxic controls; only one gene set was down-regulated (Table 5.6).

Only 2 KEGG-curated pathways were found to be differentially regulated between BALB/cByJ mice exposed to OIR and controls. Both were down-regulated in experimental OIR mice compared to control (Table 5.7).

Six KEGG-defined biological pathways were found to be up-regulated in C57BL/6ByJ mice exposed to OIR compared to OIR BALB/cByJ animals; 4 pathways were up-regulated in BALB/cByJ mice (Table 5.8).

Validation of microarray data by real-time PCR

To validate the outcome of our microarray analyses, we performed quantitative rt-PCR assays. Relative quantifications of the mRNA expression by rt-PCR were calculated for 5 genes significantly altered between strains (Table 5.9). We found excellent agreement between microarray and rt-PCR, and expression changes of each gene examined were in the same direction of regulation. These findings demonstrate the high reliability of our array results.

A

Upregulated in C57 OIR		
NAME	Enrichment Score	FDR q-val
HSA04110_CELL_CYCLE	0.525	0.021
HSA04115_P53_SIGNALING_PATHWAY	0.557	0.019
HSA04512_ECM_RECEPTOR_INTERACTION	0.511	0.040
HSA01430_CELL_COMMUNICATION	0.519	0.035
HSA05222_SMALL_CELL_LUNG_CANCER	0.472	0.116
HSA05216_THYROID_CANCER	0.587	0.097
HSA04610_COMPLEMENT_AND_COAGULATION_CASCADES	0.499	0.084
HSA05217_BASAL_CELL_CARCINOMA	0.494	0.101
HSA05219_BLADDER_CANCER	0.527	0.122
HSA04060_CYTOKINE_CYTOKINE_RECEPTOR_INTERACTION	0.411	0.112
HSA00670_ONE_CARBON_POOL_BY_FOLATE	0.622	0.111
HSA04514_CELL_ADHESION_MOLECULES	0.442	0.106
HSA04510_FOCAL_ADHESION	0.406	0.115
HSA04350_TGF_BETA_SIGNALING_PATHWAY	0.434	0.133
HSA04810_REGULATION_OF_ACTIN_CYTOSKELETON	0.392	0.173
HSA04640_HEMATOPOIETIC_CELL_LINEAGE	0.431	0.204
HSA00052_GALACTOSE_METABOLISM	0.507	0.207
Upregulated in C57 Control		
NAME	ES	FDR q-val
HSA00960_ALKALOID_BIOSYNTHESIS_II	-0.553	0.230

B

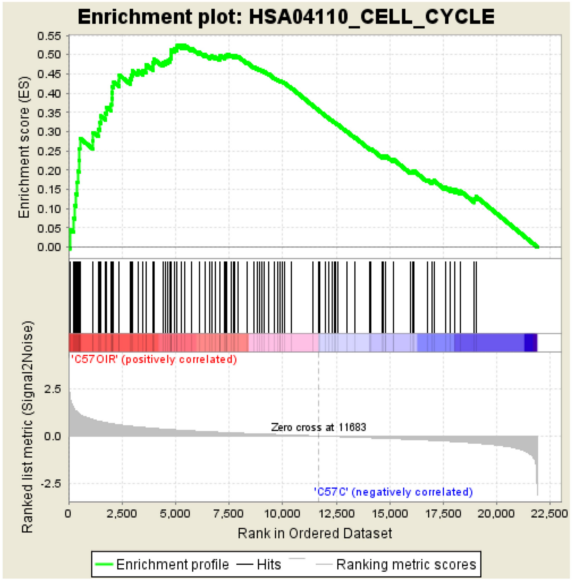

Fig 1: Enrichment plot: HSA04110_CELL_CYCLE
Profile of the Running ES Score & Positions of GeneSet Members on the Rank Ordered List

Table 5.6 GSEA results identifying KEGG-defined gene sets differentially expressed in C57BL/6ByJ mice exposed to OIR.
(**A**) GSEA was performed to reveal functional gene sets associated with our data using a false discovery rate of < 0.25 as our cut-off. Seventeen gene sets were up-regulated in the retina of C57BL/6ByJ mice exposed to OIR compared to normoxic controls; only one gene set was down-regulated. (**B**) Example enrichment plot with enrichment score profile for the KEGG-defined Cell Cycle gene set.

A

Upregulated in BALB/cByJ		
NAME	ES	FDR q-val
HSA00100_BIOSYNTHESIS_OF_STEROIDS	-0.535	0.236
HSA03320_PPAR_SIGNALING_PATHWAY	-0.416	0.244

B

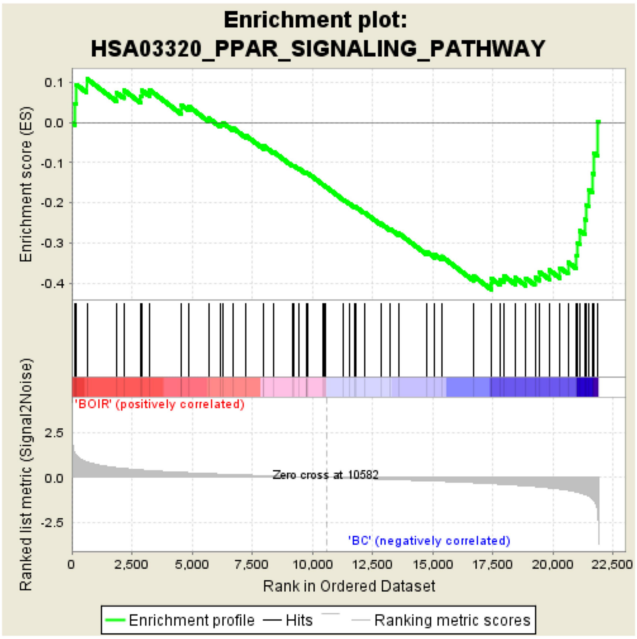

Fig 1: Enrichment plot: HSA03320_PPAR_SIGNALING_PATHWAY
Profile of the Running ES Score & Positions of GeneSet Members on the Rank Ordered List

Table 5.7 GSEA results identifying KEGG-defined gene sets differentially expressed in BALB/cByJ mice exposed to OIR.

(**A**) GSEA was performed to reveal functional gene sets associated with our data using a false discovery rate of < 0.25 as our cut-off. Two gene sets were up-regulated in the retina of BALB/cByJ mice exposed to OIR compared to normoxic controls; none were down-regulated. (**B**) Example enrichment plot with enrichment score profile for the KEGG-defined PPAR Signaling Pathway gene set.

A

Upregulated in C57BL/6ByJ OIR		
NAME	ES	FDR q-val
HSA04512_ECM_RECEPTOR_INTERACTION	0.505	0.113
HSA01430_CELL_COMMUNICATION	0.505	0.112
HSA04514_CELL_ADHESION_MOLECULES	0.443	0.253
HSA05219_BLADDER_CANCER	0.518	0.230
HSA04115_P53_SIGNALING_PATHWAY	0.467	0.227
HSA04320_DORSO_VENTRAL_AXIS_FORMATION	0.560	0.220
Upregulated in BALB/cByJ OIR		
NAME	ES	FDR q-val
HSA00271_METHIONINE_METABOLISM	-0.660	0.038
HSA03020_RNA_POLYMERASE	-0.598	0.045
HSA00260_GLYCINE_SERINE_AND_THREONINE_METABOLISM	-0.504	0.050
HSA00480_GLUTATHIONE_METABOLISM	-0.419	0.249

B

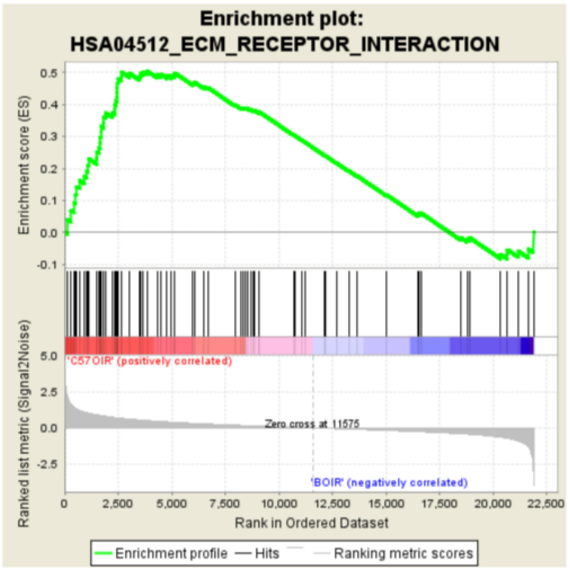

Fig 1: Enrichment plot: HSA04512_ECM_RECEPTOR_INTERACTION
Profile of the Running ES Score & Positions of GeneSet Members on the Rank Ordered List

Table 5.8 GSEA results identifying KEGG-defined gene sets differentially expressed between strains of mice exposed to OIR.

(**A**) GSEA was performed to reveal functional gene sets associated with our data using a false discovery rate of < 0.25 as our cut-off. Six gene sets were up-regulated in the retina of C57BL/6ByJ mice exposed to OIR compared to BALB/cByJ; four gene set were up-regulated in BALB/cByJ (**B**) Example enrichment plot with enrichment score profile for the KEGG-defined ECM Receptor Interaction pathway.

DISCUSSION

The purpose of this study was to identify specific genes and pathways associated with more or less successful retinal revascularization responses to the OIR model of ROP. The BALB/cByJ murine strain has been shown in multiple studies to revascularize more rapidly and in a more physiologically normal manner in the OIR model compared to the C57BL/6 strain (Ritter, Banin et al., 2006; Dorrell, Aguilar et al., 2010; O'Bryhim, Radel et al., 2012).

While several published microarray studies have elucidated gene expression changes that occur in murine OIR (Sato, Kusaka et al., 2009; Ishikawa, Yoshida et al., 2010; Recchia, Xu et al., 2010), all used the C57BL/6 strain that is highly susceptible to the development of proliferative OIR. In contrast, BALB/cByJ exhibits faster regeneration of the obliterated retinal vasculature and is less susceptible to proliferative OIR (Dorrell, Aguilar et al., 2010; O'Bryhim, Radel et al., 2012). By comparing differences in gene expression between these strains we sought to identify mechanisms associated with more or less adaptive responses to OIR.

Comparison of C57 Data with Previously Published Reports

The genes we determined to be differentially expressed in C57BL/6ByJ retinas in response to hypoxia in the OIR model largely agree with those of Ishikawa (Ishikawa, Yoshida et al., 2010) and Sato (Sato, Kusaka et al., 2009), although the other investigators used different time points. In all cases where genes were differentially expressed in our experiment as well as in the work of Ishikawa or Sato, then the direction of differential expression was concordant between the experiments.

Connective tissue growth factor (*Ctgf*) and Tumor necrosis factor receptor superfamily member 12A (*Tnfrsf12a*) were the only 2 genes up-regulated in our experiment as well as in those of Ishikawa and Sato. Inhibition of *Ctgf* has been demonstrated to hasten retinal revascularization and to inhibit NV in OIR (Pi, Shenoy et al., 2012). *Tnfrsf12a* is also known as *Fn14* and as the TWEAK receptor. *Fn14* is up-regulated in renal ischemia. Renal blockade of *Fn14* reduced proinflammatory cytokine production, decreased inflammatory infiltrate, inhibited tubular cell apoptosis, and prolonged survival of mice in a model of renal ischemia reperfusion injury (Hotta, Sho et al., 2011). Similarly, *Fn14* deficiency has been found to be neuroprotective (Frauenknecht, Bargiotas et al., 2010), and to reduce neuronal apoptosis (Haile, Echeverry et al., 2010) in an experimental model of stroke (Echeverry, Wu et al., 2012). Interestingly, *Fn14* is not up-regulated in response to the OIR model in BALB/cByJ retinas. It is possible that *Fn14* up-regulation in C57BL/6ByJ mice contributes to increased apoptosis of microglial cells and astrocytes reported previously (Dorrell, Aguilar et al., 2010), which may explain in part why C57BL/6ByJ mice revascularize more slowly in the OIR model.

Comparison of Retinal Response to Hypoxia between Strains

At P13, 24 hours after return to normoxia in the OIR model, retinae from both C57BL/6 and BALB/c mice exhibit up-regulation of genes related to inflammation compared to normoxic controls. This finding is consistent with previously published microarray studies (Sato, Kusaka et al., 2009; Ishikawa, Yoshida et al., 2010) and other data suggesting that hypoxic retinas are in an elevated state of immune responsiveness (Matsuoka, Kitamura et al., 1998; Lin, Chen et al., 2011; Sivakumar, Foulds et al., 2011). For example,

retinal microglia have been shown to increase production of tumor necrosis factor α and interleukin 1β in rat OIR models (Sivakumar, Foulds et al., 2011).

The inflammation-associated genes showing the greatest degree of differential expression are the major histocompatibility complex (MHC) class Ib gene H2-Q7 and the MHC class II gene H2-Ab1. H2-Q7, also known as H2-Qa2 and Preimplantation embryonic development (*Ped*) gene, is a non-classical class 1b MHC molecule that is widely expressed (Niederkorn, Chiang et al., 1999; Comiskey, Goldstein et al., 2003; Ohtsuka, Inoko et al., 2008). While its role in blastocyst implantation and embryonic survival are better described, there is evidence that H2-Q7 along with other class 1b MHC genes inhibit Natural Killer cells and thus cell-mediated cytotoxicity (Niederkorn, Chiang et al., 1999; Chiang, Henson et al., 2003). H2-Q7 is more highly expressed in the hypoxic retina of C57BL/6ByJ than of BALB/cByJ.

In contrast, H2-Ab1 is more highly expressed in the hypoxic retinae of BALB/cByJ than of C57BL/6ByJ mice. H2-Ab1, is class II molecule expressed on antigen presenting cells and recognized by CD4+ T cells. This serves to activate CD4+ T cells, which subsequently regulate activation and apoptosis of T cells (Tsang, Chai et al., 2003; Zhou, Ding et al., 2011). The substantial strain specific differences of expression of these MHC genes may point to a difference in polarization of the immune response in hypoxia between these strains.

Chemokine (C-C motif) ligand 3 (*Ccl3*), also known as Macrophage inhibitory protein-1 α (*MIP-1α*), is more highly expressed in C57BL/6ByJ than BALB/cByJ retinas. MIP-1α is a cytokine functions to recruit monocytes, and is produced in response to tissue ischemia. In the OIR model, MIP-1α mRNA expression was increased within 12 hours after return to normoxia. Antibody blockade delivered at P12 and P14 successfully inhibited retinal NV by

P17 (Yoshida, Yoshida et al., 2003). Up-regulation of this gene in C57BL/6ByJ retinae compared to BALB/cByJ could therefore contribute to the increased NV seen in this strain.

Complement components C3 and C4b were up-regulated in response to hypoxia. C3 was up-regulated in both strains, and C4b was up-regulated in BALB/cByJ retinae. C3-deficienct mice had worsened NV after exposure to OIR compared to wild-type littermate controls via polarization of macrophages toward an anti-angiogenic phenotype (Langer, Chung et al., 2010). Although several patents have been filed for complement inhibitors designed to treat other retinal vasculopathies (Epstein and Kurz, 2009; Fung and Yao, 2009; Hass, Jianping et al., 2011), to date no other data has been published on the role of complement activation in OIR or ROP.

Hypoxic C57BL/6ByJ retinae showed greater differential expression of angiogenic genes than did BALB/cByJ retinae. Genes related to angiogenesis that were up-regulated in response to hypoxia in C57BL/6ByJ OIR retinae included genes known to play an important role in retinal vascularization such as *Vegfa* (Chen and Smith, 2007) and *Igfbp3* (Lofqvist, Chen et al., 2007). The only 2 down-regulated angiogenic genes in this comparison were Chemokine (C-X-C motif) receptor 4 (*Cxcr4*) and *Tek. Cxcr4* is the SDF-1 receptor that mediates EPC recruitment (Ceradini, Kulkarni et al., 2004; Urbich and Dimmeler, 2004; Lima e Silva, Shen et al., 2007). EPC contribute to angiogenesis in the retina(Nakagawa, Masuda et al., 2011), and reduced recruitment of progenitor cells could potentially lead to either reduced revascularization or reduced development of pathological NV.

Tek, or *Tie*-2, is the angiopoietin 1 receptor. Angiopoietin 1 has been shown to inhibit EC apoptosis, and to promote angiogenesis, vascular perfusion and EPC recruitment (Koh, 2012). The most up-regulated angiogenesis-related gene in the hypoxic BALB/cByJ retina is

Igfbp3, which is associated with successful retinal revascularization and increased EPC recruitment in OIR (Lofqvist, Chen et al., 2007).

BALB/cByJ retinae were shown to increase expression of several metabolic genes after exposure to OIR. Several of these genes (*Gpi1, Hk2, Pfkfb3, Pfkp*) are involved in glycolysis. The HIF-1α mediated increase in glycolysis in hypoxia (Semenza, 2000; Marsin, Bouzin et al., 2002) is thought to increase cell survival in hypoxic environments by maintaining sufficient levels of ATP (Warburg, 1956; Semenza, 2009; Shi, Xie et al., 2009). It is possible that the failure of C57BL/6 to significantly up-regulate these glycolytic enzymes may be maladaptive, but we have no data regarding the consequences on differences in energy metabolism or reactive oxygen species production between the strains.

Although a number of genes demonstrate particularly pronounced differential expression between the strains in hypoxia, in most cases the function of these is insufficiently understood to allow any useful speculation linking this differential regulation with disease outcome.

Gene Set Enrichment Analysis

The goal of our gene set-based approach was to detect coordinated changes in pre-specified sets of related genes, especially those where the individual transcripts fail to meet significance criteria. The use of GSEA to identify differentially expressed KEGG curated gene sets, several expression patterns emerged in each comparison.

Comparison of hyperoxia exposed C57BL/6ByJ retinas with the retinas of normoxic control mice demonstrated up-regulation of KEGG pathways related to Cell Cycle, P53 Signaling Pathway, Extracellular Matrix Interaction, Cell Communication, Complement and

Coagulation Cascades, as well as differential expression observed in several neoplasia. The neoplasia-related gene sets encompass families of genes related to angiogenesis and Wnt signaling pathways, which have been shown to play an important role in ROP development (Hiraoka, Takahashi et al., 2010; Shastry, 2010) and other related retinal vascular diseases (Gong, Slee et al., 2001; Robitaille, MacDonald et al., 2002; Xu, Wang et al., 2004; Ye, Wang et al., 2009).

In BALB/cByJ mice, no gene sets were up-regulated in OIR retinae compared to normoxic. Control retinae were found to have relatively greater expression of genes related to the Biosynthesis of Steroids and PPAR signaling. Data regarding the role of peroxisome proliferator-activated receptors (PPAR) in angiogenesis are conflicting (Biscetti, Straface et al.). Some reports suggest that PPARγ agonists increase the number and functional activity of EPCs (Pistrosch, Herbrig et al., 2005; Chu, Lee et al., 2006; Besler, Doerries et al., 2008). Others have found that PPARα is required for EPC differentiation and stimulates angiogenesis (Benameur, Tual-Chalot et al., 2010). However, several groups reported that both PPARα and γ activation result in inhibition of angiogenesis (Murata, He et al., 2000; Panigrahy, Singer et al., 2002; Peeters, Vigne et al., 2005; Bishop-Bailey, 2011). Given that OIR-exposed retinae are revascularizing at P13, our data is in line with this latter body of evidence, but more work is needed to explore the role of these genes in OIR development.

Comparing gene set changes between strains exposed to OIR, C57BL/6ByJ retinae have greater expression of genes related to Extracellular Matrix Receptor Interaction, Cell Communication, and Cell Adhesion Molecules. These 3 pathways share many genes. The Extracellular Matrix Receptor Interaction and Cell Communication pathways were particularly driven by various collagens, integrins, fibronectins, and laminins. Additionally,

the Bladder Cancer Pathway, which includes growth factors, transcription factors, and matrix metalloprotease expression, was up-regulated in C57BL/6ByJ OIR retinae.

BALB/cByJ retinae again showed higher expression of metabolic pathways. Specifically, GSEA analysis indicated increase in expression of genes involved in metabolism of methionine, glycine/serine/threonine, and glutathione. Methionine and glycine/serine/threonine pathways have some overlap of genes with the highest enrichment scores. Up-regulation of the glutathione pathway is driven primarily by expression of glutathione S-transferase genes, which are involved in protection against chemical toxicity and oxidative stress (Raza, 2011). As glutathione is a potent anti-oxidant (Lubos, Loscalzo et al., 2011), up-regulation of this pathway may prevent oxidative damage to the retina during exposure to hyperoxia and thus minimize OIR-induced vascular damage in BALB/cByJ mice. This may explain differences in avascular area at P12. To date, neither the role of glutathione transferases specifically nor glutathione metabolism generally have been studied in ROP or OIR, but may be an intriguing avenue to explore. The higher expression of genes involved in metabolic pathways in BALB/cByJ may indicate a more adaptive response to the stress of the OIR model.

It is unclear from this study whether the more adaptive response in BALB/cByJ is in any way responsible for the faster vascular regeneration seen in this strain, or whether it is a consequence of the smaller area of avascular retina seen in BALB/cByJ mice at this time point. Similarly, the higher expression of extracellular matrix components and of cellular communications pathways in C57BL/6ByJ may simply be a consequence of the greater ischemic area in this strain rather than a sign of maladaptive angiogenic efforts. Nevertheless, this result raises the question of why retinal vascular regeneration proceeds

more slowly in C57BL/6ByJ than BALB/cByJ despite the higher levels of expression of genes that would normally promote revascularization.

CONCLUSIONS

Our comparative microarray studies in murine OIR development provide molecular insights on disease susceptibility and resistance using C57BL/6ByJ and BALB/cByJ strains, respectively. Initial experiments confirmed that BALB/cByJ mice are more resistant to initial vaso-obliteration during the hyperoxic phase of OIR, and that they revascularize more rapidly than C57BL/6ByJ mice following return to normoxia. Our microarray analysis, confirmatory rt-PCR data, and GSEA results suggest that up-regulation of angiogenic genes is associated with slower vascular regeneration and a greater degree of pathological revascularization.

Increased expression of metabolic genes was associated with improved OIR outcome in the BALB/cByJ strain. This finding may be a direct result of HIF-1α signaling in hypoxia. However, GSEA results alternatively suggest changes in expression of metabolic pathways may be related to an up-regulation of the glutathione pathway, which would likely decrease damaged related to oxidative stress. The latter mechanism may also explain why BALB/cByJ mice are more resistant to vaso-obliterative damage seen in the retina at P12.

Identifying expression patterns associated with varying outcomes can potentially identify gene targets that would allow for earlier and less invasive treatments for ROP, a leading cause of blindness in the pediatric population in the US. Future work expanding on these results may uncover additional pharmacological targets to improve the visual outcomes of premature infants affected by ROP.

CHAPTER 6

GENERAL DISCUSSION AND PROSPECTUS

LIST OF ABBREVIATIONS

BM – bone marrow
c-2J – B6(Cg)-*Tyr*$^{c-2J}$/J mouse strain
DA – dopamine
D1 – dopamine receptor 1
EPC – endothelial progenitor cell
F_2 – familial (intercross) 2nd generation
FEVR – familial exudative vitreoretinopathy
HIF-1α – hypoxia-inducible factor 1 α
HPLC-ED – high performance liquid chromatography with electrochemical detection
IGF-1– insulin-like growth factor1
IGFBP3 – insulin-like growth factor binding protein 3
OIR – oxygen-induced retinopathy
P – post-natal day
QTL – quantitative trait loci
ROP – Retinopathy of Prematurity
rt-PCR – real time polymerase chain reaction
Tyr – Tyrosinase

ROP is a major cause of vision loss in infants, and incidence of this disease is increasing worldwide. The pathogenesis of ROP is multifactorial, and several well-characterized risk factors have been identified. These include the use of oxygen therapy (Wheatley, Dickinson et al., 2002); decreased gestational age (Wheatley, Dickinson et al., 2002; Kim, Sohn et al., 2004; Good, Hardy et al., 2005; Bizzarro, Hussain et al., 2006); reduced gestational weight (Wheatley, Dickinson et al., 2002; Kim, Sohn et al., 2004; Good, Hardy et al., 2005; Bizzarro, Hussain et al., 2006) and associated reduced levels of IGF-1 (Hellstrom, Perruzzi et al., 2001); and reduced levels of IGFBP3 (Lofqvist, Chen et al., 2007; Fleck and McIntosh, 2008).

A growing body of evidence suggests that genetic component may also modulate risk of ROP development. Several epidemiological studies have identified differences in risk and severity of ROP between varieties of different ethnic groups both in the US and worldwide (Munoz and West, 2002; Tadesse, Dhanireddy et al., 2002; Lang, Blackledge et al., 2005; Yang, Donovan et al., 2006; Lad, Nguyen et al., 2008). Two inherited diseases of the retinal vasculature, FEVR and Norrie disease, share similar phenotypes with ROP; mutations in causative genes have been identified in a small number of severe cases of ROP (Shastry, Pendergast et al., 1997; Hiraoka, Berinstein et al., 2001; Talks, Ebenezer et al., 2001; Haider, Devarajan et al., 2002; Hutcheson, Paluru et al., 2005; MacDonald, Goldberg et al., 2005; Dickinson, Sale et al., 2006; Ells, Guernsey et al., 2010; Hiraoka, Takahashi et al., 2010). Additionally, a retrospective twin study suggested that as much as 70% of the variance in susceptibility to ROP is due to a heritable component (Bizzarro, Hussain et al., 2006). Despite this evidence, no genes associated with increased risk of developing ROP have been

identified to date. Therefore, the central purpose of the described studies is to identify genes related to susceptibility to ROP.

Using classical forward genetic techniques, we identified regions of the genome associated with retinal revascularization in the murine OIR model of ROP. Subsequent experiments confirmed the role of a specific candidate gene, *Tyr*, and elucidated a mechanism by which *Tyr* function alters susceptibility to OIR. These studies additionally characterize the role of EPCs in OIR development, and compare EPC response between *Tyr*-sufficient susceptible and *Tyr*-null resistant strains of mice. Finally, a microarray analysis adds insight into general transcriptional patterns associated with more or less successful responses to OIR and identified alternative mechanisms that may also play a role in OIR susceptibility.

Chapter II: Identification of QTL related to OIR

Using murine strains with known differences in susceptibility to ROP, we created a mapping cross to identify QTL associated with susceptibility to OIR. C57BL/6ByJ and BALB/cByJ animals were inbred and the resulting F_2 generation was phenotyped and selectively genotyped. Linkage analysis identified QTL associated with avascular area at P16 on chromosome 7 and chromosome 9. Positional Medline identified 185 candidate genes located within the support intervals of these 2 QTL and related to retinal angiogenesis.

Data from the F_2 generation also revealed significantly different areas of avascular retina between albino and non-albino mice. This result supports findings from a rat backcross (van Wijngaarden, Brereton et al., 2007) as well as across different strains of rats (van Wijngaarden, Coster et al., 2005). As albinism in the parental BALB/cByJ strain is

caused by homozygous loss of function of *Tyr*, these data suggest that *Tyr* or a linked gene may play a role in disease susceptibility. The QTL identified on chromosome 7 by mapping analysis includes *Tyr* (located 94.58-94.64 Mbp) within the support interval.

Chapter III: Exploration of the role of Tyr *in OIR*

The putative role of *Tyr* in OIR susceptibility was further explored in studies described in chapter 3. These experiments employed the c-2J strain of mice, which were derived from the C57BL/6J strain but had a spontaneous loss of function mutation in *Tyr* that was subsequently bred to homozygosity. Thus, c-2J mice share the same genetic background as C57BL/6J but are *Tyr* deficient. Exposure of both strains to the OIR model revealed that c-2J mice revascularize the retina more rapidly after hyperoxia-induced vaso-obliteration. This finding is associated with increased numbers of CD34+/CD133+ putative EPCs in the retina and more numerous CD45-/CD34+/CD133+ cells in both the bone marrow and in circulation. Together, these data suggest that *Tyr* function inhibits putative EPC proliferation, mobilization, and retinal recruitment *in vivo*.

We next began to explore a possible mechanism by which *Tyr* may modify retinal revascularization in OIR. HPLC-ED analysis of serum samples found higher concentrations of DA in serum of *Tyr*-functional C57BL/6J mice. This finding is in concordance with previously published work demonstrating that *Tyr* can contribute to peripheral production of DA early in murine life, prior to a developmental switch to melanin production (Eisenhofer, Tian et al., 2003). Intraperitoneal administration of DA in both C57BL/6J and c-2J mice results in inhibition of revascularization compared to saline-treated controls. Additionally, this treatment is associated with reduced recruitment of EPCs to the retina.

Use dopaminergic agonists indicate that the D1-like family of receptors mediates this response to DA signaling. These data support rt-PCR results that demonstrate expression of both D1 and D5 by BM and cultured EPCs. While our data conflict with prior work identifying D2 as the primary receptor responsible for inhibition of EPC mobilization by DA, other studies have demonstrated that DA receptor expression in EPCs is highly dynamic and responsive to the cytokine milieu present. As the aforementioned work examined the role of DA in tumor-laden adult mice, it is likely that differences in cytokine expression in our neonatal, hyperoxia-exposed mice explain these differences.

Chapter IV: Dynamic role of EPCs in OIR

Given the important role EPCs play in retinal revascularization in ROP and OIR, our next experiments were designed to better characterize changes in CD34+/CD133+ EPC populations that occur throughout the OIR protocol. Using the C57BL/6J and c-2J strains, we quantified EPC numbers in bone marrow, blood, and retina and quantified avascular area at every day from P7 through P13, and additionally at P7.5 and P9.5, 12 and 60 hours after exposure to hyperoxia.

Our data show that EPCs are highly dynamic and responsive to the stresses of the OIR model. EPCs followed different patterns in each tissue tested. Circulating EPCs were an especially variable population, which may explain some discrepancies in the literature amongst reports that suggest conflicting effects of dopaminergic regulation of this process.

Importantly, our data suggest that the customary time points used to describe the OIR model may not accurately describe the physiological changes. Traditionally, P7 through P12 are the time points used to describe the vaso-obliterative phase of OIR, and

revascularization and NV are thought to occur after P12. However, our data suggest that OIR can no longer be considered a 2-stage process. Rather, there are several stages: early vaso-obliteration, late vaso-obliteration, EPC response in the presence of hyperoxia, EPC response in the presence of normoxia, and pathological vascularization. Thus, the timing of interventions targeting these processes should be designed with this sequence in mind.

Chapter V: Microarray analysis

Our microarray analysis, confirmatory rt-PCR data, and GSEA results identified several interesting pathways that may contribute to differential susceptibility to OIR. Exposure to the OIR model led to increased expression in inflammatory genes in mice of both strains. In the C57BL/6ByJ strain, up-regulation of angiogenic genes is paradoxically associated with slower vascular regeneration and a greater degree of pathological NV. These genes may be up-regulated compared to BALB/cByJ mice due to the increased hypoxia of their larger avascular area, although more studies are need to clarify the regulation of these genes changes. Our microarray data are in line with other studies published using various C57BL sub-strains of mice.

Increased expression of metabolic genes was associated with improved OIR outcome in the BALB/cByJ strain. This finding may be a direct result of HIF-1α signaling in hypoxia. However, GSEA results alternatively suggest changes in expression of metabolic pathways may be related to an up-regulation of the glutathione pathway, which would likely decrease oxidative stress.

Identifying expression patterns associated with varying outcomes can potentially identify gene targets that would allow for earlier and less invasive treatments for ROP. Follow-up studies will explore gene candidates identified in this study.

Perspective

This study represents the first genome-wide approach to determining novel mechanisms underlying retinal revascularization in OIR. Additionally, we have identified a novel mechanism of dopaminergic control of angiogenesis in the retina. This finding is of particular importance clinically as DA is used therapeutically in the neonatal intensive care unit. Our work revives the earlier hypothesis that use of DA is associated with increased risk of severe ROP.

This pathway may offer a pharmacological target for improving ROP outcome. It is possible that improvement of EPC function and recruitment to the retina may mitigate retinal vascular arrest in the first phase of ROP, thus preventing the vision-threatening complications of the second stage. Additionally, these findings likely apply to other vascular retinopathies such as diabetic retinopathy and vein occlusion retinopathy, and potentially other diseases of angiogenesis, such as cardiovascular repair after myocardial infarction and tumor metastasis.

CHAPTER 7

REFERENCES

Allegaert, K., V. Cossey, G. Naulaers, C. Vanhole, H. Devlieger and I. Casteels (2004). "Dopamine is an indicator but not an independent risk factor for grade 3 retinopathy of prematurity in extreme low birthweight infants." Br J Ophthalmol **88**(2): 309-310.

Anand-Apte, B. and J. G. Hollyfield (2010). "Developmental Anatomy of the Retinal and Choroidal Vasculature."

Armando, I., X. Wang, V. A. Villar, J. E. Jones, L. D. Asico, C. Escano and P. A. Jose (2007). "Reactive oxygen species-dependent hypertension in dopamine D2 receptor-deficient mice." Hypertension **49**(3): 672-678.

Asahara, T., H. Masuda, T. Takahashi, C. Kalka, C. Pastore, M. Silver, M. Kearne, M. Magner and J. M. Isner (1999). "Bone marrow origin of endothelial progenitor cells responsible for postnatal vasculogenesis in physiological and pathological neovascularization." Circ Res **85**(3): 221-228.

Asahara, T., T. Murohara, A. Sullivan, M. Silver, R. van der Zee, T. Li, B. Witzenbichler, G. Schatteman and J. M. Isner (1997). "Isolation of putative progenitor endothelial cells for angiogenesis." Science **275**(5302): 964-967.

Ayoub, M. and D. E. Mather (2002). "Effectiveness of selective genotyping for detection of quantitative trait loci: an analysis of grain and malt quality traits in three barley populations." Genome **45**(6): 1116-1124.

Balasubramaniam, V., C. F. Mervis, A. M. Maxey, N. E. Markham and S. H. Abman (2007). "Hyperoxia reduces bone marrow, circulating, and lung endothelial progenitor cells in the developing lung: implications for the pathogenesis of bronchopulmonary dysplasia." Am J Physiol Lung Cell Mol Physiol **292**(5): L1073-1084.

Balogh, A., L. Derzbach, A. Vannay and B. Vasarhelyi (2006). "Lack of association between insulin-like growth factor I receptor G(+3174)A polymorphism and retinopathy of prematurity." Graefes Arch Clin Exp Ophthalmol **244**(8): 1035-1038.

Baschat, A. A., C. R. Harman, G. Farid, B. N. Chodirker and J. A. Evans (2002). "Very low second-trimester maternal serum alpha-fetoprotein: Association with high birth weight." Obstet Gynecol **99**(4): 531-536.

Basu, S., J. A. Nagy, S. Pal, E. Vasile, I. A. Eckelhoefer, V. S. Bliss, E. J. Manseau, P. S. Dasgupta, H. F. Dvorak and D. Mukhopadhyay (2001). "The neurotransmitter dopamine inhibits angiogenesis induced by vascular permeability factor/vascular endothelial growth factor." Nat Med **7**(5): 569-574.

Benameur, T., S. Tual-Chalot, R. Andriantsitohaina and M. C. Martinez (2010). "PPARalpha is essential for microparticle-induced differentiation of mouse bone marrow-derived endothelial progenitor cells and angiogenesis." PLoS One **5**(8): e12392.

Besler, C., C. Doerries, G. Giannotti, T. F. Luscher and U. Landmesser (2008). "Pharmacological approaches to improve endothelial repair mechanisms." Expert Rev Cardiovasc Ther **6**(8): 1071-1082.

Biscetti, F., G. Straface, D. Pitocco, F. Zaccardi, G. Ghirlanda and A. Flex.

Bishop-Bailey, D. (2011). "PPARs and angiogenesis." Biochem Soc Trans **39**(6): 1601-1605.

Bizzarro, M. J., N. Hussain, B. Jonsson, R. Feng, L. R. Ment, J. R. Gruen, H. Zhang and V. Bhandari (2006). "Genetic susceptibility to retinopathy of prematurity." Pediatrics **118**(5): 1858-1863.

Broderick, C., R. M. Hoek, J. V. Forrester, J. Liversidge, J. D. Sedgwick and A. D. Dick (2002). "Constitutive retinal CD200 expression regulates resident microglia and activation state of inflammatory cells during experimental autoimmune uveoretinitis." Am J Pathol **161**(5): 1669-1677.

Broman, K. W., S. Sen and Ś. Sen (2009). A Guide to Mapping with R/qtl. New York, Springer.

Broman, K. W., H. Wu, S. Sen and G. A. Churchill (2003). "R/qtl: QTL mapping in experimental crosses." Bioinformatics **19**(7): 889-890.

Campbell, K. (1951). "Intensive oxygen therapy as a possible cause of retrolental fibroplasia; a clinical approach." Med J Aust **2**(2): 48-50.

Cao, Z., L. D. Jensen, P. Rouhi, K. Hosaka, T. Lanne, J. F. Steffensen, E. Wahlberg and Y. Cao (2010). "Hypoxia-induced retinopathy model in adult zebrafish." Nat Protoc **5**(12): 1903-1910.

Case, J., D. A. Ingram and L. S. Haneline (2008). "Oxidative stress impairs endothelial progenitor cell function." Antioxid Redox Signal **10**(11): 1895-1907.

Ceradini, D. J., A. R. Kulkarni, M. J. Callaghan, O. M. Tepper, N. Bastidas, M. E. Kleinman, J. M. Capla, R. D. Galiano, J. P. Levine and G. C. Gurtner (2004). "Progenitor cell trafficking is regulated by hypoxic gradients through HIF-1 induction of SDF-1." Nat Med **10**(8): 858-864.

Chakroborty, D., U. R. Chowdhury, C. Sarkar, R. Baral, P. S. Dasgupta and S. Basu (2008). "Dopamine regulates endothelial progenitor cell mobilization from mouse bone marrow in tumor vascularization." J Clin Invest **118**(4): 1380-1389.

Chakroborty, D., C. Sarkar, B. Basu, P. S. Dasgupta and S. Basu (2009). "Catecholamines regulate tumor angiogenesis." Cancer Res **69**(9): 3727-3730.

Chan, C. K., L. N. Pham, J. Zhou, C. Spee, S. J. Ryan and D. R. Hinton (2005). "Differential expression of pro- and antiangiogenic factors in mouse strain-dependent hypoxia-induced retinal neovascularization." Lab Invest **85**(6): 721-733.

Chan-Ling, T. "Vasculogenesis and Angiogenesis in Formation of the Human Retinal Vasculature." 119-138.

Chan-Ling, T. and J. Stone (1993). "Retinopathy of Prematurity: Origins in the architecture of the Retina." Progress in Retinal Research **12**(2): 1-4.

Chen, J., K. M. Connor, C. M. Aderman and L. E. Smith (2008). "Erythropoietin deficiency decreases vascular stability in mice." J Clin Invest **118**(2): 526-533.

Chen, J., K. M. Connor, C. M. Aderman, K. L. Willett, O. P. Aspegren and L. E. Smith (2009). "Suppression of retinal neovascularization by erythropoietin siRNA in a mouse model of proliferative retinopathy." Invest Ophthalmol Vis Sci **50**(3): 1329-1335.

Chen, J. and L. E. Smith (2007). "Retinopathy of prematurity." Angiogenesis **10**(2): 133-140.

Chen, J. and L. E. Smith (2008). "A double-edged sword: erythropoietin eyed in retinopathy of prematurity." J AAPOS **12**(3): 221-222.

Chen, J., A. Stahl, A. Hellstrom and L. E. Smith (2011). "Current update on retinopathy of prematurity: screening and treatment." Curr Opin Pediatr **23**(2): 173-178.

Chiang, E. Y., M. Henson and I. Stroynowski (2003). "Correction of defects responsible for impaired Qa-2 class Ib MHC expression on melanoma cells protects mice from tumor growth." J Immunol **170**(9): 4515-4523.

Chidlow, J. H., Jr., J. D. Glawe, J. S. Alexander and C. G. Kevil (2010). "VEGF differentially regulates neutrophil and T cell adhesion through ItgaL- and ItgaM-dependent mechanisms." Am J Physiol Gastrointest Liver Physiol **299**(6): G1361-1367.

Chu, K., S. T. Lee, J. S. Koo, K. H. Jung, E. H. Kim, D. I. Sinn, J. M. Kim, S. Y. Ko, S. J. Kim, E. C. Song, M. Kim and J. K. Roh (2006). "Peroxisome proliferator-activated receptor-gamma-agonist, rosiglitazone, promotes angiogenesis after focal cerebral ischemia." Brain Res **1093**(1): 208-218.

Churchill, G. A. and R. W. Doerge (1994). "Empirical threshold values for quantitative trait mapping." Genetics **138**(3): 963-971.

Coats, D. K. (2005). "Retinopathy of prematurity: involution, factors predisposing to retinal detachment, and expected utility of preemptive surgical reintervention." Trans Am Ophthalmol Soc **103**: 281-312.

Comiskey, M., C. Y. Goldstein, S. R. De Fazio, M. Mammolenti, J. A. Newmark and C. M. Warner (2003). "Evidence that HLA-G is the functional homolog of mouse Qa-2, the Ped gene product." Hum Immunol **64**(11): 999-1004.

Cooke, R. W., J. A. Drury, R. Mountford and D. Clark (2004). "Genetic polymorphisms and retinopathy of prematurity." Invest Ophthalmol Vis Sci **45**(6): 1712-1715.

Crewe, J. M., G. Lam, A. Clark, K. Spilsbury, A. S. Mukhtar, N. Morlet, W. H. Morgan, M. Crowley and J. B. Semmens (2013). "Hospitalization rates of children who are blind." Clin Experiment Ophthalmol.

Darvasi, A. (1997). "The effect of selective genotyping on QTL mapping accuracy." Mamm Genome **8**(1): 67-68.

Davies, M. H., J. P. Eubanks and M. R. Powers (2003). "Increased retinal neovascularization in Fas ligand-deficient mice." Invest Ophthalmol Vis Sci **44**(7): 3202-3210.

Dickinson, J. L., M. M. Sale, A. Passmore, L. M. FitzGerald, C. M. Wheatley, K. P. Burdon, J. E. Craig, S. Tengtrisorn, S. M. Carden, H. Maclean and D. A. Mackey (2006). "Mutations in the NDP gene: contribution to Norrie disease, familial exudative vitreoretinopathy and retinopathy of prematurity." Clin Experiment Ophthalmol **34**(7): 682-688.

Diez-Roux, G., M. Argilla, H. Makarenkova, K. Ko and R. A. Lang (1999). "Macrophages kill capillary cells in G1 phase of the cell cycle during programmed vascular regression." Development **126**(10): 2141-2147.

Dorrell, M., H. Uusitalo-Jarvinen, E. Aguilar and M. Friedlander (2007). "Ocular neovascularization: basic mechanisms and therapeutic advances." Surv Ophthalmol **52 Suppl 1**: S3-19.

Dorrell, M. I., E. Aguilar, R. Jacobson, S. A. Trauger, J. Friedlander, G. Siuzdak and M. Friedlander (2010). "Maintaining retinal astrocytes normalizes revascularization and prevents vascular pathology associated with oxygen-induced retinopathy." Glia **58**(1): 43-54.

Dorrell, M. I. and M. Friedlander (2006). "Mechanisms of endothelial cell guidance and vascular patterning in the developing mouse retina." Prog Retin Eye Res **25**(3): 277-295.

Dorrell, M. I., M. Friedlander and L. E. H. Smith (2007). Retinal Vascular Development. Retinal Vascular Disease. A. M. Joussen, T. W. Gardner, B. Kirchhof and S. J. Ryan, Springer Berlin Heidelberg**:** 24-37.

Echeverry, R., F. Wu, W. B. Haile, J. Wu and M. Yepes (2012). "The cytokine tumor necrosis factor-like weak inducer of apoptosis and its receptor fibroblast growth factor-

inducible 14 have a neuroprotective effect in the central nervous system." J Neuroinflammation **9**: 45.

Eisenhofer, G., H. Tian, C. Holmes, J. Matsunaga, S. Roffler-Tarlov and V. J. Hearing (2003). "Tyrosinase: a developmentally specific major determinant of peripheral dopamine." FASEB J **17**(10): 1248-1255.

Ells, A., D. L. Guernsey, K. Wallace, B. Zheng, M. Vincer, A. Allen, A. Ingram, O. DaSilva, L. Siebert, T. Sheidow, J. Beis and J. M. Robitaille (2010). "Severe retinopathy of prematurity associated with FZD4 mutations." Ophthalmic Genet **31**(1): 37-43.

Epstein, D. and J. C. Kurz (2009). Patent. Complement Binding Aptamers and Anti-C5 Agents Useful in the Treatment of Ocular Disorders. US. **US 20090269356 A1**.

Fadini, G. P., C. Agostini and A. Avogaro (2005). "Endothelial progenitor cells and vascular biology in diabetes mellitus: current knowledge and future perspectives." Curr Diabetes Rev **1**(1): 41-58.

Fleck, B. W. and N. McIntosh (2008). "Pathogenesis of retinopathy of prematurity and possible preventive strategies." Early Hum Dev **84**(2): 83-88.

Fraisl, P., M. Mazzone, T. Schmidt and P. Carmeliet (2009). "Regulation of angiogenesis by oxygen and metabolism." Dev Cell **16**(2): 167-179.

Frauenknecht, K., P. Bargiotas, H. Bauer, P. von Landenberg, M. Schwaninger and C. Sommer (2010). "Neuroprotective effect of Fn14 deficiency is associated with induction of the granulocyte-colony stimulating factor (G-CSF) pathway in experimental stroke and enhanced by a pathogenic human antiphospholipid antibody." J Neuroimmunol **227**(1-2): 1-9.

Fruttiger, M. (2007). "Development of the retinal vasculature." Angiogenesis **10**(2): 77-88.

Fung, S. C. and Z. Yao (2009). Patent. Use of Complement Inhibitors to Treat Ocular Diseases. Genentech. US. **US20090214538 A1**.

Gallagher, K. A., Z. J. Liu, M. Xiao, H. Chen, L. J. Goldstein, D. G. Buerk, A. Nedeau, S. R. Thom and O. C. Velazquez (2007). "Diabetic impairments in NO-mediated endothelial progenitor cell mobilization and homing are reversed by hyperoxia and SDF-1 alpha." J Clin Invest **117**(5): 1249-1259.

Gariano, R. F. and T. W. Gardner (2005). "Retinal angiogenesis in development and disease." Nature **438**(7070): 960-966.

Gerhardt, H., M. Golding, M. Fruttiger, C. Ruhrberg, A. Lundkvist, A. Abramsson, M. Jeltsch, C. Mitchell, K. Alitalo, D. Shima and C. Betsholtz (2003). "VEGF guides angiogenic sprouting utilizing endothelial tip cell filopodia." J Cell Biol **161**(6): 1163-1177.

Gibson, D. L., S. B. Sheps, S. H. Uh, M. T. Schechter and A. Q. McCormick (1990). "Retinopathy of prematurity-induced blindness: birth weight-specific survival and the new epidemic." Pediatrics **86**(3): 405-412.

Gilbert, C. (2008). "Retinopathy of prematurity: a global perspective of the epidemics, population of babies at risk and implications for control." Early Hum Dev **84**(2): 77-82.

Gilbert, C. and A. Foster (2001). "Childhood blindness in the context of VISION 2020--the right to sight." Bull World Health Organ **79**(3): 227-232.

Gilbert, C. and M. Muhit (2012). "Eye conditions and blindness in children: priorities for research, programs, and policy with a focus on childhood cataract." Indian J Ophthalmol **60**(5): 451-455.

Gomez R Fau - Gonzalez-Izquierdo, M., R. C. Gonzalez-Izquierdo M Fau - Zimmermann, E. Zimmermann Rc Fau - Novella-Maestre, I. Novella-Maestre E Fau - Alonso-Muriel, J. Alonso-Muriel I Fau - Sanchez-Criado, J. Sanchez-Criado J Fau - Remohi, C. Remohi J Fau - Simon, A. Simon C Fau - Pellicer and A. Pellicer (2006). "Low-dose dopamine agonist administration blocks vascular endothelial growth factor (VEGF)-mediated vascular hyperpermeability without altering VEGF receptor 2-dependent luteal angiogenesis in a rat ovarian hyperstimulation model." Endocrinology(0013-7227 (Print)).

Gong, Y., R. B. Slee, N. Fukai, G. Rawadi, S. Roman-Roman, A. M. Reginato, H. Wang, T. Cundy, F. H. Glorieux, D. Lev, M. Zacharin, K. Oexle, J. Marcelino, W. Suwairi, S. Heeger, G. Sabatakos, S. Apte, W. N. Adkins, J. Allgrove, M. Arslan-Kirchner, J. A. Batch, P. Beighton, G. C. Black, R. G. Boles, L. M. Boon, C. Borrone, H. G. Brunner, G. F. Carle, B. Dallapiccola, A. De Paepe, B. Floege, M. L. Halfhide, B. Hall, R. C. Hennekam, T. Hirose, A. Jans, H. Juppner, C. A. Kim, K. Keppler-Noreuil, A. Kohlschuetter, D. LaCombe, M. Lambert, E. Lemyre, T. Letteboer, L. Peltonen, R. S. Ramesar, M. Romanengo, H. Somer, E. Steichen-Gersdorf, B. Steinmann, B. Sullivan, A. Superti-Furga, W. Swoboda, M. J. van den Boogaard, W. Van Hul, M. Vikkula, M. Votruba, B. Zabel, T. Garcia, R. Baron, B. R. Olsen and M. L. Warman (2001). "LDL receptor-related protein 5 (LRP5) affects bone accrual and eye development." Cell **107**(4): 513-523.

Good, W. V., R. J. Hardy, V. Dobson, E. A. Palmer, D. L. Phelps, M. Quintos and B. Tung (2005). "The incidence and course of retinopathy of prematurity: findings from the early treatment for retinopathy of prematurity study." Pediatrics **116**(1): 15-23.

Guo, S., W. J. Kim, J. Lok, S. R. Lee, E. Besancon, B. H. Luo, M. F. Stins, X. Wang, S. Dedhar and E. H. Lo (2008). "Neuroprotection via matrix-trophic coupling between cerebral endothelial cells and neurons." Proc Natl Acad Sci U S A **105**(21): 7582-7587.

Haider, M. Z., L. V. Devarajan, M. Al-Essa and H. Kumar (2002). "A C597-->A polymorphism in the Norrie disease gene is associated with advanced retinopathy of prematurity in premature Kuwaiti infants." J Biomed Sci **9**(4): 365-370.

Haile, W. B., R. Echeverry, F. Wu, J. Guzman, J. An, J. Wu and M. Yepes (2010). "Tumor necrosis factor-like weak inducer of apoptosis and fibroblast growth factor-inducible 14 mediate cerebral ischemia-induced poly(ADP-ribose) polymerase-1 activation and neuronal death." Neuroscience **171**(4): 1256-1264.

Hartnett, M. E. (2010). "Studies on the pathogenesis of avascular retina and neovascularization into the vitreous in peripheral severe retinopathy of prematurity (an american ophthalmological society thesis)." Trans Am Ophthalmol Soc **108**: 96-119.

Hartnett, M. E. and J. S. Penn (2012). "Mechanisms and management of retinopathy of prematurity." N Engl J Med **367**(26): 2515-2526.

Hass, P., Y. Jianping, J. K. Katschke, M. Steffek, M. Van Lookeren Campagne and C. Wiesmann (2011). Patent. Prevention and treatment of complement-associated eye conditions. Genentech. **US 8007791 B2**.

Hatfield, E. M. (1972). "Blindness in infants and young children." Sight Sav Rev **42**(2): 69-89.

Hellstrom, A., D. Ley, I. Hansen-Pupp, A. Niklasson, L. Smith, C. Lofqvist and A. L. Hard (2010). "New insights into the development of retinopathy of prematurity--importance of early weight gain." Acta Paediatr **99**(4): 502-508.

Hellstrom, A., C. Perruzzi, M. Ju, E. Engstrom, A. L. Hard, J. L. Liu, K. Albertsson-Wikland, B. Carlsson, A. Niklasson, L. Sjodell, D. LeRoith, D. R. Senger and L. E. Smith (2001). "Low IGF-I suppresses VEGF-survival signaling in retinal endothelial cells: direct correlation with clinical retinopathy of prematurity." Proc Natl Acad Sci U S A **98**(10): 5804-5808.

Hellstrom, M., L. K. Phng, J. J. Hofmann, E. Wallgard, L. Coultas, P. Lindblom, J. Alva, A. K. Nilsson, L. Karlsson, N. Gaiano, K. Yoon, J. Rossant, M. L. Iruela-Arispe, M. Kalen, H. Gerhardt and C. Betsholtz (2007). "Dll4 signalling through Notch1 regulates formation of tip cells during angiogenesis." Nature **445**(7129): 776-780.

Hiraoka, M., D. M. Berinstein, M. T. Trese and B. S. Shastry (2001). "Insertion and deletion mutations in the dinucleotide repeat region of the Norrie disease gene in patients with advanced retinopathy of prematurity." J Hum Genet **46**(4): 178-181.

Hiraoka, M., H. Takahashi, H. Orimo, T. Ogata and N. Azuma (2010). "Genetic screening of Wnt signaling factors in advanced retinopathy of prematurity." Mol Vis **16**: 2572-2577.

Holmstrom, G., P. van Wijngaarden, D. J. Coster and K. A. Williams (2007). "Genetic susceptibility to retinopathy of prematurity: the evidence from clinical and experimental animal studies." Br J Ophthalmol **91**(12): 1704-1708.

Holvoet, P. (2008). "Relations between metabolic syndrome, oxidative stress and inflammation and cardiovascular disease." Verh K Acad Geneeskd Belg **70**(3): 193-219.

Horuk, R. and S. C. Peiper (1996). "Chemokines: molecular double agents." Curr Biol **6**(12): 1581-1582.

Hotta, K., M. Sho, I. Yamato, K. Shimada, H. Harada, T. Akahori, S. Nakamura, N. Konishi, H. Yagita, K. Nonomura and Y. Nakajima (2011). "Direct targeting of fibroblast growth factor-inducible 14 protein protects against renal ischemia reperfusion injury." Kidney Int **79**(2): 179-188.

Huber, G., S. C. Beck, C. Grimm, A. Sahaboglu-Tekgoz, F. Paquet-Durand, A. Wenzel, P. Humphries, T. M. Redmond, M. W. Seeliger and M. D. Fischer (2009). "Spectral domain optical coherence tomography in mouse models of retinal degeneration." Invest Ophthalmol Vis Sci **50**(12): 5888-5895.

Hughes, S., H. Yang and T. Chan-Ling (2000). "Vascularization of the human fetal retina: roles of vasculogenesis and angiogenesis." Invest Ophthalmol Vis Sci **41**(5): 1217-1228.

Hutcheson, K. A., P. C. Paluru, S. L. Bernstein, J. Koh, E. F. Rappaport, R. A. Leach and T. L. Young (2005). "Norrie disease gene sequence variants in an ethnically diverse population with retinopathy of prematurity." Mol Vis **11**: 501-508.

Ilia, M. and G. Jeffery (1999). "Retinal mitosis is regulated by dopa, a melanin precursor that may influence the time at which cells exit the cell cycle: analysis of patterns of cell production in pigmented and albino retinae." J Comp Neurol **405**(3): 394-405.

Ishikawa, K., S. Yoshida, K. Kadota, T. Nakamura, H. Niiro, S. Arakawa, A. Yoshida, K. Akashi and T. Ishibashi (2010). "Gene expression profile of hyperoxic and hypoxic retinas in a mouse model of oxygen-induced retinopathy." Invest Ophthalmol Vis Sci **51**(8): 4307-4319.

Ito, S., T. Kato, K. Shinpo and K. Fujita (1984). "Oxidation of tyrosine residues in proteins by tyrosinase. Formation of protein-bonded 3,4-dihydroxyphenylalanine and 5-S-cysteinyl-3,4-dihydroxyphenylalanine." Biochem J **222**(2): 407-411.

Jakobsson, L., C. A. Franco, K. Bentley, R. T. Collins, B. Ponsioen, I. M. Aspalter, I. Rosewell, M. Busse, G. Thurston, A. Medvinsky, S. Schulte-Merker and H. Gerhardt (2010). "Endothelial cells dynamically compete for the tip cell position during angiogenic sprouting." Nat Cell Biol **12**(10): 943-953.

Jeffery, G. (1997). "The albino retina: an abnormality that provides insight into normal retinal development." Trends Neurosci **20**(4): 165-169.

Jia, L. Y., X. X. Li, W. Z. Yu, W. T. Zeng and C. Liang (2010). "Novel frizzled-4 gene mutations in chinese patients with familial exudative vitreoretinopathy." Arch Ophthalmol **128**(10): 1341-1349.

Kase, S., S. He, S. Sonoda, M. Kitamura, C. Spee, E. Wawrousek, S. J. Ryan, R. Kannan and D. R. Hinton (2010). "alphaB-crystallin regulation of angiogenesis by modulation of VEGF." Blood **115**(16): 3398-3406.

Katoh, M. (2009). "FGFR2 abnormalities underlie a spectrum of bone, skin, and cancer pathologies." J Invest Dermatol **129**(8): 1861-1867.

Kaya, M., M. Cokakli, A. T. Berk, A. Yaman, D. Yesilirmak, A. Kumral and N. Atabey (2013). "Associations of VEGF/VEGF-Receptor and HGF/c-Met Promoter Polymorphisms With Progression/Regression of Retinopathy of Prematurity." Curr Eye Res **38**(1): 137-142.

Kim, T. I., J. Sohn, S. Y. Pi and Y. H. Yoon (2004). "Postnatal risk factors of retinopathy of prematurity." Paediatr Perinat Epidemiol **18**(2): 130-134.

Klettner, A. and J. Roider (2009). "Constitutive and oxidative-stress-induced expression of VEGF in the RPE are differently regulated by different Mitogen-activated protein kinases." Graefes Arch Clin Exp Ophthalmol **247**(11): 1487-1492.

Koh, G. Y. (2012). "Orchestral actions of angiopoietin-1 in vascular regeneration." Trends Mol Med.

Kolb, H. (2005, 2007 Jul 5). "Facts and Figures Concerning the Human Retina." Webvision: The Organization of the Retina and Visual System, 2013, from http://www.ncbi.nlm.nih.gov/books/NBK11556/.

Kosaka, N., H. Sakamoto, M. Terada and T. Ochiya (2009). "Pleiotropic function of FGF-4: its role in development and stem cells." Dev Dyn **238**(2): 265-276.

Kralj-Hans, I., M. Tibber, G. Jeffery and P. Mobbs (2006). "Differential effect of dopamine on mitosis in early postnatal albino and pigmented rat retinae." J Neurobiol **66**(1): 47-55.

Lad, E. M., T. C. Nguyen, J. M. Morton and D. M. Moshfeghi (2008). "Retinopathy of prematurity in the United States." Br J Ophthalmol **92**(3): 320-325.

Lang, D. M., J. Blackledge and R. W. Arnold (2005). "Is Pacific race a retinopathy of prematurity risk factor?" Arch Pediatr Adolesc Med **159**(8): 771-773.

Lang, R. A. and J. M. Bishop (1993). "Macrophages are required for cell death and tissue remodeling in the developing mouse eye." Cell **74**(3): 453-462.

Lange, C., C. Ehlken, A. Stahl, G. Martin, L. Hansen and H. T. Agostini (2009). "Kinetics of retinal vaso-obliteration and neovascularisation in the oxygen-induced retinopathy (OIR) mouse model." Graefes Arch Clin Exp Ophthalmol **247**(9): 1205-1211.

Langer, H. F., K. J. Chung, V. V. Orlova, E. Y. Choi, S. Kaul, M. J. Kruhlak, M. Alatsatianos, R. A. DeAngelis, P. A. Roche, P. Magotti, X. Li, M. Economopoulou, S. Rafail, J. D. Lambris and T. Chavakis (2010). "Complement-mediated inhibition of neovascularization reveals a point of convergence between innate immunity and angiogenesis." Blood **116**(22): 4395-4403.

Ligi, I., S. Simoncini, E. Tellier, P. F. Vassallo, F. Sabatier, B. Guillet, E. Lamy, G. Sarlon, C. Quemener, A. Bikfalvi, M. Marcelli, A. Pascal, B. Dizier, U. Simeoni, F. Dignat-George and F. Anfosso (2011). "A switch toward angiostatic gene expression impairs the angiogenic properties of endothelial progenitor cells in low birth weight preterm infants." Blood **118**(6): 1699-1709.

Lima e Silva, R., J. Shen, S. F. Hackett, S. Kachi, H. Akiyama, K. Kiuchi, K. Yokoi, M. C. Hatara, T. Lauer, S. Aslam, Y. Y. Gong, W. H. Xiao, N. H. Khu, C. Thut and P. A. Campochiaro (2007). "The SDF-1/CXCR4 ligand/receptor pair is an important contributor to several types of ocular neovascularization." FASEB J **21**(12): 3219-3230.

Lin, M., Y. Chen, J. Jin, Y. Hu, K. K. Zhou, M. Zhu, Y. Z. Le, J. Ge, R. S. Johnson and J. X. Ma (2011). "Ischaemia-induced retinal neovascularisation and diabetic retinopathy in mice with conditional knockout of hypoxia-inducible factor-1 in retinal Muller cells." Diabetologia **54**(6): 1554-1566.

Liu, F., J. Smith, Z. Zhang, R. Cole and B. J. Herron (2010). "Genetic heterogeneity of skin microvasculature." Dev Biol **340**(2): 480-489.

Lofqvist, C., J. Chen, K. M. Connor, A. C. Smith, C. M. Aderman, N. Liu, J. E. Pintar, T. Ludwig, A. Hellstrom and L. E. Smith (2007). "IGFBP3 suppresses retinopathy through suppression of oxygen-induced vessel loss and promotion of vascular regrowth." Proc Natl Acad Sci U S A **104**(25): 10589-10594.

Lofqvist, C., I. Hansen-Pupp, E. Andersson, K. Holm, L. E. Smith, D. Ley and A. Hellstrom (2009). "Validation of a new retinopathy of prematurity screening method monitoring longitudinal postnatal weight and insulinlike growth factor I." Arch Ophthalmol **127**(5): 622-627.

Lofqvist, C., K. L. Willett, O. Aspegren, A. C. Smith, C. M. Aderman, K. M. Connor, J. Chen, A. Hellstrom and L. E. Smith (2009). "Quantification and localization of the IGF/insulin system expression in retinal blood vessels and neurons during oxygen-induced retinopathy in mice." Invest Ophthalmol Vis Sci **50**(4): 1831-1837.

Long, E. O. (2011). "ICAM-1: getting a grip on leukocyte adhesion." J Immunol **186**(9): 5021-5023.

Lubos, E., J. Loscalzo and D. E. Handy (2011). "Glutathione peroxidase-1 in health and disease: from molecular mechanisms to therapeutic opportunities." Antioxid Redox Signal **15**(7): 1957-1997.

Lutty, G. A., T. Chan-Ling, D. L. Phelps, A. P. Adamis, K. I. Berns, C. K. Chan, C. H. Cole, P. A. D'Amore, A. Das, W. T. Deng, V. Dobson, J. T. Flynn, M. Friedlander, A. Fulton, W. V. Good, M. B. Grant, R. Hansen, W. W. Hauswirth, R. J. Hardy, D. R. Hinton, S. Hughes, D. S. McLeod, E. A. Palmer, A. Patz, J. S. Penn, B. J. Raisler, M. X. Repka, M. Saint-Geniez, L. C. Shaw, D. T. Shima, B. T. Smith, L. E. Smith, S. G. Tahija, W. Tasman and M. T. Trese (2006). "Proceedings of the Third International Symposium on Retinopathy of Prematurity: an update on ROP from the lab to the nursery (November 2003, Anaheim, California)." Mol Vis **12**: 532-580.

MacDonald, M. L., Y. P. Goldberg, J. Macfarlane, M. E. Samuels, M. T. Trese and B. S. Shastry (2005). "Genetic variants of frizzled-4 gene in familial exudative vitreoretinopathy and advanced retinopathy of prematurity." Clin Genet **67**(4): 363-366.

Machalinska, A., M. Kotowski, K. Safranow, J. Lewandowska, M. Modrzejewska, J. Rudnicki, R. Czajka and B. Machalinski (2011). "[The role of circulating endothelial progenitor cells in the progression of retinopathy of prematurity--a prospective study]." Klin Oczna **113**(7-9): 223-227.

Marsin, A. S., C. Bouzin, L. Bertrand and L. Hue (2002). "The stimulation of glycolysis by hypoxia in activated monocytes is mediated by AMP-activated protein kinase and inducible 6-phosphofructo-2-kinase." J Biol Chem **277**(34): 30778-30783.

Matsuoka, Y., Y. Kitamura, M. Okazaki, M. Sakata, T. Tsukahara and T. Taniguchi (1998). "Induction of heme oxygenase-1 and major histocompatibility complex antigens in transient forebrain ischemia." J Cereb Blood Flow Metab **18**(8): 824-832.

Mazzone, A. and G. Ricevuti (1995). "Leukocyte CD11/CD18 integrins: biological and clinical relevance." Haematologica **80**(2): 161-175.

Mintz-Hittner, H. A., K. A. Kennedy and A. Z. Chuang (2011). "Efficacy of intravitreal bevacizumab for stage 3+ retinopathy of prematurity." N Engl J Med **364**(7): 603-615.

Mizoguchi, M. B., T. G. Chu, F. M. Murphy, N. Willits and L. S. Morse (1999). "Dopamine use is an indicator for the development of threshold retinopathy of prematurity." Br J Ophthalmol **83**(4): 425-428.

Munoz, B. and S. K. West (2002). "Blindness and visual impairment in the Americas and the Caribbean." Br J Ophthalmol **86**(5): 498-504.

Murata, T., S. He, M. Hangai, T. Ishibashi, X. P. Xi, S. Kim, W. A. Hsueh, S. J. Ryan, R. E. Law and D. R. Hinton (2000). "Peroxisome proliferator-activated receptor-gamma ligands inhibit choroidal neovascularization." Invest Ophthalmol Vis Sci **41**(8): 2309-2317.

Nakagawa, Y., H. Masuda, R. Ito, M. Kobori, M. Wada, T. Shizuno, A. Sato, T. Suzuki, K. Kawai and T. Asahara (2011). "Aberrant kinetics of bone marrow-derived endothelial progenitor cells in the murine oxygen-induced retinopathy model." Invest Ophthalmol Vis Sci **52**(11): 7835-7841.

Nakamura, R. E., D. D. Hunter, H. Yi, W. J. Brunken and A. S. Hackam (2007). "Identification of two novel activities of the Wnt signaling regulator Dickkopf 3 and characterization of its expression in the mouse retina." BMC Cell Biol **8**: 52.

Nallathambi, J., D. Shukla, A. Rajendran, P. Namperumalsamy, R. Muthulakshmi and P. Sundaresan (2006). "Identification of novel FZD4 mutations in Indian patients with familial exudative vitreoretinopathy." Mol Vis **12**: 1086-1092.

Niederkorn, J. Y., E. Y. Chiang, T. Ungchusri and I. Stroynowski (1999). "Expression of a nonclassical MHC class Ib molecule in the eye." Transplantation **68**(11): 1790-1799.

Nikopoulos, K., C. Gilissen, A. Hoischen, C. E. van Nouhuys, F. N. Boonstra, E. A. Blokland, P. Arts, N. Wieskamp, T. M. Strom, C. Ayuso, M. A. Tilanus, S. Bouwhuis, A. Mukhopadhyay, H. Scheffer, L. H. Hoefsloot, J. A. Veltman, F. P. Cremers and R. W. Collin (2010). "Next-generation sequencing of a 40 Mb linkage interval reveals TSPAN12 mutations in patients with familial exudative vitreoretinopathy." Am J Hum Genet **86**(2): 240-247.

Nikopoulos, K., H. Venselaar, R. W. Collin, R. Riveiro-Alvarez, F. N. Boonstra, J. M. Hooymans, A. Mukhopadhyay, D. Shears, M. van Bers, I. J. de Wijs, A. J. van Essen, R. H. Sijmons, M. A. Tilanus, C. E. van Nouhuys, C. Ayuso, L. H. Hoefsloot and F. P. Cremers (2010). "Overview of the mutation spectrum in familial exudative vitreoretinopathy and Norrie disease with identification of 21 novel variants in FZD4, LRP5, and NDP." Hum Mutat **31**(6): 656-666.

O'Bryhim, B. E., J. Radel, S. J. Macdonald and R. C. Symons (2012). "The genetic control of avascular area in mouse oxygen-induced retinopathy." Mol Vis **18**: 377-389.

Ohtsuka, M., H. Inoko, J. K. Kulski and S. Yoshimura (2008). "Major histocompatibility complex (Mhc) class Ib gene duplications, organization and expression patterns in mouse strain C57BL/6." BMC Genomics **9**: 178.

Owens, W. C. and E. U. Owens (1950). "Retrolental Fibroplasia." Am J Public Health Nations Health **40**(4): 405-408.

Ozerdem, U. and W. B. Stallcup (2004). "Pathological angiogenesis is reduced by targeting pericytes via the NG2 proteoglycan." Angiogenesis **7**(3): 269-276.

Panigrahy, D., S. Singer, L. Q. Shen, C. E. Butterfield, D. A. Freedman, E. J. Chen, M. A. Moses, S. Kilroy, S. Duensing, C. Fletcher, J. A. Fletcher, L. Hlatky, P. Hahnfeldt, J. Folkman and A. Kaipainen (2002). "PPARgamma ligands inhibit primary tumor growth and metastasis by inhibiting angiogenesis." J Clin Invest **110**(7): 923-932.

Patz, A., L. E. Hoeck and E. De La Cruz (1952). "Studies on the effect of high oxygen administration in retrolental fibroplasia. I. Nursery observations." Am J Ophthalmol **35**(9): 1248-1253.

Peeters, L. L., J. L. Vigne, M. K. Tee, D. Zhao, L. L. Waite and R. N. Taylor (2005). "PPAR gamma represses VEGF expression in human endometrial cells: implications for uterine angiogenesis." Angiogenesis **8**(4): 373-379.

Penn, J. S., B. L. Tolman and L. A. Lowery (1993). "Variable oxygen exposure causes preretinal neovascularization in the newborn rat." Invest Ophthalmol Vis Sci **34**(3): 576-585.

Perez-Munuzuri, A., J. R. Fernandez-Lorenzo, M. L. Couce-Pico, M. J. Blanco-Teijeiro and J. M. Fraga-Bermudez (2010). "Serum levels of IGF1 are a useful predictor of retinopathy of prematurity." Acta Paediatr **99**(4): 519-525.

Pi, L., A. K. Shenoy, J. Liu, S. Kim, N. Nelson, H. Xia, W. W. Hauswirth, B. E. Petersen, G. S. Schultz and E. W. Scott (2012). "CCN2/CTGF regulates neovessel formation via targeting structurally conserved cystine knot motifs in multiple angiogenic regulators." FASEB J **26**(8): 3365-3379.

Pistrosch, F., K. Herbrig, U. Oelschlaegel, S. Richter, J. Passauer, S. Fischer and P. Gross (2005). "PPARgamma-agonist rosiglitazone increases number and migratory activity of cultured endothelial progenitor cells." Atherosclerosis **183**(1): 163-167.

Polverini, P. J., P. S. Cotran, M. A. Gimbrone, Jr. and E. R. Unanue (1977). "Activated macrophages induce vascular proliferation." Nature **269**(5631): 804-806.

Qiao, H., K. H. Sonoda, Y. Ikeda, T. Yoshimura, K. Hijioka, Y. J. Jo, Y. Sassa, C. Tsutsumi-Miyahara, Y. Hata, S. Akira and T. Ishibashi (2007). "Interleukin-18 regulates pathological intraocular neovascularization." J Leukoc Biol **81**(4): 1012-1021.

Qiao, H., K. H. Sonoda, Y. Sassa, T. Hisatomi, H. Yoshikawa, Y. Ikeda, T. Murata, S. Akira and T. Ishibashi (2004). "Abnormal retinal vascular development in IL-18 knockout mice." Lab Invest **84**(8): 973-980.

Rachel, R. A., G. Dolen, N. L. Hayes, A. Lu, L. Erskine, R. S. Nowakowski and C. A. Mason (2002). "Spatiotemporal features of early neuronogenesis differ in wild-type and albino mouse retina." J Neurosci **22**(11): 4249-4263.

Raza, H. (2011). "Dual localization of glutathione S-transferase in the cytosol and mitochondria: implications in oxidative stress, toxicity and disease." FEBS J **278**(22): 4243-4251.

Recchia, F. M., L. Xu, J. S. Penn, B. Boone and P. J. Dexheimer (2010). "Identification of genes and pathways involved in retinal neovascularization by microarray analysis of two animal models of retinal angiogenesis." Invest Ophthalmol Vis Sci **51**(2): 1098-1105.

Reis, R. A., A. L. Ventura, R. C. Kubrusly, M. C. de Mello and F. G. de Mello (2007). "Dopaminergic signaling in the developing retina." Brain Res Rev **54**(1): 181-188.

Rios, M., B. Habecker, T. Sasaoka, G. Eisenhofer, H. Tian, S. Landis, D. Chikaraishi and S. Roffler-Tarlov (1999). "Catecholamine synthesis is mediated by tyrosinase in the absence of tyrosine hydroxylase." J Neurosci **19**(9): 3519-3526.

Ritter, M. R., E. Banin, S. K. Moreno, E. Aguilar, M. I. Dorrell and M. Friedlander (2006). "Myeloid progenitors differentiate into microglia and promote vascular repair in a model of ischemic retinopathy." J Clin Invest **116**(12): 3266-3276.

Robitaille, J., M. L. MacDonald, A. Kaykas, L. C. Sheldahl, J. Zeisler, M. P. Dube, L. H. Zhang, R. R. Singaraja, D. L. Guernsey, B. Zheng, L. F. Siebert, A. Hoskin-Mott, M. T. Trese, S. N. Pimstone, B. S. Shastry, R. T. Moon, M. R. Hayden, Y. P. Goldberg and M. E. Samuels (2002). "Mutant frizzled-4 disrupts retinal angiogenesis in familial exudative vitreoretinopathy." Nat Genet **32**(2): 326-330.

Rohan, R. M., A. Fernandez, T. Udagawa, J. Yuan and R. J. D'Amato (2000). "Genetic heterogeneity of angiogenesis in mice." FASEB J **14**(7): 871-876.

Romagnani, P., L. Lasagni, F. Annunziato, M. Serio and S. Romagnani (2004). "CXC chemokines: the regulatory link between inflammation and angiogenesis." Trends Immunol **25**(4): 201-209.

Rozen, S. and H. Skaletsky (2000). "Primer3 on the WWW for general users and for biologist programmers." Methods Mol Biol **132**: 365-386.

Rusai, K., A. Vannay, B. Szebeni, G. Borgulya, A. Fekete, B. Vasarhelyi, T. Tulassay and A. J. Szabo (2008). "Endothelial nitric oxide synthase gene T-786C and 27-bp repeat gene polymorphisms in retinopathy of prematurity." Mol Vis **14**: 286-290.

Ryan, S. J. (2001). Retina. St. Louis, Mosby.

Safranow, K., M. Kotowski, J. Lewandowska, A. Machalinska, V. Dziedziejko, R. Czajka, Z. Celewicz, J. Rudnicki and B. Machalinski (2012). "Circulating endothelial progenitor cells in premature infants: is there an association with premature birth complications?" J Perinat Med **40**(4): 455-462.

Saint-Geniez, M. and P. A. D'Amore (2004). "Development and pathology of the hyaloid, choroidal and retinal vasculature." Int J Dev Biol **48**(8-9): 1045-1058.

Saito, A., T. Hayashi, S. Okuno, T. Nishi and P. H. Chan (2004). "Oxidative stress affects the integrin-linked kinase signaling pathway after transient focal cerebral ischemia." Stroke **35**(11): 2560-2565.

Sakurai, K. and T. Sawamura (2003). "Stress and vascular responses: endothelial dysfunction via lectin-like oxidized low-density lipoprotein receptor-1: close relationships with oxidative stress." J Pharmacol Sci **91**(3): 182-186.

Sapieha, P. (2012). "Eyeing central neurons in vascular growth and reparative angiogenesis." Blood **120**(11): 2182-2194.

Sapieha, P., J. S. Joyal, J. C. Rivera, E. Kermorvant-Duchemin, F. Sennlaub, P. Hardy, P. Lachapelle and S. Chemtob (2010). "Retinopathy of prematurity: understanding ischemic retinal vasculopathies at an extreme of life." J Clin Invest **120**(9): 3022-3032.

Sato, T., S. Kusaka, N. Hashida, Y. Saishin, T. Fujikado and Y. Tano (2009). "Comprehensive gene-expression profile in murine oxygen-induced retinopathy." Br J Ophthalmol **93**(1): 96-103.

Schwertfeger, K. L. (2009). "Fibroblast growth factors in development and cancer: insights from the mammary and prostate glands." Curr Drug Targets **10**(7): 632-644.

Sekiguchi, H., M. Ii, K. Jujo, A. Yokoyama, N. Hagiwara and T. Asahara (2011). "Improved culture-based isolation of differentiating endothelial progenitor cells from mouse bone marrow mononuclear cells." PLoS One **6**(12): e28639.

Semenza, G. L. (2000). "Expression of hypoxia-inducible factor 1: mechanisms and consequences." Biochem Pharmacol **59**(1): 47-53.

Semenza, G. L. (2009). "Regulation of oxygen homeostasis by hypoxia-inducible factor 1." Physiology (Bethesda) **24**: 97-106.

Shastry, B. S. (2010). "Genetic susceptibility to advanced retinopathy of prematurity (ROP)." J Biomed Sci **17**: 69.

Shastry, B. S., S. D. Pendergast, M. K. Hartzer, X. Liu and M. T. Trese (1997). "Identification of missense mutations in the Norrie disease gene associated with advanced retinopathy of prematurity." Arch Ophthalmol **115**(5): 651-655.

Shi, D. Y., F. Z. Xie, C. Zhai, J. S. Stern, Y. Liu and S. L. Liu (2009). "The role of cellular oxidative stress in regulating glycolysis energy metabolism in hepatoma cells." Mol Cancer **8**: 32.

Sivakumar, V., W. S. Foulds, C. D. Luu, E. A. Ling and C. Kaur (2011). "Retinal ganglion cell death is induced by microglia derived pro-inflammatory cytokines in the hypoxic neonatal retina." J Pathol **224**(2): 245-260.

Smith, L. E., E. Wesolowski, A. McLellan, S. K. Kostyk, R. D'Amato, R. Sullivan and P. A. D'Amore (1994). "Oxygen-induced retinopathy in the mouse." Invest Ophthalmol Vis Sci **35**(1): 101-111.

Smyth, G. K., and Speed, T. P. (2003). "Normalization of cDNA microarray data." Methods **31**: 265-273.

Spiegel, A., S. Shivtiel, A. Kalinkovich, A. Ludin, N. Netzer, P. Goichberg, Y. Azaria, I. Resnick, I. Hardan, H. Ben-Hur, A. Nagler, M. Rubinstein and T. Lapidot (2007). "Catecholaminergic neurotransmitters regulate migration and repopulation of immature human CD34+ cells through Wnt signaling." Nat Immunol **8**(10): 1123-1131.

Stefater, J. A., 3rd, I. Lewkowich, S. Rao, G. Mariggi, A. C. Carpenter, A. R. Burr, J. Fan, R. Ajima, J. D. Molkentin, B. O. Williams, M. Wills-Karp, J. W. Pollard, T. Yamaguchi, N. Ferrara, H. Gerhardt and R. A. Lang (2011). "Regulation of angiogenesis by a non-canonical Wnt-Flt1 pathway in myeloid cells." Nature **474**(7352): 511-515.

Strieter, R. M., J. A. Belperio, M. D. Burdick, S. Sharma, S. M. Dubinett and M. P. Keane (2004). "CXC chemokines: angiogenesis, immunoangiostasis, and metastases in lung cancer." Ann N Y Acad Sci **1028**: 351-360.

Subramanian, A., P. Tamayo, V. K. Mootha, S. Mukherjee, B. L. Ebert, M. A. Gillette, A. Paulovich, S. L. Pomeroy, T. R. Golub, E. S. Lander and J. P. Mesirov (2005). "Gene set enrichment analysis: a knowledge-based approach for interpreting genome-wide expression profiles." Proc Natl Acad Sci U S A **102**(43): 15545-15550.

Summers, C. G. (1996). "Vision in albinism." Trans Am Ophthalmol Soc **94**: 1095-1155.

Suriano, R., D. Chaudhuri, R. S. Johnson, E. Lambers, B. T. Ashok, R. Kishore and R. K. Tiwari (2008). "17Beta-estradiol mobilizes bone marrow-derived endothelial progenitor cells to tumors." Cancer Res **68**(15): 6038-6042.

Symons, R. C., M. E. Swaim, T. W. Lauer and P. A. Campochiaro (2009). "Genetic Control of Vaso-Obliteration in Mouse Oxygen Induced Retinopathy." Invest. Ophthalmol. Vis. Sci. **50**(5): 5695-.

Tadesse, M., R. Dhanireddy, M. Mittal and R. D. Higgins (2002). "Race, Candida sepsis, and retinopathy of prematurity." Biol Neonate **81**(2): 86-90.

Talks, S. J., N. Ebenezer, P. Hykin, G. Adams, F. Yang, E. Schulenberg, K. Gregory-Evans and C. Y. Gregory-Evans (2001). "De novo mutations in the 5' regulatory region of the Norrie disease gene in retinopathy of prematurity." J Med Genet **38**(12): E46.

Terry, T. L. (1942). "Fibroblastic Overgrowth of Persistent Tunica Vasculosa Lentis in Infants Born Prematurely: II. Report of Cases-Clinical Aspects." Trans Am Ophthalmol Soc **40**: 262-284.

Terry, T. L. (1944). "Retrolental Fibroplasia in the Premature Infant: V. Further Studies on Fibroplastic Overgrowth of the Persistent Tunica Vasculosa Lentis." Trans Am Ophthalmol Soc **42**: 383-396.

Tsang, J. Y. S., J. G. Chai and R. Lechler (2003). "Antigen presentation by mouse CD4+ T cells involving acquired MHC class II:peptide complexes: another mechanism to limit clonal expansion?" Blood **101**(7): 2704-2710.

Tsimafeyeu, I., L. Demidov, E. Stepanova, N. Wynn and H. Ta (2011). "Overexpression of fibroblast growth factor receptors FGFR1 and FGFR2 in renal cell carcinoma." Scand J Urol Nephrol.

Urbich, C. and S. Dimmeler (2004). "Endothelial progenitor cells: characterization and role in vascular biology." Circ Res **95**(4): 343-353.

Valentine, P. H., J. C. Jackson, R. E. Kalina and D. E. Woodrum (1989). "Increased survival of low birth weight infants: impact on the incidence of retinopathy of prematurity." Pediatrics **84**(3): 442-445.

Vallet, J. L., J. R. Miles and B. A. Freking (2009). "Development of the pig placenta." Soc Reprod Fertil Suppl **66**: 265-279.

Van Gestel, S., J. J. Houwing-Duistermaat, R. Adolfsson, C. M. van Duijn and C. Van Broeckhoven (2000). "Power of selective genotyping in genetic association analyses of quantitative traits." Behav Genet **30**(2): 141-146.

van Wijngaarden, P., H. M. Brereton, D. J. Coster and K. A. Williams (2007). "Genetic influences on susceptibility to oxygen-induced retinopathy." Invest Ophthalmol Vis Sci **48**(4): 1761-1766.

van Wijngaarden, P., H. M. Brereton, I. L. Gibbins, D. J. Coster and K. A. Williams (2007). "Kinetics of strain-dependent differential gene expression in oxygen-induced retinopathy in the rat." Exp Eye Res **85**(4): 508-517.

van Wijngaarden, P., D. J. Coster, H. M. Brereton, I. L. Gibbins and K. A. Williams (2005). "Strain-dependent differences in oxygen-induced retinopathy in the inbred rat." Invest Ophthalmol Vis Sci **46**(4): 1445-1452.

Vannay, A., G. Dunai, I. Banyasz, M. Szabo, R. Vamos, A. Treszl, J. Hajdu, T. Tulassay and B. Vasarhelyi (2005). "Association of genetic polymorphisms of vascular endothelial growth factor and risk for proliferative retinopathy of prematurity." Pediatr Res **57**(3): 396-398.

Walsh, N., A. Bravo-Nuevo, S. Geller and J. Stone (2004). "Resistance of photoreceptors in the C57BL/6-c2J, C57BL/6J, and BALB/cJ mouse strains to oxygen stress: evidence of an oxygen phenotype." Curr Eye Res **29**(6): 441-447.

Warburg, O. (1956). "On the origin of cancer cells." Science **123**(3191): 309-314.

Watanabe, D., K. Suzuma, S. Matsui, M. Kurimoto, J. Kiryu, M. Kita, I. Suzuma, H. Ohashi, T. Ojima, T. Murakami, T. Kobayashi, S. Masuda, M. Nagao, N. Yoshimura and H. Takagi (2005). "Erythropoietin as a retinal angiogenic factor in proliferative diabetic retinopathy." N Engl J Med **353**(8): 782-792.

Wesolowski, E. and L. E. Smith (1994). "Effect of light on oxygen-induced retinopathy in the mouse." Invest Ophthalmol Vis Sci **35**(1): 112-119.

Wheatley, C. M., J. L. Dickinson, D. A. Mackey, J. E. Craig and M. M. Sale (2002). "Retinopathy of prematurity: recent advances in our understanding." Br J Ophthalmol **86**(6): 696-700.

Wheatley, C. M., J. L. Dickinson, D. A. Mackey, J. E. Craig and M. M. Sale (2002). "Retinopathy of prematurity: recent advances in our understanding." Arch Dis Child Fetal Neonatal Ed **87**(2): F78-82.

Xu, Q., Y. Wang, A. Dabdoub, P. M. Smallwood, J. Williams, C. Woods, M. W. Kelley, L. Jiang, W. Tasman, K. Zhang and J. Nathans (2004). "Vascular development in the retina and inner ear: control by Norrin and Frizzled-4, a high-affinity ligand-receptor pair." Cell **116**(6): 883-895.

Yang, J., M. Ii, N. Kamei, C. Alev, S. M. Kwon, A. Kawamoto, H. Akimaru, H. Masuda, Y. Sawa and T. Asahara (2011). "CD34+ cells represent highly functional endothelial progenitor cells in murine bone marrow." PLoS One **6**(5): e20219.

Yang, M. B., E. F. Donovan and J. R. Wagge (2006). "Race, gender, and clinical risk index for babies (CRIB) score as predictors of severe retinopathy of prematurity." J AAPOS **10**(3): 253-261.

Yanni, S. E., G. W. McCollum and J. S. Penn (2008). Rodent Models of Oxygen-Induced Retinopathy. Retinal and Choroidal Angiogenesis. J. S. Penn, Springer Netherlands**:** 57-80.

Ye, X., Y. Wang, H. Cahill, M. Yu, T. C. Badea, P. M. Smallwood, N. S. Peachey and J. Nathans (2009). "Norrin, frizzled-4, and Lrp5 signaling in endothelial cells controls a genetic program for retinal vascularization." Cell **139**(2): 285-298.

Yoshida, S., A. Yoshida, T. Ishibashi, S. G. Elner and V. M. Elner (2003). "Role of MCP-1 and MIP-1alpha in retinal neovascularization during postischemic inflammation in a mouse model of retinal neovascularization." J Leukoc Biol **73**(1): 137-144.

Yoshida, Y., Y. Makita, N. Heida, S. Asano, A. Matsushima, M. Ishii, Y. Mochizuki, H. Masuya, S. Wakana, N. Kobayashi and T. Toyoda (2009). "PosMed (Positional Medline): prioritizing genes with an artificial neural network comprising medical documents to accelerate positional cloning." Nucleic Acids Res **37**(Web Server issue): W147-152.

Zeng, H., L. Li and J. X. Chen (2012). "Overexpression of angiopoietin-1 increases CD133+/c-kit+ cells and reduces myocardial apoptosis in db/db mouse infarcted hearts." PLoS One **7**(4): e35905.

Zeng, L., S. Ding, Z. Yan, C. Chen, W. Sang, J. Cao, H. Cheng and K. Xu (2012). "Irradiation induces homing of donor endothelial progenitor cells in allogeneic hematopoietic stem cell transplantation." Int J Hematol **95**(2): 189-197.

Zhang, H., J. Tse, X. Hu, M. Witte, M. Bernas, J. Kang, F. Tilahun, Y. K. Hong, M. Qiu and L. Chen (2010). "Novel discovery of LYVE-1 expression in the hyaloid vascular system." Invest Ophthalmol Vis Sci **51**(12): 6157-6161.

Zhao, L., W. Ma, R. N. Fariss and W. T. Wong (2009). "Retinal vascular repair and neovascularization are not dependent on CX3CR1 signaling in a model of ischemic retinopathy." Exp Eye Res **88**(6): 1004-1013.

Zhou, G., Z.-C. Ding, J. Fu and H. I. Levitsky (2011). "Presentation of Acquired Peptide-MHC Class II Ligands by CD4+ Regulatory T Cells or Helper Cells Differentially Regulates Antigen-Specific CD4+ T Cell Response." The Journal of Immunology **186**(4): 2148-2155.

Zhu, W. H., M. Iurlaro, A. MacIntyre, E. Fogel and R. F. Nicosia (2003). "The mouse aorta model: influence of genetic background and aging on bFGF- and VEGF-induced angiogenic sprouting." Angiogenesis **6**(3): 193-199.

Zubilewicz, A., C. Hecquet, J. C. Jeanny, G. Soubrane, Y. Courtois and F. Mascarelli (2001). "Two distinct signalling pathways are involved in FGF2-stimulated proliferation of choriocapillary endothelial cells: a comparative study with VEGF." Oncogene **20**(12): 1403-1413.